INAUGURAL-DISSERTATION

zur

Erlangung der Doktorwürde

der Naturwissenschaftlich-Mathematischen

Gesamtfakultät

der Ruprecht-Karls-Universität

Heidelberg

vorgelegt von

Master of Science Dan Domide

aus Sibiu, Rumänien

Tag der mündlichen Prüfung: 12 *November* 2010

A new synthetic route to heterobimetallic carbamato complexes and their use as precursors to nanosized magnetic oxide particles

Gutachter: Prof. Dr. Dr. Hans-Jörg Himmel
                          Prof. Dr. Gerald Linti

carpe diem

Table of contents

Zusammenfassung

Die vorliegende Arbeit beschäftigt sich mit der Synthese und Charakterisierung von neuen heterobimetalischen Carbamat-Komplexen und ihren chemischen Eigenschaften. CO_2-Fixierung durch Insertion in die Zn-N Bindung von $EtZnN(iPr)_2$ führt zur Bildung des tetrameren Carbamat-Komplexes $[ZnEt(O_2CN(iPr)_2)]_4$, welcher in dieser Arbeit als Ausgangsverbindung eingesetzt wurde. Die thermische Zersetzung dieses Carbamat-Komplexes wurde mit verschiedenen Methoden analysiert, wobei die Untersuchungen zeigen, dass der Komplex $[ZnEt(O_2CN(iPr)_2)]_4$ eine gute Vorläuferverbindung für ZnO-Nanopartikel darstellt. Die ZnO-Nanopartikel mit einer Partikelgröße von ca. 10 nm können unter milden Reaktionsbedingungen erhalten werden, wobei die Sauerstoff-Atome des Oxids aus dem CO_2 stammen.

Das tetramere Carbamat $[ZnEt(O_2CN(iPr)_2)]_4$ wurde mit den verschiedenen Stickstoffbasen Pyridin, N,N,N',N'-Tetramethylguanidin und bis-N,N,N',N'-Tetramethylguanidinonaphthalin umgesetzt, wobei eine Vielzahl neuer mono-, bi- und trinuklearer Zn-Carbamat-Komplexe erhalten werden konnte. Der erste strukturell charakterisierte mononukleare Zn-Biscarbamat-Komplex mit η^1-koordinierten Carbamat-Liganden entstand bei der Reaktion von $[ZnEt(O_2CN(iPr)_2)]_4$ und einer Guanidin-Base.

Die Reaktion von $[ZnEt(O_2CN(iPr)_2)]_4$ mit Co(II)- und Mn(II)-dichlorid-Komplexen, welche 2-(Methylamino)pyridin als weiteren Ligand enthalten, führt zu neuen tetra- und oktanuklearen gemischten Zn/Co und Zn/Mn Carbamat-Komplexen. Im Fall von Kobalt entstanden tetranukleare ($[M_4R_2(O_2CN(iPr)_2)_6]$ (M = Zn, Co; R = Et, Me)) und oktanukleare Komplexe ($[M_8(\mu_4\text{-}O)_2(O_2CN(iPr)_2)_6]$ (M = Zn, Co)), während mit Mn der oktanukleare Komplex $[Zn_2Mn_6(\mu_4\text{-}O)_2(O_2CN(iPr)_2)_6]$ gebildet wurde. Bei der Oxidation des oktanuklearen Zn/Mn-Komplexes $[Zn_2Mn_6(\mu_4\text{-}O)_2(O_2CN(iPr)_2)_6]$ mit Sauerstoff entsteht der neue Komplex $[Zn_2Mn_6(\mu_4\text{-}O)_2(\mu_3\text{-}O)(O_2CN(iPr)_2)_6]$.

Die thermische Zersetzung der gemischten Zn/Co und Zn/Mn Carbamat-Komplexe unter milden Bedingungen (200-300°C) führt zu magnetischen gemischten Oxid-Nanopartikeln.

Abstract

This work is concerned with the synthesis and characterization of new heterobimetallic carbamate complexes and their chemistry. CO_2 fixation by insertion into the Zn-N bond of the molecular compound $EtZnN(iPr)_2$ leads to the formation of the tetrameric carbamate complex $[ZnEt(O_2CN(iPr)_2)]_4$ used further on in this work as starting material. Thermal decomposition of the carbamate complexe $[ZnEt(O_2CN(iPr)_2)]_4$ was studied by applying a variety of different analytical techniques. These studies show that this compound is a suitable precursor for nanosized ZnO particles of ca. 10 nm diameter synthesised under mild conditions (< 200°C) with the oxygen atoms originating from the reactant CO_2.

The tetrameric carbamate $[ZnEt(O_2CN(iPr)_2)]_4$ is then reacted with the nitrogen bases pyridine, N,N,N',N'-tetramethylguanidine and bis-N,N,N',N'-tetramethylguanidine naphthalene. Using this top-down approach the synthesis of a variety of new mono-, bi- and trinuclear carbamato-Zn complexes becomes possible. The first structurally characterized mononuclear biscarbamate complex of Zn with η^1-coordinated carbamate ligands can be prepared by reaction between $[ZnEt(O_2CN(iPr)_2)]_4$ and a guanidine base.

Reaction of the tetrameric carbamate $[ZnEt(O_2CN(iPr)_2)]_4$ with Co(II) and Mn(II) dichloride complexes, containing as ligands a nitrogen base [2-(Methylamino)pyridine], afforded new tetra- and octanuclear mixed Zn/Co and Zn/Mn carbamate complexes. Hence, with Co the tetranuclear $[M_4R_2(O_2CN(iPr)_2)_6]$ (R = Et, Me) and octanuclear $[M_8(\mu_4-O)_2(O_2CN(iPr)_2)_6]$ (M =Zn, Co) complexes were formed, and with Mn the octanuclear complex $[Zn_2Mn_6(\mu_4-O)_2(O_2CN(iPr)_2)_6]$ was obtained. Oxidation of the carbamate $[Zn_2Mn_6(\mu_4-O)_2(O_2CN(iPr)_2)_6]$ by filling the empty void with one oxygen atom leads to the formation of a new carbamate complex $[Zn_2Mn_6(\mu_4-O)_2(\mu_3-O)(O_2CN(iPr)_2)_6]$. Thermal decomposition of these mixed Zn/Co and Zn/Mn carbamates, at mild conditions (200-300°C), is shown to lead to magnetic mixed oxide nanoparticles.

Abbreviations

General Abbreviations

AAS	Atomic Absorption Spectroscopy
BTMGN	Bis-N,N,N',N'-Tetramethylguanidine naphthalene
EA	Elemental Analysis
EPR	Electron Paramagnetic Resonance
Et	Ethyl
eq	equivalent
FD+	Positive Field Desorption Mass Spectrometry
*i*Bu	Isobutyl
ICP	Inductively Coupled Plasma Mass Spectrometry
*i*Pr	Isopropyl
IR	Infrared
LIFDI	Liquid Injection Field Desorption Ionization
MAEP	2-[2-(Methylamino)-ethyl]-pyridine
MAP	2-(Methylamino)pyridine
Me	Methyl
MS	Mass Spectrometry
NMR	Nuclear Magnetic Resonance
Py	Pyridine
R	Alkyl
RT	Room temperature
SET	Single electron transfer
SQUID	Superconducting Quantum Interference Device
TEM	Transmission Electron Microscopy
THF	Tetrahydrofuran
TG	Thermogravimetrie
TMEDA	Tetramethylethylenediamine
TMG	N,N,N',N'-Tetramethylguanidine
UV/Vis	Ultraviolet, Visible
XRD	X-ray diffraction

Abbreviations referring to spectroscopic methods

a, b, c	unit cell length dimensions [Å]
α, β, γ	angles of the unit cell [°]
δ	chemical shift [ppm]
ε	extinction coefficient
J	coupling constant [Hz]
λ	wavelength
$\tilde{\upsilon}$	wavenumber
m/z	mass-to-charge ratio
d	doublet (NMR spectroscopy)
s	singlet (NMR spectroscopy), strong (IR spectroscopy)
t	triplet (NMR spectroscopy)
m	multiplet (NMR spectroscopy), medium (IR spectroscopy)
b	broad (NMR spectroscopy)
w	weak (IR spectroscopy)
ν	stretching vibration (Raman spectroscopy)

1. Introduction

The chemistry of carbon dioxide at metal centres, for example the coordination of CO_2, its activation and conversion into organic compounds, is a rapidly increasing domain of coordination chemistry, organometallic chemistry and catalysis. The fundamental challenge and motivation of this chemistry are based on the discrepancy between the highly advanced apparatus employed by nature to convert CO_2 into organic matter and the difficulties encountered by chemistry in converting this molecule via effective catalytic reactions into high quality products. In nature CO_2 is selectively transformed under mild conditions employing highly organised enzymatic systems in which metal centres are instrumental.[1]

1.1 CO$_2$ fixation in nature

The motivation of CO_2 chemistry, inspired by nature is not only to understand the fundamental processes of nature and to mimic them in artificial systems but also to look for key steps useful in chemical synthesis.
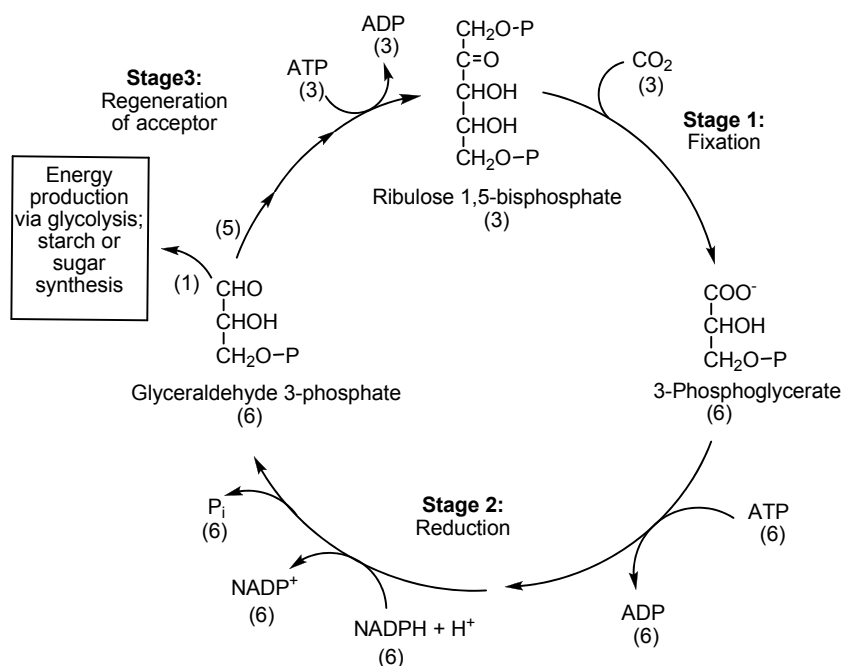
Figure 1.1 Calvin cycle

Carbamate complexes of the elements zinc and magnesium were identified at the active site of phosphotriesterase and rubisco enzymes.[2] The *rubisco (Ribulose-1,5-bisphosphate carboxylase oxygenase)* enzyme is probably the most abundant enzyme of the biosphere. The fixation of CO_2 and its transfer to organic substrates in the Calvin cycle[3,4,5] (**Figure 1.1**) leads by way of starch to an annual production of 10^{11} tons of biomass.

Green plants contain in their chloroplasts unique enzymatic machinery that catalyzes the conversion of CO_2 to simple (reduced) organic compounds, a process called *CO_2 assimilation*. This process has also been called *CO_2 fixation*. Carbon dioxide is assimilated via a cyclic pathway, its key intermediates constantly regenerated. The pathway was elucidated in the early 1950s by Melvin Calvin, Andrew Benson and James A. Bassham, and is often called the *Calvin cycle* or, more descriptively, the *photosynthetic carbon reduction cycle*.[3] Carbon dioxide assimilation occurs in three stages.

The first stage (**Figure 1.2**) in the assimilation of CO_2 into biomolecules is the carbon-fixation reaction.
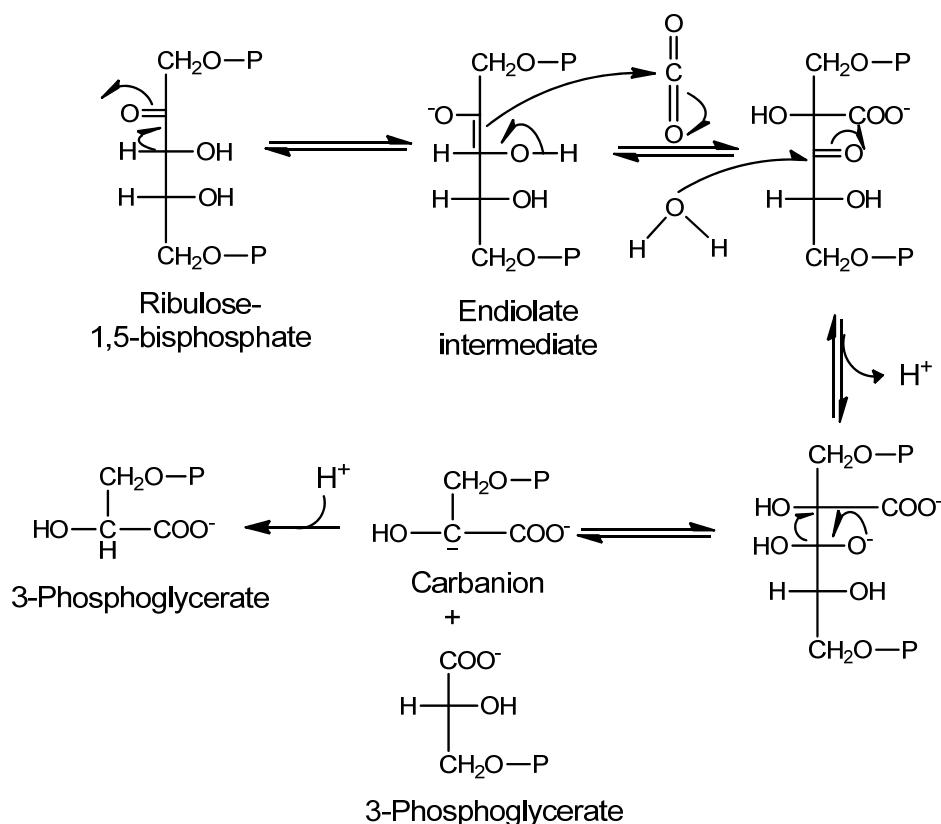
Figure 1.2 The first stage of the Calvin cycle

The enzyme that catalyzes incorporation of CO_2 into organic form is *ribulose-1,5 bisphosphate carboxylase oxygenase.* As a carboxylaze, rubisco catalyzes the covalent attachment of CO_2 to the five-carbon sugar ribulose 1,5-bisphosphate and cleavage of the unstable six-carbon intermediate to form two molecules of 3-phosphoglycerate, one of which bears the carbon introduced as CO_2 in its carboxyl group.

The active site of rubisco (**Figure 1.3**) consists of an octahedrally coordinated Mg atom with six oxygen atoms: one oxygen in the carbamate on Lys[201]; two in the carboxyl group of Glu[204] and Asp[203]; two at C-2 and C-3 of the substrate ribulose 1,5-bisphosphate. One of the ligands is a presumably μ_1,η^1-coordinated carbamate.[6]
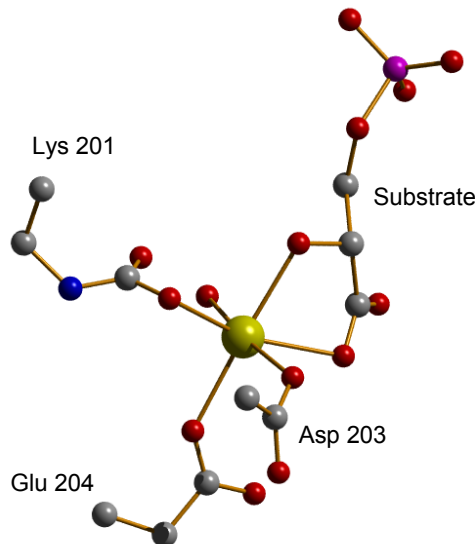
Figure 1.3 Rubisco active site; yellow Mg, red O, blue N, violet P, grey C

In the second stage of the Calvin cycle the conversion of 3-phosphoglycerate to glyceraldehyde 3-phosphate occurs in two steps. In the first step the 3-phosphoglycerate kinase catalyzes the transfer of a phosphoryl group from ATP to 3-phosphoglycerate, yielding 1,3-bisphosphoglycerate. Next, NADPH donates electrons in a reduction catalyzed by the chloroplast-specific isozyme of glyceraldehyde 3-phosphate dehydrogenase, producing glyceraldehyde 3-phosphate. Triose phosphate isomerase then interconverts glyceraldehyde 3-phosphate and dihydroxyacetone phosphate.

The third stage is regeneration of ribulose 1,5-bisphosphate from triose phosphate. This is accomplished in a series of reactions that, together with stages one and two, constitute the cyclic pathway shown in **Figure 1.1**. The product of the first assimilation reaction (3-phosphoglycerate) thus undergoes transformations that regenerate ribulose 1,5-bisphosphate. Every year photoautotrophic organisms assimilate circa 275 billions tones of CO_2 and release circa 200 billions tones O_2 in atmosphere.[7]

The possibility of using CO_2 as the starting material for the synthesis of fine chemicals provides an attractive alternative to compounds presently derived from petroleum[8] and efforts to convert CO_2 to useful chemicals will inevitably center on transition metal catalysts.[9,10,11] Furthermore, efforts are made to enhance the yield of hydrogen in water gas shift reactions and also to focus on carbon dioxide interactions with transition metal catalysts.[12] For all these reasons, a broader understanding of the coordination chemistry of CO_2 is being investigated by researchers around the world.[13,14] Also, studies of the stoichiometric reactions of CO_2 with active metal complexes can provide useful synthetic routes to a variety of organic compounds and have formed the basis for some new catalytic procedures.[15,16]

1.2 Formation of carbamato complexes by CO_2 fixation

Carbamato complexes of main groups and transition metals can be synthesised by following methods:

Reaction of CO_2 with secondary amines in the presence of metal halides:

$$2n\ R_2NH\ +\ n\ CO_2\ +\ MX_n \longrightarrow (R_2N\text{-}COO)_nM\ +\ n\ [R_2NH_2]^+ +\ n\ X^- \quad (A)$$

Insertion of CO_2 into metal amide bonds:

$$(R_2N)_nM\ +\ n\ CO_2 \longrightarrow (R_2N\text{-}COO)_nM \quad (B)$$
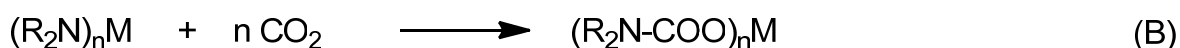
Oxidative coupling of CO_2 with Schiff bases:

$$R\text{-}CH=N\text{-}R\ +\ CO_2\ +\ NiL_2 \longrightarrow R\text{-}\underline{CH\text{-}N\text{-}(R)\text{-}COO\text{-}Ni}\ +\ 2\ L \quad (C)$$

8

Calderazzo's pioneering work resulted in a wide variety of homoleptic carbamato complexes prepared according to reaction **A**.[17,18] Many of these compounds have been structurally elucidated by X-ray analysis.[19,20]

Organometallic carbamato complexes especially of zinc and aluminium have been synthesised analogous to reaction **B**.[21,22] In addition insertion reactions in complexes stabilised by additional ligands have also been reported.

Reaction **C** is limited to Ni(0) resulting in the formation of cyclic carbamato complexes possessing an additional Ni–C bond.[23,24,25]

Synthesis, studies of bonding and structures of carbamate complexes[26,27] have been well developed in recent years as well the synthesis and characterization of metal complexes because of their perceived relationships to intermediates in the catalytic activation of carbon dioxide.

Particularly in the past decade, many carbamate complexes have been identified. Various coordination modes of the carbamato ligands have been reported[17,18] indicating that they might display a rich coordination chemistry.
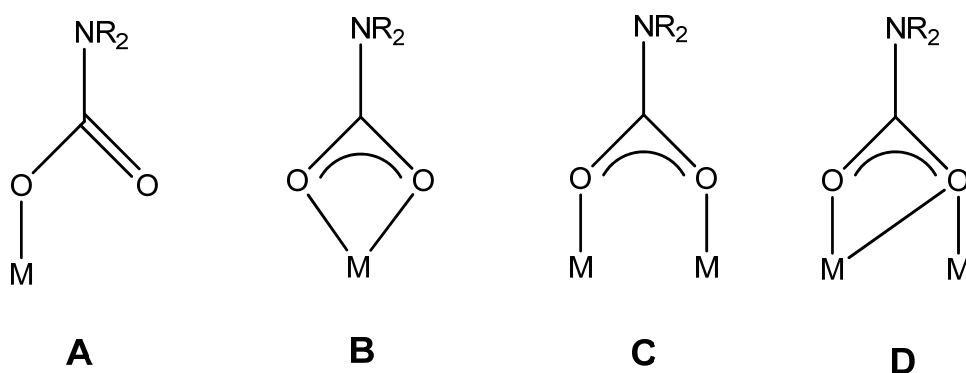
A η^1, μ_1; **B** η^2, μ_1; **C** η^1: η^1, μ_2; **D** η^2: η^1, μ_2

Figure 1.4a Coordination mode in carbamato complexes

E η^3, μ_3; **F** η^4, μ_3; **G** η^4, μ_4
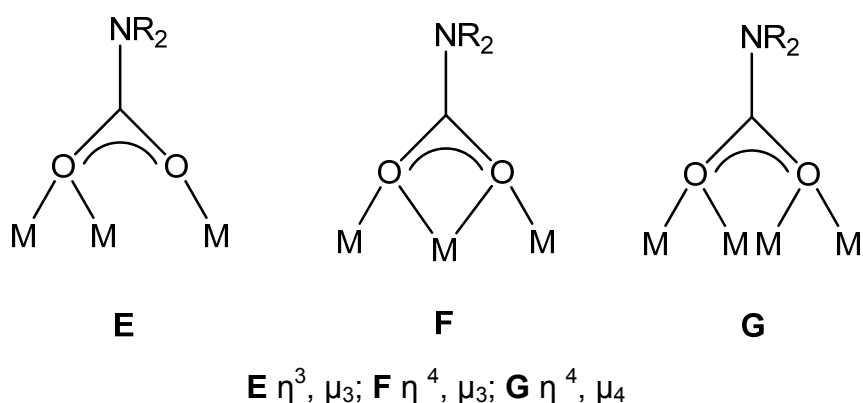
Figure 1.4b Coordination mode in carbamato complexes

In **Figure 1.4a** and **Figure 1.4b** are shown the most important coordination modes present in the carbamate complexes. However their chemistry is still in their infancy considering the small number of structurally well characterised complexes and the lack of systematic investigations to prove the reactivity of the carbamato groups.

1.3 Dialkylcarbamato metal complexes

Among alkali- and earth-alkali metal cations, lithium and magnesium carbamato complexes have been studied to some extent. The diethylcarbamato derivatives of formula $M(O_2CNEt_2)$, M = Li, Na, K, have been prepared[28,29] by treating a suspension of the alkali metal in toluene at about 50°C with the appropriate amine, in the presence of CO_2. The products were found to be insoluble in ethers or in hydrocarbons and soluble in the presence of an excess of amine or in polar solvents such as methanol or dimethylformamide. Similar results were obtained[30,31] when the reaction between the alkali metal and diethylamine or primary amines was carried out in THF as medium at room temperature followed by reflux.

Scheme 1.1 refers to dialkylcarbamates of magnesium(II) being obtained by carbonation of the appropriate bis-amido derivative, either prepared in situ from MgR_2/NHR_2 [32] or preformed.[33] The additional neutral ligand eventually found in the composition of the final product originates from the solvent used for the reaction.

$$Mg(NR_2)_2 + 2\,CO_2 \xrightarrow{\;m/n\;L\;} 1/n\,[Mg_n(O_2CNR_2)_{2n}L_m]$$
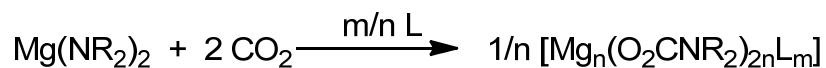
R	L	n	m
Me	THF	3	2
Me	HMPA	3	2
Et	-	6	0
Ph	-	6	0

Scheme 1.1 Preparation of dialkylcarbamates of magnesium(II)

Alternatively, the diethylcarbamato complex of magnesium can be prepared[34] via the $MgBr_2/CO_2/NHEt_2$ route.

The compounds $Mg_6(O_2CNEt_2)_{12}$, $Mg_6(O_2CNPh_2)_{12}$, and $Mg_3(O_2CNMe_2)_6$ $(HMPA)_2$ were studied by X-ray diffraction methods. Of particular interest is the hexanuclear compound of magnesium $Mg_6(O_2CNEt_2)_{12}$ (**Figure 1.5**) which has been structurally studied by two different research groups.[32,33]
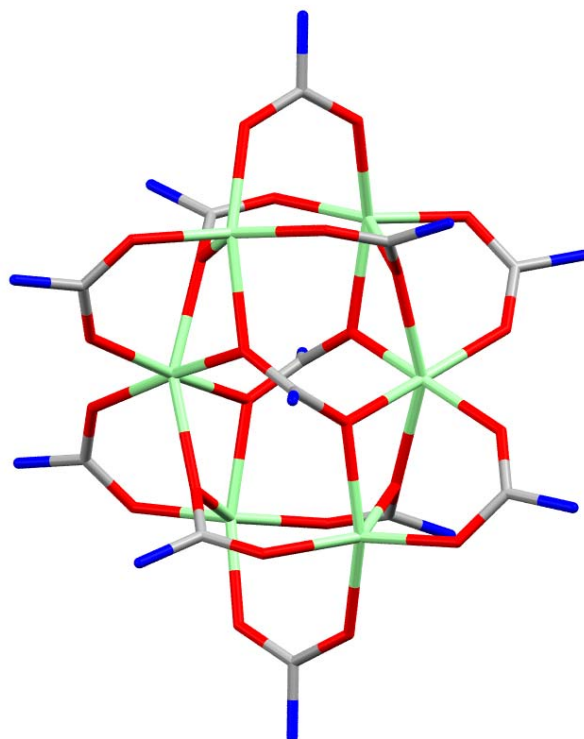
Figure 1.5 Schematic molecular structure of $Mg_6(O_2CNEt_2)_{12}$

light-green Mg, blue N, red O, grey C, alkyl groups not shown

Carbamato complexes of group 13, the aluminum(III) derivatives, as prepared from Al_2Br_6, CO_2 and the appropriate amine, have been described (**Scheme 1.2**). Aluminum bromide, which is well soluble in the reaction medium (toluene), is more advantageously used than the corresponding chloride.

$$Al_2Br_6 + 12\ iPr_2NH\ +\ 6\ CO_2\ \xrightarrow{\text{toluene}}\ Al_2(O_2CN(iPr)_2)_6 + 6\ [iPr_2NH_2]Br$$
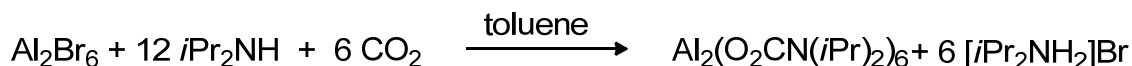
Scheme 1.2 Preparation of $Al_2(O_2CN(iPr)_2)_6$

In $Al_2(O_2CN(iPr)_2)_6$ (**Figure 1.6**) each of the two hexacoordinated aluminum atoms is surrounded by four oxygen atoms of two terminal bidentate- and by two oxygens of two bridging groups.[35] The *iso*-propyl derivative maintains its nuclearity in benzene and is fluxional, as suggested by the NMR data. The ^1H NMR spectrum showed one type only of *iso*-propyl groups at room temperature, suggesting fast exchange between terminal and bridging positions. By lowering the temperature to -55°C, two carbamato ^{13}C resonances appear at 165.4 and 156.8 ppm, and two types of quaternary C atoms at 46.8 and 43.8 ppm, while the methyl groups give a single resonance at 20.6 ppm, even at low temperature, suggesting that they are averaged out.

Figure 1.6 Schematic molecular structure of $Al_2(O_2CN(iPr)_2)_6$
orange Al, blue N, red O, grey C, alkyl groups not shown

     N,N-dialkylcarbamato derivatives of silicon(IV) have been prepared from $SiCl_4$ and the appropriate secondary amine[35, 36] in toluene. The **Scheme 1.3** presents the synthetic route to obtain these carbamates.

$$SiCl_4 \ + \ 8 \ R_2NH \ + \ 4 \ CO_2 \ \xrightarrow{\text{toluene}} \ Si(O_2CNR_2)_4 \ + \ 4 \ [R_2NH_2]Cl$$

$$R = Me, \ Et, \ i\text{Pr}$$
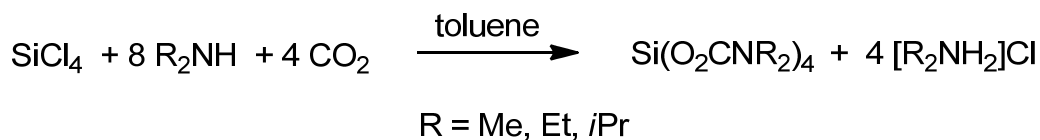
Scheme 1.3 Preparation of dialkylcarbamates of silicon(IV)

X-ray diffractometry has shown the *iso*-propyl (**Figure 1.7**) and the ethyl derivatives to be both mononuclear with four monodentate carbamato groups. The IR absorption at about 1710 cm^{-1}, one of the highest values so far observed for the entire family of compounds, was readily assigned to the C=O stretching vibration of the monodentate ligands.
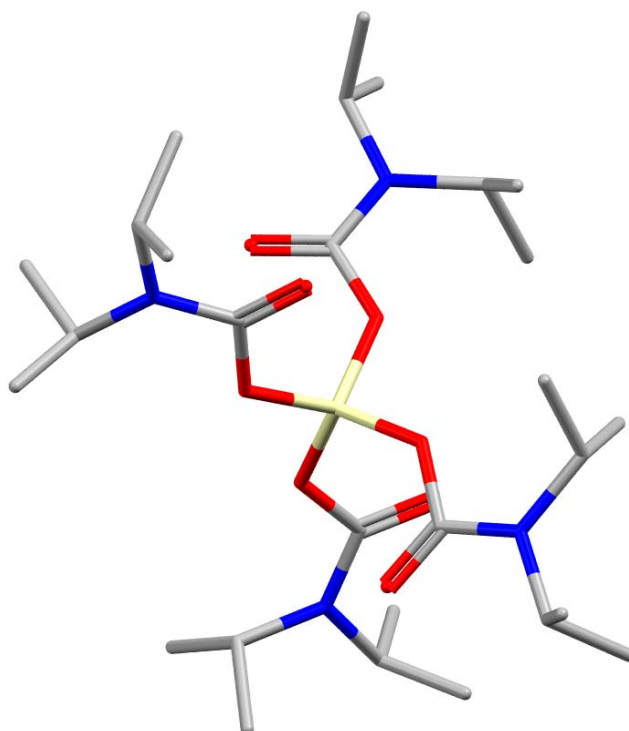
Figure 1.7 Schematic molecular structure of $Si(O_2CN(i\text{Pr}_2)_4$

light-yellow Si, blue N, red O, grey C

The homoleptic derivatives of antimony(III) $Sb(O_2CNR_2)_3$ (R = Me, Et, *i*Pr) have been prepared[37] by carbonation of the dimethylamido derivative, or by the $SbCl_3/NHR_2$ reaction to give the amido intermediate, followed by its carbonation in situ (**Scheme 1.4**).

$$Sb(NMe_2)_3 \quad + \quad 3\,CO_2 \quad \longrightarrow \quad Sb(O_2CNMe_2)_3$$

$$SbCl_3 + 6\,NHR_2 \; + \; 3\,CO_2 \quad \longrightarrow \quad Sb(O_2CNR_2)_3 \quad + \; 3\,[NH_2R_2]Cl$$

$$R = Me,\; Et,\; \textit{i}Pr$$
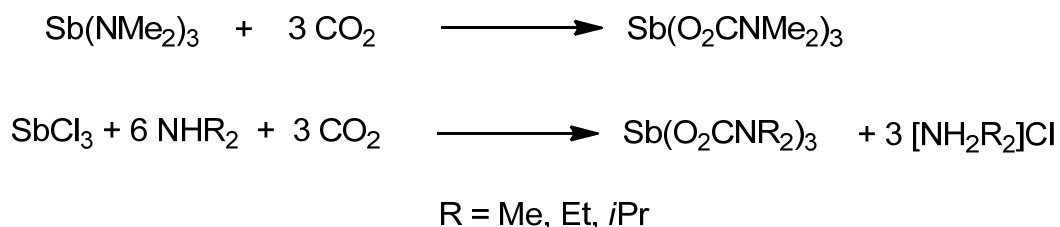
Scheme 1.4 Preparation of dialkylcarbamates of antimony(III)

The X-ray structural investigation of the three compounds has been previously reported and the structure of $Sb(O_2CNEt_2)_3$ is visualised in **Figure 1.8**.
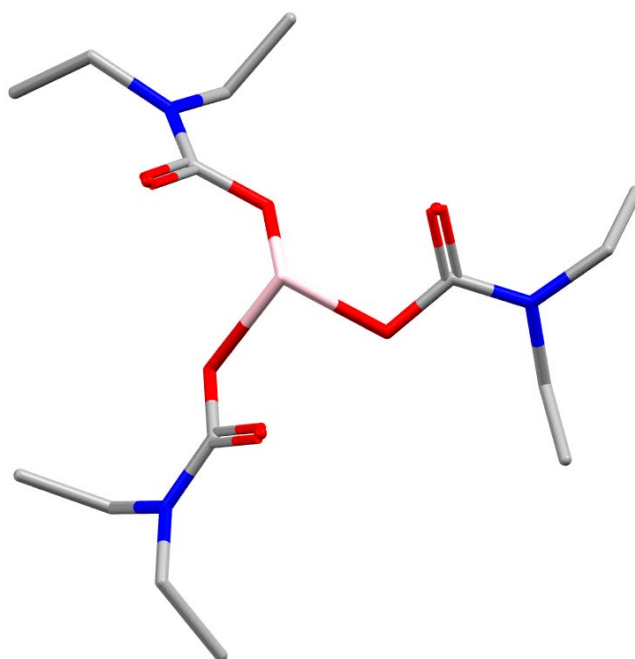
Figure 1.8 Schematic molecular structure of $Sb(O_2CNEt_2)_3$
pink Sb, blue N, red O, grey C

The ethyl derivative of manganese(II) of formula $Mn_6(O_2CNEt_2)_{12}$ was prepared[38,39] by two different methods, starting either from bis(cyclopentadienyl) manganese(II) $(MnCp_2)$[40] or from the anhydrous chloride (**Scheme 1.5**). The molecular structure consists of four five-coordinated manganese atoms in approximately trigonal bipyramidal coordination, the remaining two manganese atoms displaying a distorted octahedral geometry. The manganese(II) derivative is isostructural with the corresponding cobalt(II) compound.[41]

$$6\ MnCp_2\ +\ 12\ CO_2\ +\ 12\ NHEt_2\ \longrightarrow\ Mn_6(O_2CNEt_2)_{12}\ +\ 12\ CpH$$

$$6\ MnCl_2\ +\ 12\ CO_2\ +\ 24\ NHEt_2\ \longrightarrow\ Mn_6(O_2CNEt_2)_{12}\ +\ 12\ [NH_2Et_2]Cl$$
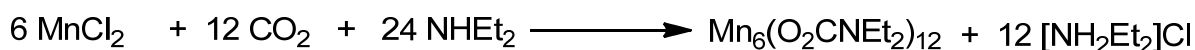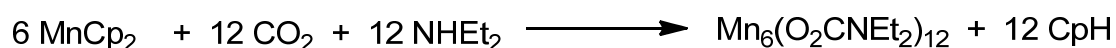
Scheme 1.5 Preparation of $Mn_6(O_2CNEt_2)_{12}$

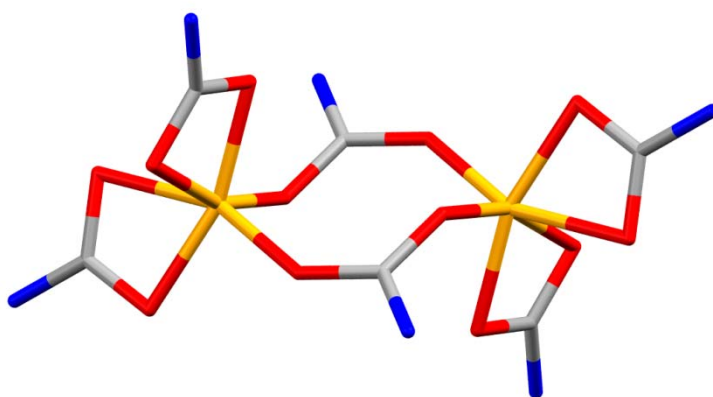The schematic molecular structure of $Mn_6(O_2CNEt_2)_{12}$ is presented in **Figure 1.9**.
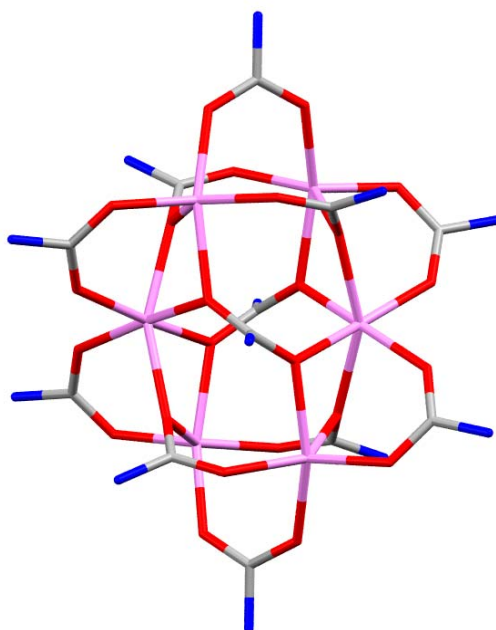
Figure 1.9 Schematic molecular structure of $Mn_6(O_2CNEt_2)_{12}$

violet Mn, blue N, red O, grey C, alkyl groups not shown

The hexanuclear cobalt derivatives[41] $Co_6(O_2CNR_2)_{12}$ (R = Et, *i*Pr) were prepared by reacting anhydrous cobalt(II) chloride with the appropriate amine under carbon dioxide at atmospheric pressure in toluene (**Scheme 1.6**).

$$6\ CoCl_2\ +\ 12\ CO_2\ +\ 24\ NHR_2\ \xrightarrow{\text{toluene}}\ Co_6(O_2CNR_2)_{12}\ +\ 12\ [NH_2R_2]Cl$$

$$R = Et,\ i\text{Pr}$$
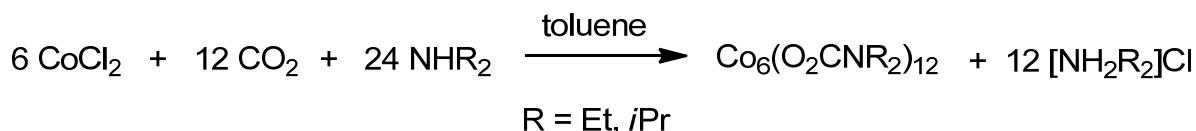
Scheme 1.6 Preparation of dialkylcarbamates of cobalt(II)

The following crystallographic data were obtained for $Co_6(O_2CNEt_2)_{12}$ (**Figure 1.10**) crystalized from *iso*-octane upon refluxing and cooling, space group *C*2/*c*, monoclinic, *a* = 18.428, *b* = 19.189, *c* = 24.654 Å, *β* = 95.90°, *U* = 8672 Å^3, *T* = 298 K. These data are to be compared with those obtained later for the same compound recrystallized under different conditions from acetonitril, space group *Ccca*, orthorhombic, *a* = 20.712, *b* = 25.040, *c* = 16.498 Å, *U* = 8557 Å^3, *T* = 298 K. This sets an example of systems for which the different recrystallization conditions may produce a different crystal packing.
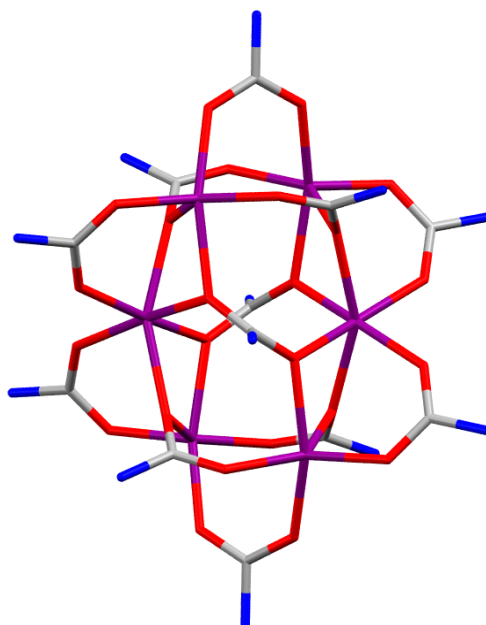
Figure 1.10 Schematic molecular structure of $Co_6(O_2CNEt_2)_{12}$

purple Co, blue N, red O, grey C, alkyl groups not shown

A number of zinc carbamate complexes have been synthesized in the past decades.[42] In these complexes the carbamate ligands usually bridge two Zn atoms (η^2, η_2-bonding mode). One possible access to these species is reaction of an alkyl zinc amide with CO_2 (**Scheme 1.7a**) and representative examples for products of this route include $[ZnMe(O_2CNR_2)]_4$ (R = Et, *i*Bu and *i*Pr[43]) and $[Zn_4Me_2(O_2CNR_2)_6]$.[44]

$$4\ MeZnNR_2\ +\ 4\ CO_2\ \longrightarrow\ [ZnMe(O_2CNR_2)]_4$$
$$R = Et, iPr, iBu$$
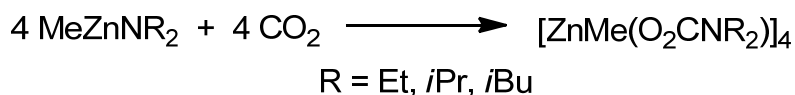
Scheme 1.7a Preparation of dialkylcarbamates of zinc

Other complexes of the general formula $[ZnMe(O_2CNR_2)]_4$ (R = *i*Pr and *i*Bu) were synthesized directly from $ZnMe_2$, the corresponding secondary amine and CO_2 (**Scheme 1.7b**).[45]

$$4\ ZnMe_2 + 4\ NHR_2\ + 4\ CO_2\ \longrightarrow\ [ZnMe(O_2CNR_2)]_4 + 4\ MeH$$
$$R = iPr, iBu$$
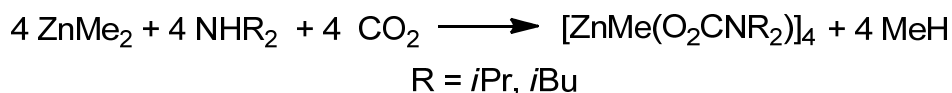
Scheme 1.7b Preparation of dialkylcarbamates of zinc

From these examples it can already be concluded that slight modifications could lead to different products indicating that the carbamato ligands could easily be replaced by other ligands and that the complex sizes could vary.
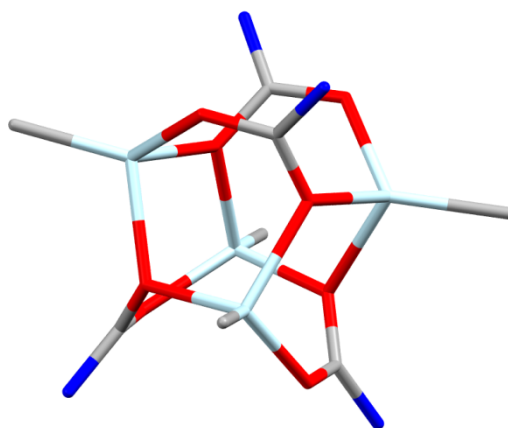
Figure 1.11 Schematic molecular structure of $[ZnMe(O_2CNR_2)]_4$
light-blue Zn, blue N, red O, grey C, alkyl groups not shown

Interestingly, these complexes (**Figure 1.11**) can be split into smaller units by introduction of a base which binds to the Zn atoms. Thus reaction between $[ZnMe(O_2CNR_2)]_4$ and pyridine leads to the dinuclear complex $[(py)ZnMe(O_2CNR_2)]_2$[43]. Treatment of the zinc carbamate $[Zn_4Me_2(O_2CNEt_2)_6]$ with TMEDA results in formation of the mononuclear bis-carbamate complex $[(Et_2NCO_2)_2Zn(TMEDA)]$.[45] (**Figure 1.12**)
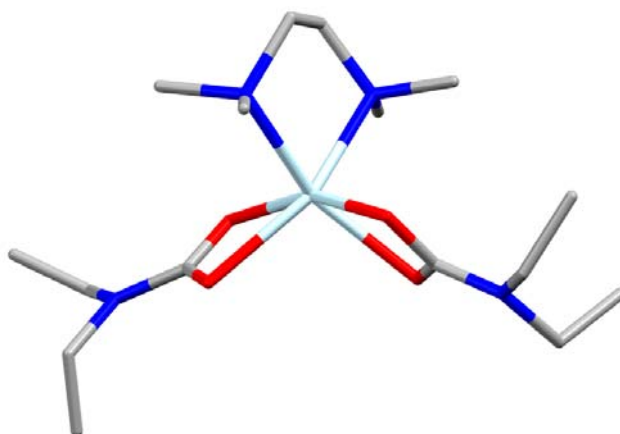
Figure 1.12 Schematic molecular structure of $[(Et_2NCO_2)_2Zn(TMEDA)]$
light-blue Zn, blue N, red O, grey C

In this rare example of a structurally characterized mononuclear bis-carbamate complex of zinc the carbamate ligands adopt a η^2-coordination mode. In the absence of further coordinating ligands, $[Zn(O_2CNR_2]_2$ is a solid sparingly soluble in common organic solvents, for which spectroscopic data (mainly IR) and elemental analysis, but no structural analysis has yet been reported.[46] The physical and chemical properties suggest an extended structure, presumably with bridging η^2, μ_2-coordinated carbamate units.

The η^1, μ_1-coordination mode is very rare, being restricted to not much more than the dinuclear anionic complex $[Zn_2(O_2CNMe_2)_5]^-$ (**Figure 1.13**) which features one terminal η^1-coordinated carbamate group per Zn and three bridging carbamate units.[47]

18
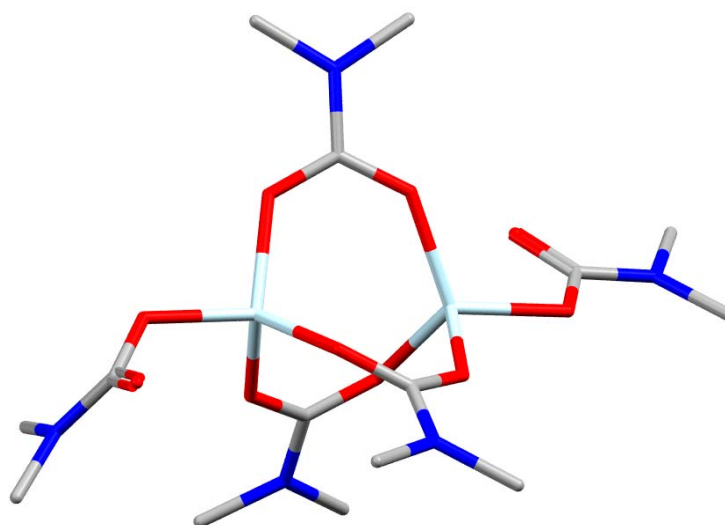
Figure 1.13 Schematic molecular structure of $[Zn_2(O_2CNMe_2)_5]^-$
light-blue Zn, blue N, red O, grey C

Structurally characterized mononuclear Zn complexes with η^1-coordinated carbamates were so far unknown.[48]

Complexes of the formula $[Zn_4O(O_2CR)_6]$ (R = N-diethylamido, N-piperidyl, and N-pyrrolidyl) are also accessible using standard Schlenk techniques, for example by addition of H_2O to a mixture of dialkyl zinc and the secondary amine (in a two-fold excess) into which CO_2 had been introduced.[49,50]

A new series of (diisopropylcarbamato)(oxido)zinc complexes were obtained by innovative synthetic approaches. The carbamato zinc clusters $[Zn_4(\mu_4\text{-}O)(O_2CN(iPr)_2)_6]$ and $[Zn_8(\mu_4\text{-}O)_2(O_2CN(iPr)_2)_{12}]$ were synthesised by an identical reaction procedure involving reaction of $ZnEt_2$ with iPr_2NH/CO_2 followed by stoichiometric hydrolysis. Recrystallisation of the reaction product from nitrile solvents yielded the tetrazinc complex (**Figure 1.14** left side). Conversely, recrystallisation from alkane solvents yielded crystals of the octazinc complex (**Figure 1.14** right side).[51]
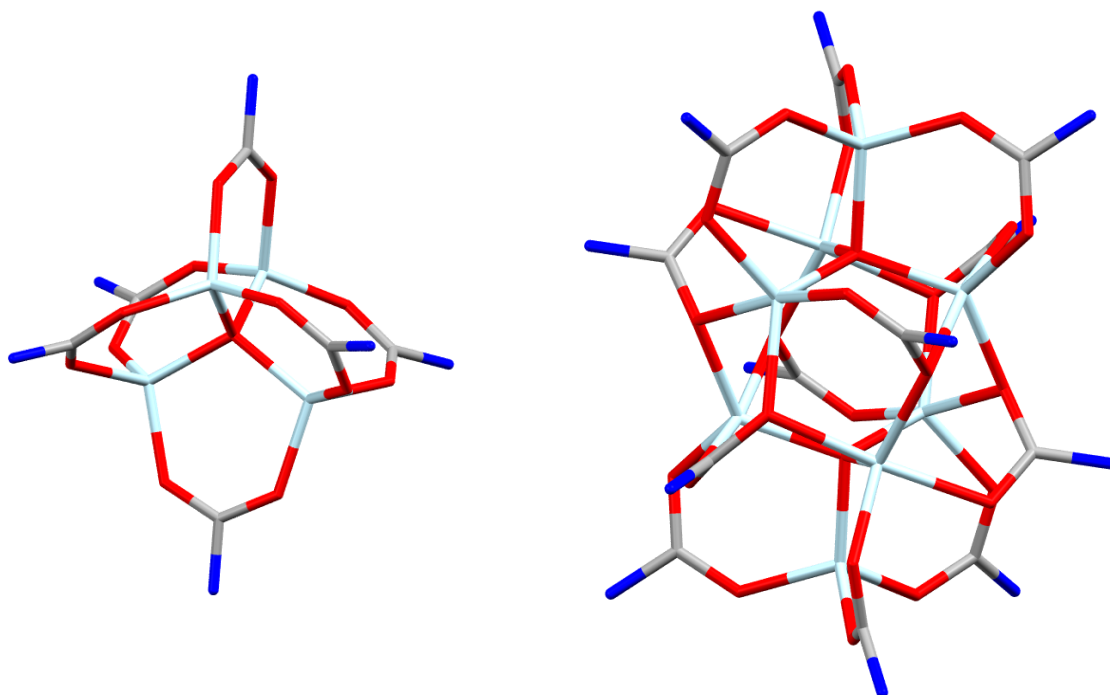
Figure 1.14 Schematic molecular structure of
[Zn$_4$(μ_4-O)(O$_2$CN(iPr)$_2$)$_6$] (left side) and [Zn$_8$(μ_4-O)$_2$(O$_2$CN(iPr)$_2$)$_{12}$] (right side);
light-blue Zn, blue N, red O, grey C, alkyl groups not shown

The tetrazinc complex easily dimerised to give the octazinc complex as the respective solvate simply by recrystallisation from heptane. Likewise the octazinc complex reverted to its monomeric form when recrystallised from acetonitrile. The combination of these steps is a reversible cycle.

Although this type of process has not yet been observed for molecules of the [M$_4$(μ_4-O)(O$_2$CNR$_2$)$_6$]$_x$ type, the fragmentation and recombination of metallocarbamates is not an entirely new concept. The solution dynamics of the hexanuclear complex [Co$_6$(O$_2$CNEt$_2$)$_{12}$] and its dinuclear dissociation isomer [Co$_2$(O$_2$CNEt$_2$)$_4$] were studied intensively using UV/Vis techniques, with the result that the lower nuclearity dinuclear species dominates in solution.[34] Despite this dominance, the existence of a facile isomerisation pathway allowed the deposition of the hexanuclear isomer as the sole solid product. This isomerisation pathway was reported to be necessary to the formation of mixed-metal [Co$_n$Mg$_{6-n}$(O$_2$CNEt$_2$)$_{12}$] complexes.

1.4 Heterobimetallic carbamato complexes

Heteronuclear diethylcarbamato complexes of the form $[Co_nMg_{6-n}(Et_2NCO_2)_{12}]$ (**Figure 1.15**) were prepared from the isostructural homonuclear precursors $Mg_6(Et_2NCO_2)_{12}$ and $Co_6(Et_2NCO_2)_{12}$ via a solvothermal methodology.
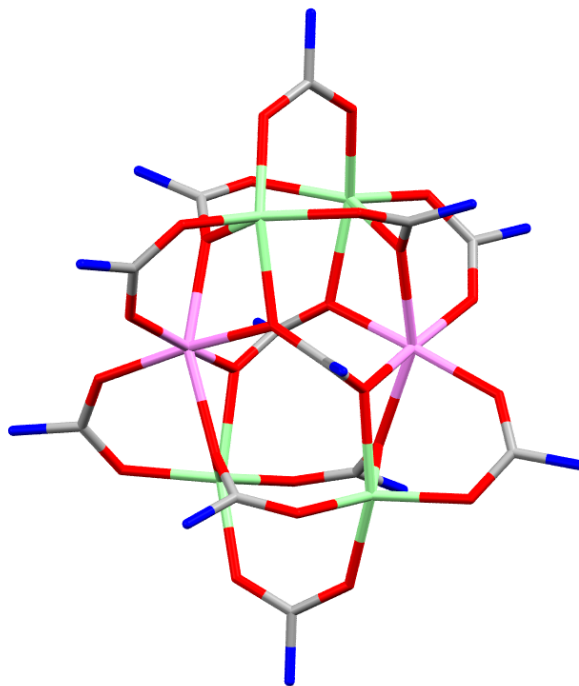
Figure 1.15 Schematic molecular structure of $[Co_nMg_{6-n}(Et_2NCO_2)_{12}]$ violet Co/Mg, light-green Mg, blue N, red O, grey C, alkyl groups not shown

The heteronuclear Co/Mg complexes were prepared by the reaction of $Co_6(Et_2NCO_2)_{12}$ with $Mg_6(Et_2NCO_2)_{12}$ in *n*-heptane. Two materials were selected for single-crystal X-ray diffraction analysis: $Co_{1.6}Mg_{4.4}(Et_2NCO_2)_{12}$ and $Co_{2.7}Mg_{3.3}(Et_2NCO_2)_{12}$.[34] The molecular structure is best described as two trinuclear M3 units cross-linked by diethylcarbamate ligands and twisted about one another so that the complex has overall D_2 symmetry and is chiral. Each trinuclear unit consists of two terminal pentacoordinate metal ions and one central hexacoordinate metal ion.

The reaction between $Mn_6(Et_2NCO_2)_{12}$ and $Mg_6(Et_2NCO_2)_{12}$ results in isolation of heteronuclear complexes $[Mn_nMg_{6-n}(Et_2NCO_2)_{12}]$. A series was prepared with different doping factors *n* by varying the Mn/Mg ratio in the crystallization solutions.[52]

In a different but related study, Calderazzo *et al.* reported on future works concerning metal redistribution phenomena for the entire Mn-to-Ni sequence of $[M_8(\mu_4\text{-}O)_2(O_2CN(iPr)_2)_{12}]$ complexes.[53] In the presence of moisture, the mixed octanuclear carbamates $[Co_xMn_{6-x}(MnO)(CoO)(O_2CNEt_2)_{12}]$ were promptly formed and detected by DCI/MS measurements. Bacchi *et al.* reported on the formation of $[Zn_2Ni_6(\mu_4\text{-}O)_2(O_2CN(iPr)_2)_{12}]$[54] (**Figure 1.16**) as a side product in 3% yield when $[Ni(MeCN)_6][ZnCl_4]$ was exposed to $iPr_2NH\text{--}CO_2$. Within the octameric core, there were tetrahedral and trigonal bypyramidal sites for metal coordination, with the zinc atoms showing a preference for residence in the tetrahedral sites.
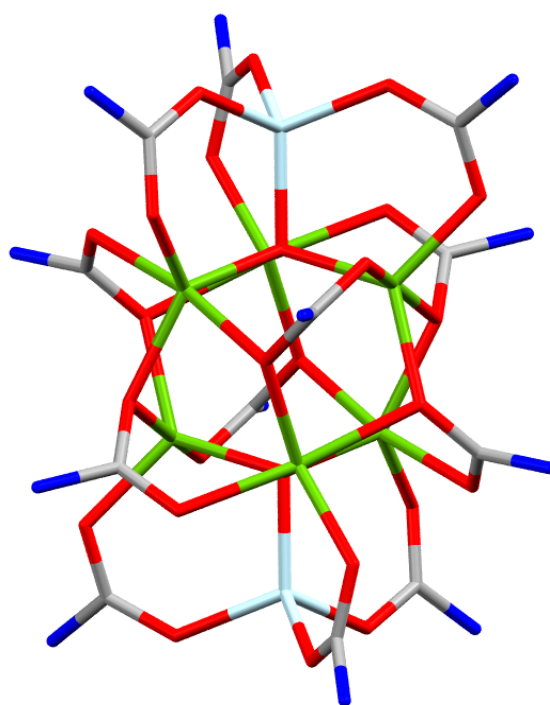
Figure 1.16 Schematic molecular structure of $[Zn_2Ni_6(\mu_4\text{-}O)_2(O_2CN(iPr)_2)_{12}]$
green Ni, light-blue Zn, blue N, red O, grey C, alkyl groups not shown

Heterobimetallic carbamato complexes are attractive from a metal oxide film growth perspective. The homonuclear complex $[Mg_6(O_2CNEt_2)_{12}]$ is already a proven precursor for MgO thin-film growth,[55] and when mixed with the (μ-oxido)zinc analogue $[Zn_4(\mu_4\text{-}O)(O_2CNEt_2)_6]$ has been used to deposit dimetallic $Zn_xMg_{1-x}O$ films of high quality and reproducibility.[56]

The first mixed-metal Zn–Mg carbamates have been synthesised using a novel strategy of coreaction between zinc and magnesium alkylamido intermediates. The complexes were structurally characterised by single-crystal X-ray diffraction; the nuclearity of these carbamato core subunits was found to vary from tetrameric to octameric with respect to the level of magnesium incorporated. The presence of magnesium in the predominantly zinc carbamato lattice was confirmed by refinement of the site occupancies of the metal atoms during the crystal data analysis, and it was found that displacement of up to 7.8% of zinc sites by magnesium atoms could be achieved before breakdown of the structure (**Scheme 1.9**).

n $MgBu_2$ + iPr_2NH $\qquad\qquad\qquad\qquad$ (8-n) $ZnEt_2$ + 2(8-n) iPr_2NH

hexane, reflux 24h $\qquad\qquad\qquad\qquad$ benzene, reflux 3h

n [BuMgNiPr_2] + (8-n) (EtZnNiPr_2) + (8-n) (iPr_2NH)

CO_2

$[Zn_{8-n}Mg_n(O_2CNiPr_2)_2]_x$ $\qquad$ n= 1- 4

1/8 H_2O, THF

$[Zn_{8-n}Mg_nO_2(O_2CNiPr_2)_2]_{12}$
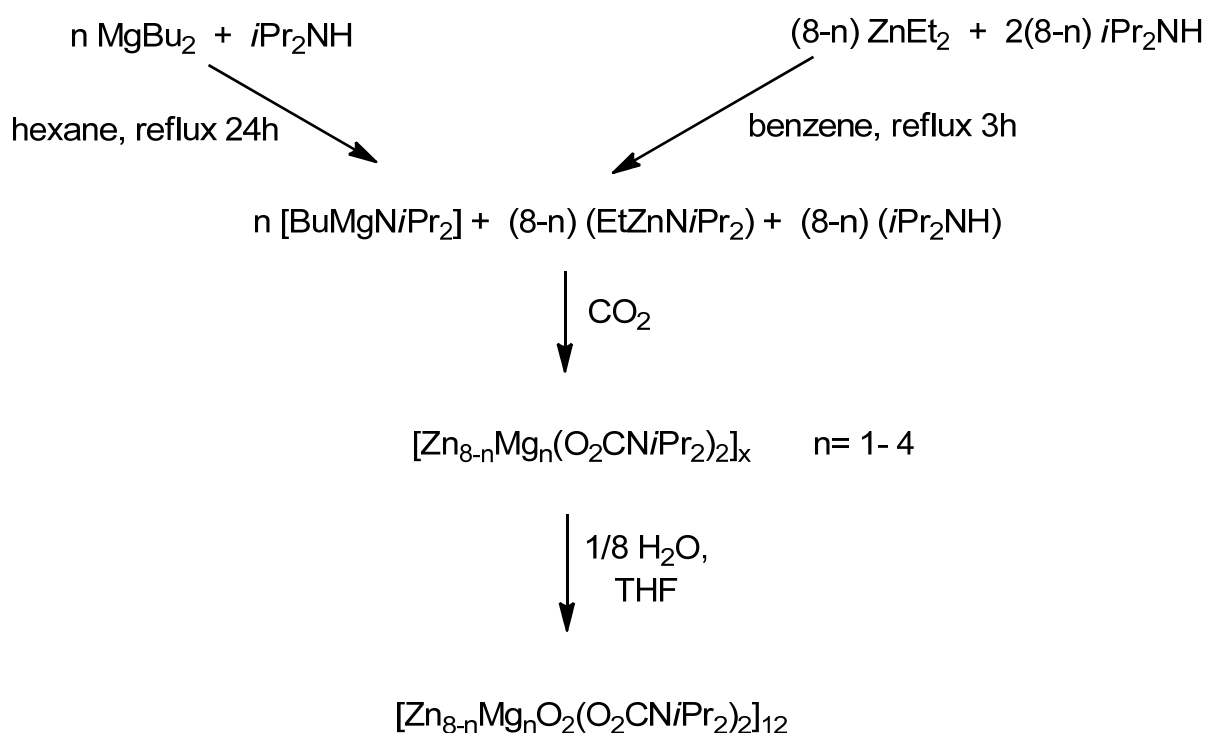
Scheme 1.9 Proposed reaction pathway for Zn-Mg carbamato complexes

Characterisation of the complexes physicochemical properties revealed that they were suitable for use as single-source chemical vapour deposition (SSCVD) precursors in the deposition of $Zn_xMg_{1-x}O$ thin films, an emerging material with promising band-gap engineering prospects.[57]

1.5 Semiconducting metal oxides and bimetallic oxides

ZnO nanoparticles are of interest for a variety of applications. Hence ZnO is a wide band gap seminconductor (3.37 eV at room temperature). The emission spectra of ZnO nanoparticles were intensively studied,[58-60] displaying luminescent properties in the near ultraviolet and visible regions. The possible application of ZnO in dye-sensitized solar cells[61] in replacement for the currently favoured TiO_2 is unfortunately still hampered by its instability in acidic dye solutions[62,63] leading to Zn(II)/dye complexes or agglomerates. However, ZnO nano-crystallites have recently been shown to exhibit high conversion efficiency,[64] and coating of the ZnO particles resulting in core-shell structures can improve their stability. Hence despite of the instability compared with TiO_2 which is also due to the relatively small Zn-O bond energy in ZnO in comparison to the Ti-O bond energies in TiO_2, research with ZnO nanoparticles is continuing in this field. Especially TiO_2-coated ZnO nanowire arrays seem to be highly efficient. One of the various possible ways to obtain ZnO nanoparticles is the use of organo metallic precursors. Studied precursors include dialkyl zinc compounds like $ZnCy_2$ (Cy = cyclohexyl) or $ZnEt_2$,[65-69] tetranuclear alkoxyde clusters of the general formula $[RZnOR']_4$ (R, R' = alkyl, e.g. R = Me and R' = *i*Pr or *t*Bu),[70-75] salts of cationic clusters like $[Zn_4(LH)_4]^{4+}$ (with LH_2 = dipyridyldiol).[76-79] $Zn_xMg_{1-x}O$ thin films were recently fabricated using mixed-metal Zn-Mg carbamates.[56,57]

Nanoparticles,[80,81] in particular those of semiconducting metal oxides like ZnO, have received increasing attention because of their high potential as components in nanotechnological devices. In general, materials containing more than one type of metal should display higher complexity and a wider range of properties.[82] So far only little attention has been paid to bi- or multimetallic oxide nanostructures, although a diverse spectrum of properties can be envisioned for such oxides.[83] Multimetallic oxides have been known in solid-state chemistry for a long time, but the high processing temperatures typically applied make them less suitable for the preparation of nanoscaled materials.[84] In addition, optimum dispersity of the two metals inside the nanostructures would play a pivotal role for the rational synthesis and adjustment of properties of those systems.

Optimum dispersity is ensured when the respective elements are distributed on the molecular level.[85] In this respect, the use of molecular single-source precursors could potentially solve this problem by the creation of molecular building blocks suitable for bottom-up formation of oxides or other materials. Correlated to the molecular design of the precursor are low thermolysis temperatures resulting in reduced particle growth.[86] However, the preparation of a specific precursor resulting in a specific oxide is difficult,[87] especially if bi- or multimetallic oxide nanostructures are targeted.[88] Some examples for such single-source precursors exist already.[89-95] In most cases these heterometallic precursors are alkoxides and are thus very moisture sensitive.[96-98]

Alloy oxides containing transition metals with unpaired electrons are also of considerable interest, e.g. for the fabrication of magnetic and optoelectronic devices.[99-101] Hence oxides such as $Zn_{1-x}Co_xO$ (x usually being much smaller than 1) represent magnetic semiconductors and the control over x allows "band-gap and spin engineering".[102] Several methods (including solid-state reactions at high temperatures, hydrolysis of ionic salts in an aqueous solution or an organic polyol, then often in combination with various film-producing techniques such as sol-gel dip-coating or spray pyrolysis, or decomposition of organo metallic precursors in aqueous solutions) have been developed to get access to these mixed oxides. Still challenging but important for a number of applications is the synthesis of nanosized particles with diameters in the range of not more than several nm and narrow size distribution.

Recently Polarz and Driess *et al.* reported a method to synthesize heteronuclear tetranuclear alkoxyde clusters which can be decomposed thermally at relatively mild conditions (T ≥ 250°C) to give nanosized two-component magnetic oxides.[76] It was shown that the average diameter of the particles can be relatively easily controlled by the decomposition temperature. In the first instance mixtures of precursor clusters were obtained in which one, two or three Zn atoms of a tetranuclear Zn compound with heterocubane-type structure are replaced by Co, Ni or Mn atoms. These clusters had to be purified in a second step prior to decomposition to the alloy oxides.

1.6 Aim of the present research

The main purpose of this dissertation was to identify a new precursor system that enables access to a large variety of nanoscaled heterobimetallic oxides under mild conditions. One particular type of heterobimetallic oxide of current interest is metal oxide semiconductors (for instance ZnO) mixed with paramagnetic metal ions like Mn^{2+} and Co^{2+}.

The precursors were synthesized by reaction between the tetrameric carbamate $[ZnEt(O_2CN(iPr)_2)]_4$ and Co(II) or Mn(II) dichloride complexes, containing as ligands a nitrogen base.

2. Results and discussions

2.1 Synthesis, characterisation and thermal decomposition of some new tetrameric zinc carbamate complexes

Herein is reported on CO_2 fixation by insertion into the Zn-N bonds of the two molecular compounds $EtZnN(iPr)_2$ and $EtZnN(iBu)_2$. The tetrameric carbamate complexes $[ZnEt(O_2CNR_2)]_4$ (R = *i*Pr and *i*Bu) were found to be the products of these reactions (**Scheme 2.1**). The structures of the complexes were analysed by single crystal X-ray diffraction.

$$ZnEt_2 \ + \ HNR_2 \longrightarrow 1/n \ [EtZnNR_2]_n \ + \ EtH$$

$$R = iPr, \ iBu$$

$$1/n \ [EtZnNR_2]_n \ + \ n \ CO_2 \longrightarrow 1/m \ [ZnEt(O_2CNR_2)]_m$$
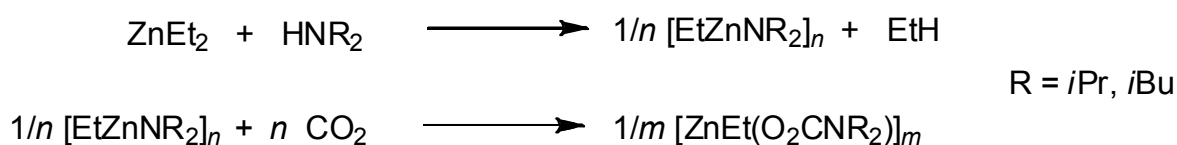
Scheme 2.1

A toluene solution containing equimolar quantities of diethyl zinc and the secondary amine $HN(iPr)_2$ was stirred for 3 h at 70°C. The ^1H NMR spectrum (**Figure 2.1**) recorded after this period turned out to be basically a superposition of the signals of the starting reagents $ZnEt_2$ and $HN(iPr)_2$.
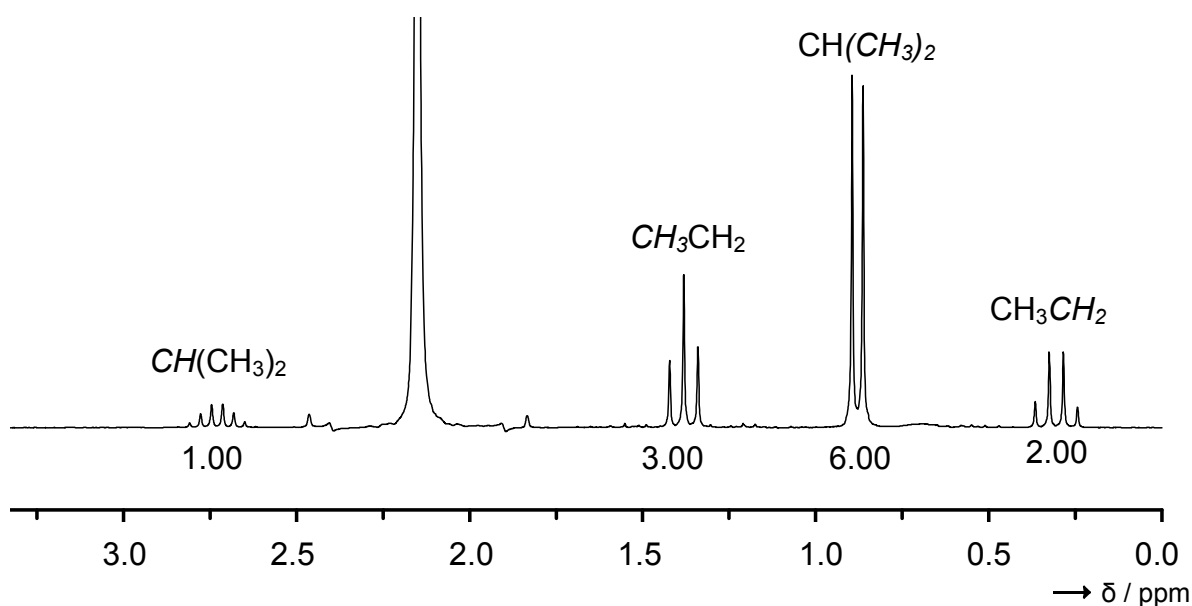
Figure 2.1 ^1H NMR spectrum (400 MHz, C_6D_6) of Et_2Zn and $HN(iPr)_2$ mixture

On the other hand, after stirring at room temperature for 3 days, the spectra (**Figure 2.2**) showed the quantitative formation of EtZnN(iPr)$_2$.
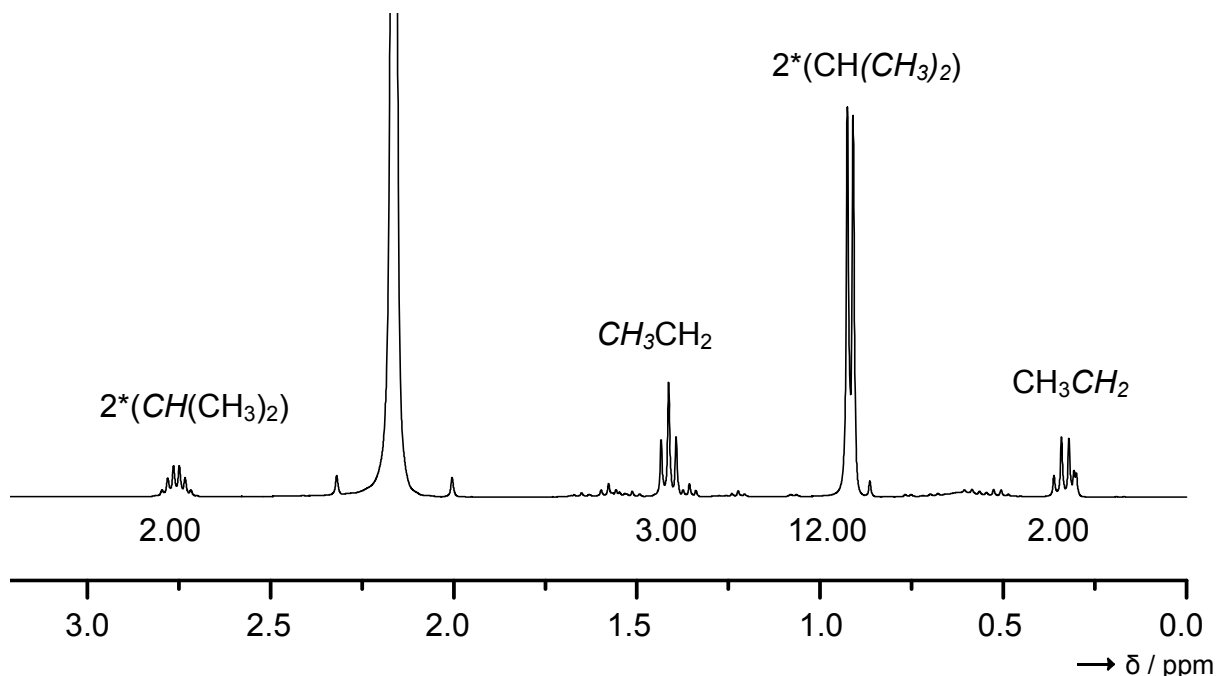
Figure 2.2 ^{1}H NMR spectrum (400 MHz, C$_6$D$_6$) for EtZnN(iPr)$_2$

Previous reports indicate that zincation of amines in toluene is a relatively slow reaction. For example, MeZnN(H)Si(iPr)$_3$ has been synthesised by stirring H$_2$NSi(iPr)$_3$ together with ZnMe$_2$ in toluene at room temperature for 10 h and subsequently under reflux for additional 2 h.[103] The purpose is not to isolate the alkyl zinc amide EtZnN(iPr)$_2$, since crystal structures for related compounds such as [EtZnNHSi(iPr)$_3$]$_2$[104] are already known and reveal the presence of dimeric units. In solution dimers and monomers should exist in equilibrium (see below) (**Scheme 2.2**).
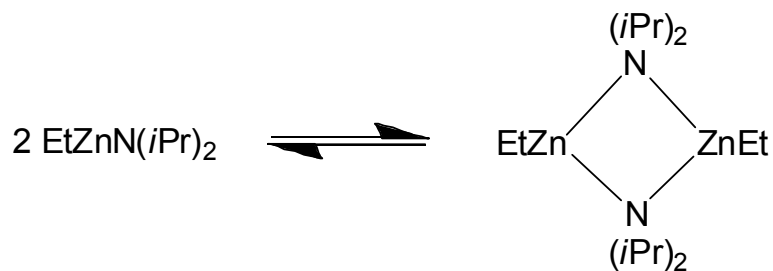
Scheme 2.2 Schematic monomer-dimer equilibrium of EtZnN(iPr)$_2$

The ^{13}C NMR spectrum taken upon CO_2 insertion showed very clearly the presence of carbamate units. Thus signals at δ = 163.04 can be assigned to the central C atom of the carbamate ligands in [ZnEt(O$_2$CN(iPr)$_2$)]$_4$ (**1**) (**Figure 2.3**).
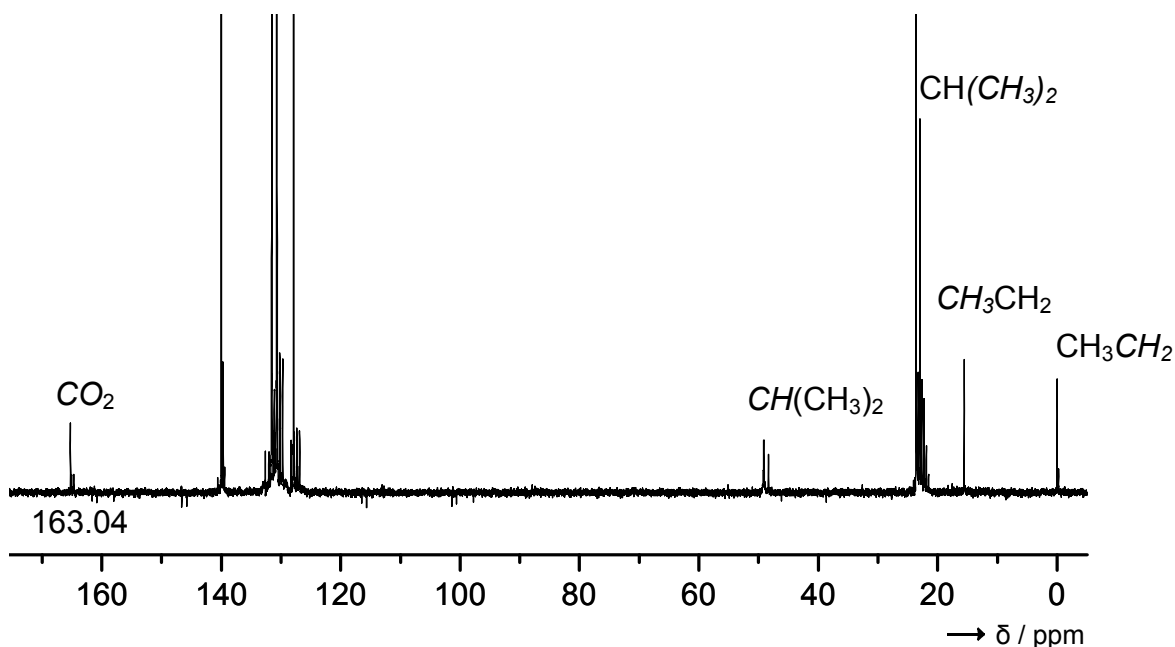
Figure 2.3 ^{13}C NMR spectrum (100.56 MHz, C$_6$D$_6$) for **1**

Colourless crystals of the two carbamate complexes in good yield were grown from these solutions. [ZnEt(O$_2$CN(iPr)$_2$)]$_4$ (**1**) crystallizes in the tetragonal space group P4(1) and [ZnEt(O$_2$CN(iBu)$_2$)]$_4$ (**2**) adopts the triclinic space group P-1. In **Figure 2.4** and **Figure 2.5** the structures as determined by X-ray diffraction are illustrated. **Table 2.1** and **Table 2.2** summarise some important parameters for these two compounds.
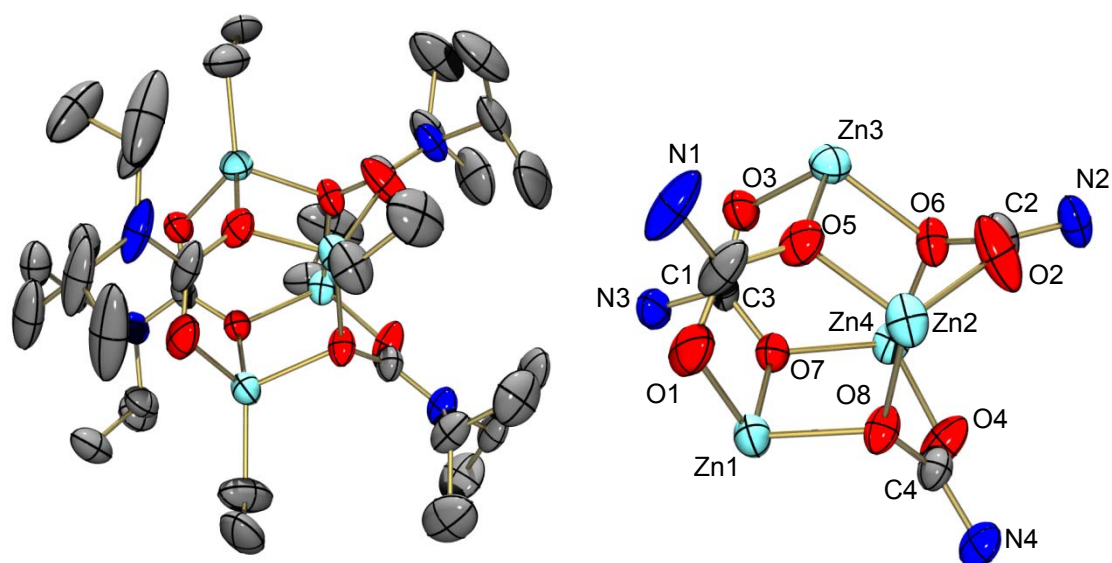
Figure 2.4 Molecular structure of **1**. Thermal ellipsoids are drawn at the 50% probability level; light-blue Zn, blue N, red O, grey C

Table 2.1 Selected bond distances (in pm) and angles (in deg.) for **1** as determined by X-ray diffraction.

Zn1-C	196.6(4)	Zn2-C	1.968(4)
Zn1-O1	196.6(4)	Zn2-O2	196.5(3)
Zn1-O7	206.2(3)	Zn2-O5	209.9(2)
Zn1-O8	208.8(3)	Zn2-O8	207.4(3)
Zn3-C	195.8(5)	Zn4-C	196.2(4)
Zn3-O3	198.5(3)	Zn4-O4	195.0(3)
Zn3-O5	204.8(3)	Zn4-O6	207.1(2)
Zn3-O6	206.6(2)	Zn4-O7	205.8(3)
O1-C1	125.6(4)	O5-C1	130.5(4)
O2-C2	125.9(4)	O6-C2	130.6(4)
O3-C3	127.4(6)	O7-C3	130.1(5)
O4-C4	127.2(5)	O8-C4	130.1(4)
N1-C1	134.4(5)	N3-C3	133.0(5)
N2-C2	134.9(5)	N4-C4	133.1(5)

C-Zn1-O1	124.29(17)	C-Zn3-O3	118.2(2)
C-Zn1-O7	120.58(19)	C-Zn3-O5	125.29(17)
C-Zn1-O8	112.79(19)	C-Zn3-O6	112.39(19)
O1-Zn1-O7	97.28(11)	O3-Zn3-O5	100.99(12)
O1-Zn1-O8	102.41(11)	O3-Zn3-O6	102.80(12)
O7-Zn1-O8	94.14(10)	O5-Zn3-O6	92.42(10)
C-Zn2-O2	129.11(17)	C-Zn4-O4	124.51(16)
C-Zn2-O5	108.89(18)	C-Zn4-O6	118.28(17)
C-Zn2-O8	119.19(15)	C-Zn4-O7	118.85(16)
O2-Zn2-O5	98.75(11)	O4-Zn4-O6	100.22(13)
O2-Zn2-O8	98.43(12)	O4-Zn4-O7	95.94(13)
O5-Zn2-O8	96.26(10)	O6-Zn4-O7	92.47(10)

According to the X-ray diffraction experiments, both molecules feature two Zn_2O_3C rings which are linked by bridging O atoms. Thus as anticipated the structures are similar to those reported for $[ZnMe(O_2CN(iPr)_2)]_4$ and $[ZnMe(O_2CN(iBu)_2)]_4$.[45]
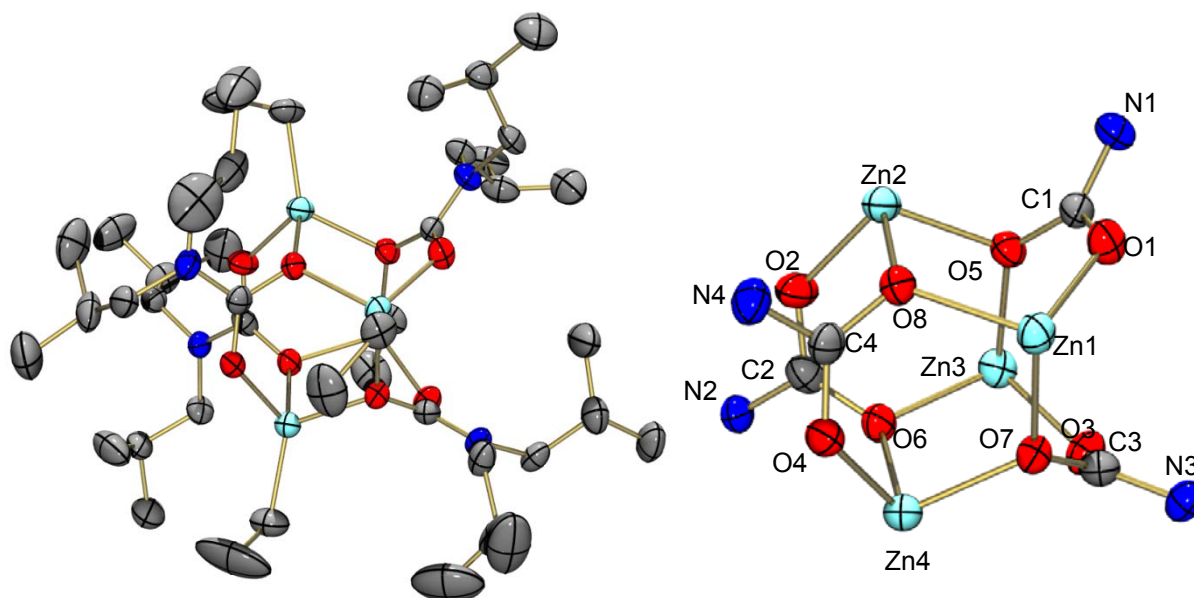
Figure 2.5 Molecular structure of **2**. Thermal ellipsoids are drawn at the 50% probability level; light-blue Zn, blue N, red O, grey C

Table 2.2 Selected bond distances (in pm) and angles (in deg.) for **2** as determined by X-ray diffraction.

Zn1-C	198.3(4)	Zn2-C	196.4(5)
Zn1-O1	195.6(3)	Zn2-O2	199.4(3)
Zn1-O7	210.2(3)	Zn2-O5	206.2(3)
Zn1-O8	209.6(3)	Zn2-O8	210.6(3)
Zn3-C	197.2(4)	Zn4-C	197.4(4)
Zn3-O3	197.9(3)	Zn4-O4	197.1(3)
Zn3-O5	208.1(3)	Zn4-O6	206.6(3)
Zn3-O6	207.0(3)	Zn4-O7	206.9(3)
O1-C1	125.5(5)	O5-C1	130.9(5)
O2-C2	126.8(5)	O6-C2	130.5(5)
O3-C3	126.9(5)	O7-C3	131.0(5)
O4-C4	125.6(5)	O8-C4	130.1(5)
N1-C1	133.3(5)	N3-C3	133.8(5)
N2-C2	134.1(5)	N4-C4	134.3(5)
C-Zn1-O1	123.73(17)	C-Zn3-O3	127.35(15)
C-Zn1-O7	116.43(16)	C-Zn3-O5	116.96(15)
C-Zn1-O8	116.18(16)	C-Zn3-O6	116.80(16)
O1-Zn1-O7	100.47(11)	O3-Zn3-O5	97.19(12)
O1-Zn1-O8	98.83(13)	O3-Zn3-O6	97.27(12)
O7-Zn1-O8	96.45(11)	O5-Zn3-O6	94.85(10)
C-Zn2-O2	122.02(18)	C-Zn4-O4	112.79(16)
C-Zn2-O5	118.96(19)	C-Zn4-O6	126.29(17)
C-Zn2-O8	118.97(17)	C-Zn4-O7	120.33(18)
O2-Zn2-O5	97.52(11)	O4-Zn4-O6	98.53(13)
O2-Zn2-O8	97.94(12)	O4-Zn4-O7	102.90(12)
O5-Zn2-O8	96.04(11)	O6-Zn4-O7	91.40(11)

The center of inversion as the only symmetry operation for crystals of **2** is clearly visible in **Figure 2.6**, showing a section of the three-dimensional arrangement of molecules hosting the *b* and *c* axis of the unit cell [*a* = 12.8820(16) Å, *b* = 13.4530(27) Å and *c* = 18.0890(36) Å] in the paper plane.
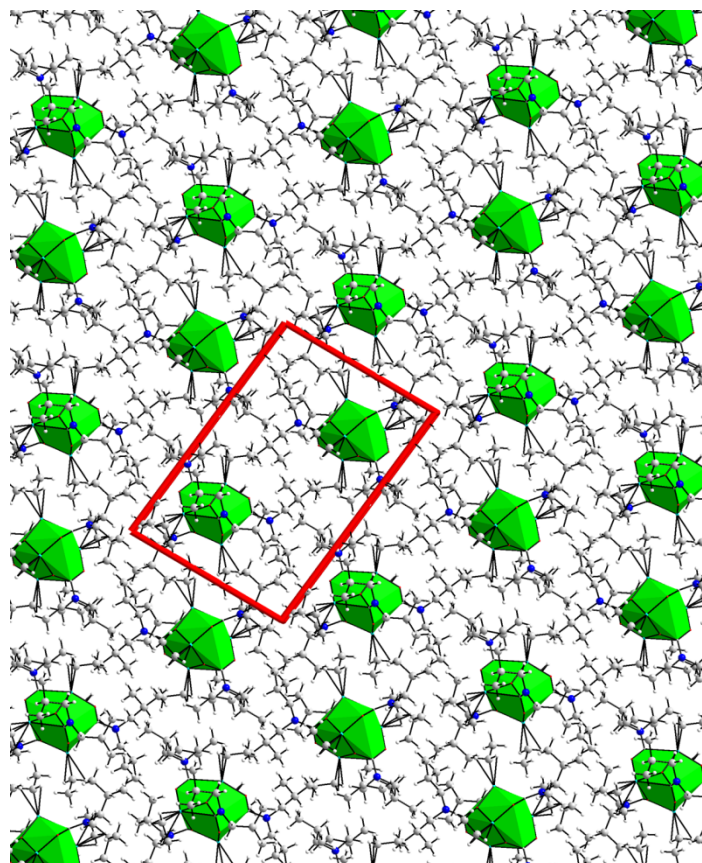
Figure 2.6 Arrangement of molecules of **2** in the crystalline phase
as determined by X-ray diffraction

The crystal structure of [ZnMe(O$_2$CN(*i*Bu)$_2$)]$_4$ was shown to be of much higher symmetry. Crystal symmetries for the four carbamate complexes [ZnMe(O$_2$CN(*i*Pr)$_2$)]$_4$, [ZnEt(O$_2$CN(*i*Pr)$_2$)]$_4$, [ZnMe(O$_2$CN(*i*Bu)$_2$)]$_4$ and [ZnEt(O$_2$CN(*i*Bu)$_2$)]$_4$ are presented in **Table 2.3**.[45]

Table 2.3 Crystal symmetries for the four carbamate complexes [ZnMe(O$_2$CN(*i*Pr)$_2$)]$_4$, [ZnEt(O$_2$CN(*i*Pr)$_2$)]$_4$, [ZnMe(O$_2$CN(*i*Bu)$_2$)]$_4$ and [ZnEt(O$_2$CN(*i*Bu)$_2$)]$_4$

Complex	crystal system	point group	unit cell volume / [Å^3]
[ZnMe(O$_2$CN(*i*Pr)$_2$)]$_4$	tetragonal	P4(1)	4510.3
[ZnEt(O$_2$CN(*i*Pr)$_2$)]$_4$	tetragonal	P4(1)	4745.3
[ZnMe(O$_2$CN(*i*Bu)$_2$)]$_4$	tetragonal	I4	2655.9
[ZnEt(O$_2$CN(*i*Bu)$_2$)]$_4$	triclinic	P-1	2815.5

If small amounts of water are added to the reaction mixture, the carbamate complex [Zn$_4$(μ$_4$-O)(O$_2$CN(*i*Bu)$_2$)$_6$] (**3**) is formed instead of **2**. Complex **3** crystallises in the orthorhombic space group Fdd2. A molecular C$_2$ rotational axis is running through atoms N1-C1-C2-N2 (**Figure 2.7**).
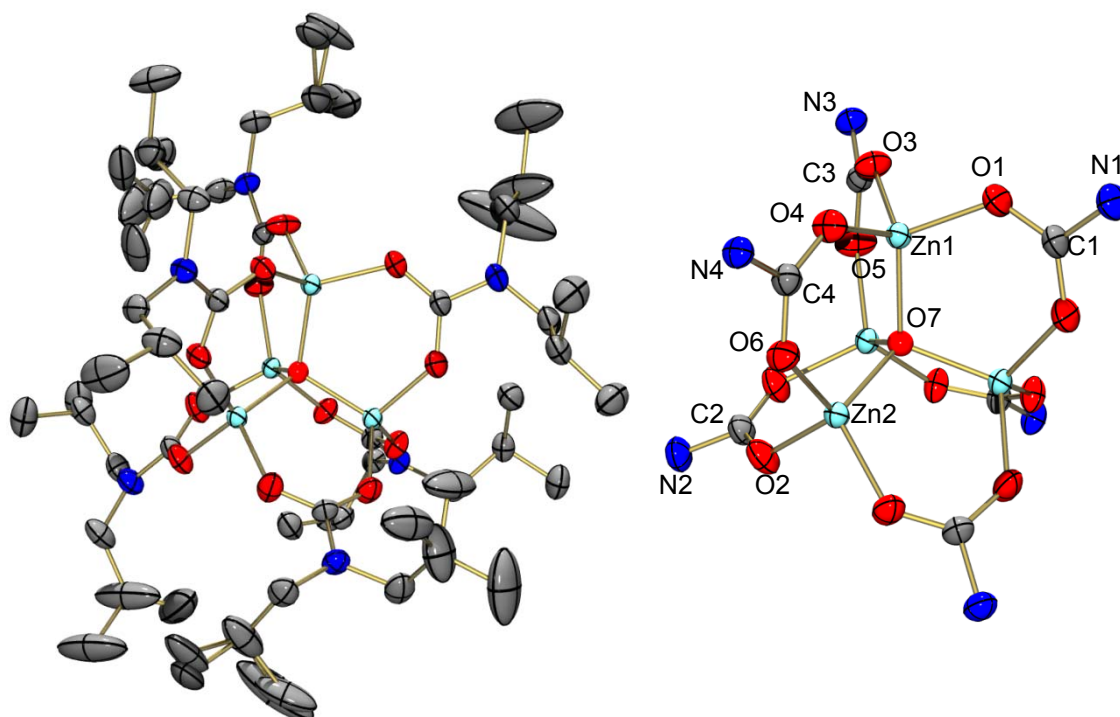
**Figure 2.7** Molecular structure of **3**. Thermal ellipsoids are drawn at the 50% probability level; light-blue Zn, blue N, red O, grey C

Figure 2.8 shows a LIFDI spectrum of **3** together with a simulation of the isotopic structure indicating that the molecule is stable in solution. In addition to the signal centered at m/z = 1310.5 due to $[Zn_4(\mu_4\text{-}O)(O_2CN(i\text{Bu})_2)_6]$ a small signal centered at m/z = 1418.5 was found.
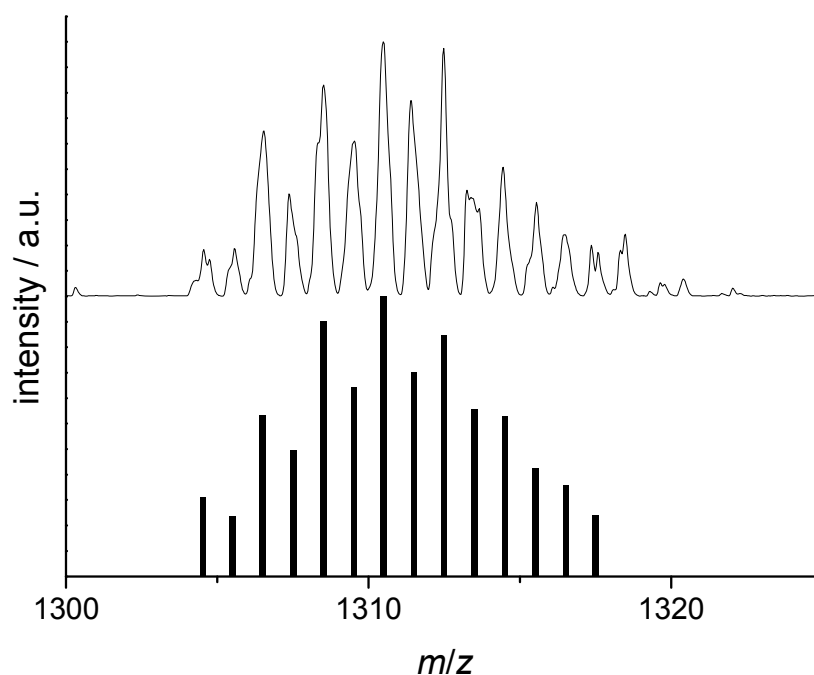
Figure 2.8 LIFDI spectrum of $[Zn_4(\mu_4\text{-}O)(O_2CN(i\text{Bu})_2)_6]$ in solution.
Measured spectrum (top) together with
a simulation of the most intense isotopic peaks

The central OZn_4 unit resembles the structure of solid ZnO, in which Zn^{2+} cations occupy alternative tetrahedral holes in an hcp array of O^{2-}. The O1-Zn bond distances of ca. 194 pm (**Table 2.4** summarise some important parameters for this complex) are very close to the Zn-O distances in solid (wurtzite) ZnO (193 pm).[105] In the case of $[OZn_4(acetate)_6]$,[106] absorption and emission spectra have been measured confirming also the analogy to the electronic properties of ZnO.

35

Table 2.4 Selected bond distances (in pm) and angles (in deg.) for **3** as determined by X-ray diffraction.

Zn1-O7	193.6(2)	Zn2-O7	194.6(2)
Zn1-O1	194.2(2)	Zn2-O2	194.5(2)
Zn1-O3	193.6(2)	Zn2-O5	193.4(2)
Zn1-O4	192.7(2)	Zn2-O6	192.2(2)
O1-C1	126.8(3)	O4-C4	127.5(4)
O2-C2	126.6(3)	O5-C3	127.2(4)
O3-C3	127.3(4)	O6-C4	128.1(4)
N1-C1	136.4(5)	N3-C3	134.9(4)
N2-C2	136.1(6)	N4-C4	134.2(4)
O7-Zn1-O1	108.89(10)	O7-Zn2-O2	108.58(10)
O7-Zn1-O3	111.15(8)	O7-Zn2-O5	112.21(8)
O7-Zn1-O4	113.39(8)	O7-Zn2-O6	112.48(7)
O1-Zn1-O3	107.38(10)	O2-Zn2-O5	113.54(10)
O1-Zn1-O4	111.78(10)	O2-Zn2-O6	105.94(10)
O3-Zn1-O4	104.04(11)	O5-Zn2-O6	103.93(11)
Zn1-O7-Zn1'	113.15(14)	O1-C1-O1'	125.7(4)
Zn1-O7-Zn2	108.143(14)	O2-C2-O2'	125.7(4)
Zn1'-O7-Zn2	107.558(14)	O3-C3-O5	124.9(3)
Zn2-O7-Zn2'	112.37(14)	O4-C4-O6	124.5(3)
Zn1-O7-Zn2'	107.563(14)		
Zn1'-O7-Zn2'	108.145(14)		
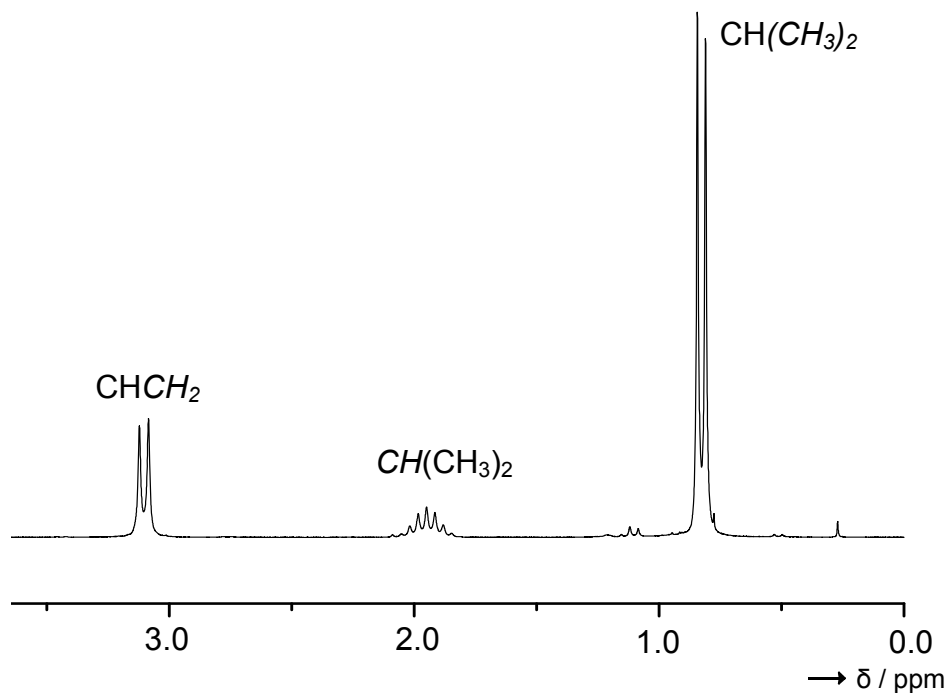
Figure 2.9 ^{1}H NMR spectrum (400 MHz, C_6D_6) for **3**

As visible from **Figure 2.9** and **Figure 2.10**, the only signals present are those from the iso-butyl groups and in the ^{13}C NMR spectrum the signal from 164.69 ppm is assigned to the central C atom of the carbamate ligands.
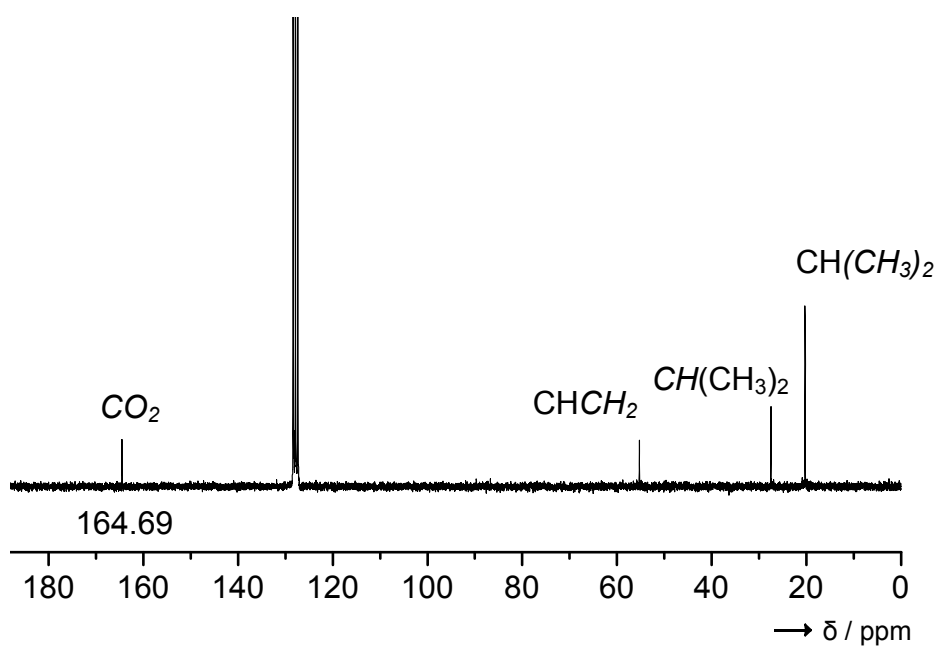
Figure 2.10 ^{13}C NMR spectrum (100.56 MHz, C_6D_6) for **3**

The tetrameric carbamate complex **1** and **2** decompose at relatively low temperatures. **Figure 2.11** shows thermogravimetric (TG) curves recorded for **1** for different heating rates (2, 5 and 10°C min^{-1}). It can be seen that the heating rate effects the decomposition.
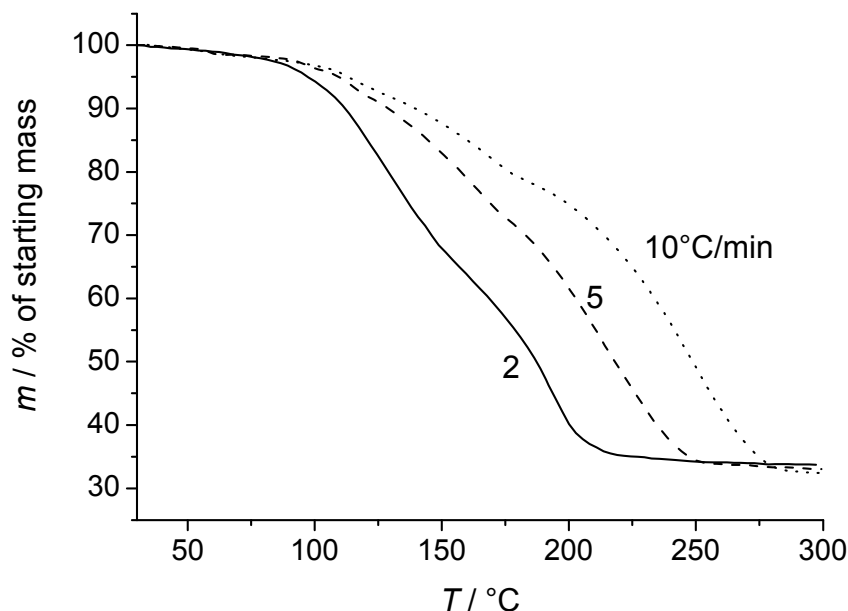
Figure 2.11 Thermogravimetric (TG) curves obtained for [ZnEt(O$_2$CN(iPr)$_2$)]$_4$
with different heating rates (2, 5 and 10°C min^{-1})

Thus decomposition is completed at higher temperatures for larger heating rates, arguing for a non-equilibrium process under these conditions. In **Figure 2.12** the first derivative of the TG curve for a heating rate of 2°C min^{-1} is plotted. Two minima are visible at ca. 130 and 192°C. Thus, as shown previously for [RZnOR']$_4$ precursor compounds [e.g. R = CH$_3$, R' = CH(CH$_3$)$_2$], decomposition occurs in two steps.[76] The mass loss of the two combined steps is ca. 67% fitting thus well with decomposition to give ZnO.
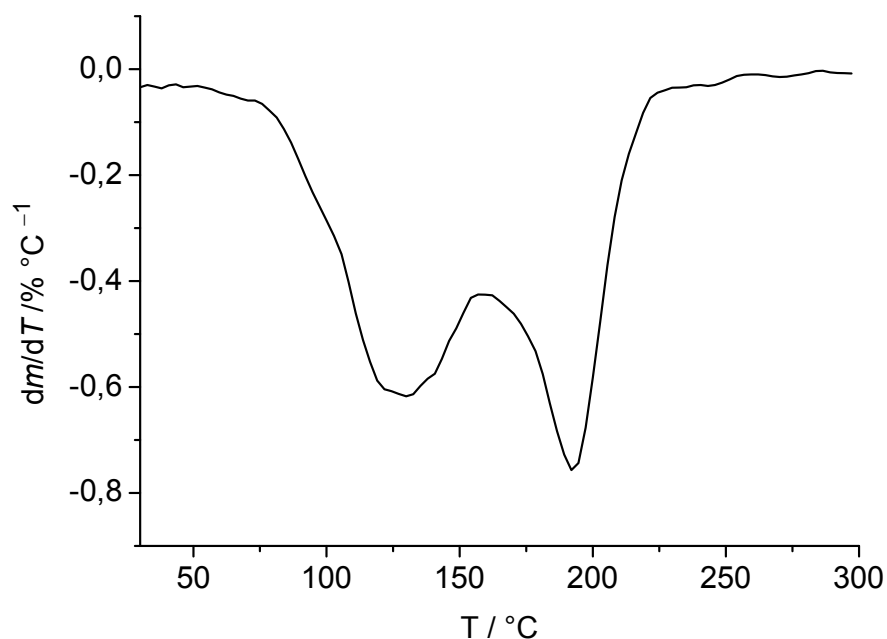
Figure 2.12 First derivative of the TG curve recorded for a

heating rate of 2°C min^{-1}

Raman spectra were recorded before and after decomposition to obtain further information. **Figure 2.13** displays the Raman signal of [ZnEt(O$_2$CN(iPr)$_2$)]$_4$ in the region around 450 cm^{-1}. An additionally measured wurtzite ZnO reference (trace c) shows the characteristic two intense (allowed) E_2 phonon modes of ZnO at 98 and 437 cm^{-1} (E_2^{low} and E_2^{high}, literature values 99 and 439 cm^{-1}).[107] Other signals at ca. 330, 380 and 580 cm^{-1} were previously assigned to E_2^{high}-E_2^{low}, A_1(TO) and E_1(LO) (TO and LO should denote the transverse and longitudinal components, in which the infrared active optical phonon mode is split).[108] Finally, a broad signal around 1140 cm^{-1} is due to 2E_1(LO), gaining intensity due to the presence of a resonance Raman effect.[109] All these signals are absent in the spectrum recorded for **1** prior to heating (trace a). The appearance of the signals characteristic for ZnO in the spectrum recorded after heating the sample to 300°C (trace b) confirms that decomposition of **1** leads to ZnO.

Importantly, the spectra show no sign of any signals besides those due to ZnO. Therefore decomposition appears to be a clean process and the use of the carbamate complexes as ZnO precursors is attractive.
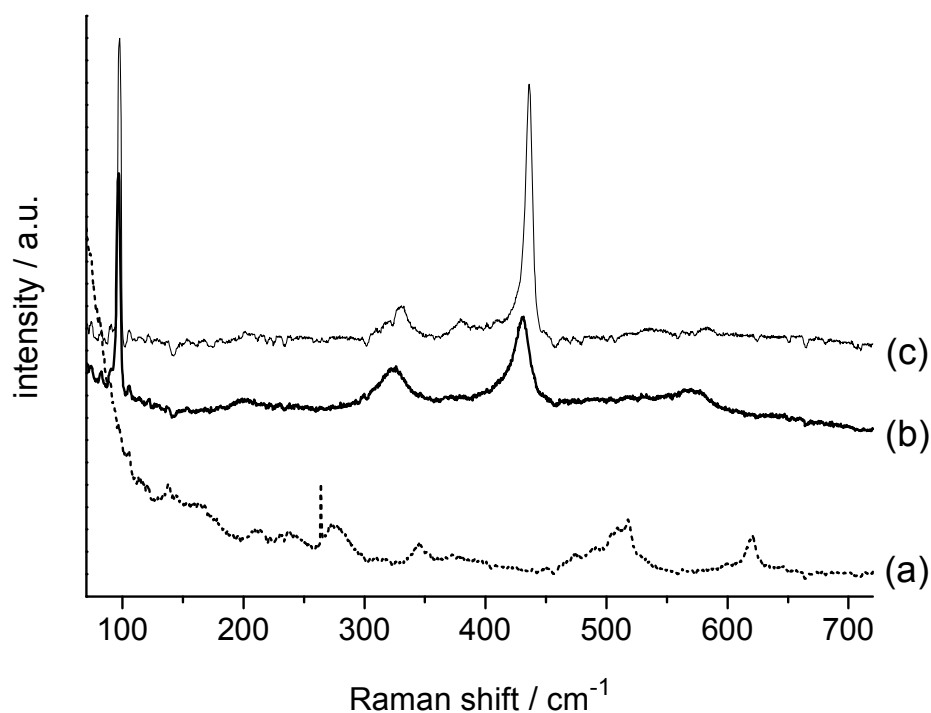
Figure 2.13 Raman spectra in the region around 450 cm^{-1} (excited with the
514 nm line of an Ar$^+$ ion laser) measured for [ZnEt(O$_2$CN(*i*Pr)$_2$)]$_4$
(a) before heating and (b) after heating to 300°C, together with (c) a reference
Raman spectrum of a purchased ZnO sample

X-ray powder diffraction (XRD) data in reflection with Cu radiation was
measured after heating of [ZnEt(O$_2$CN(*i*Pr)$_2$)]$_4$ to 300°C with a heating rate of 5°C
min^{-1}. The ZnO can be identified from the powder diffractogramme as the hexagonal
in the space group P6$_3$mc crystallising form (*a* = *b* = 324.98 pm, *c* = 520.66 pm, see
Figure 2.14). The mean particle size calculated from the line broadening in the
diffractogramme is calculated to be 10.3 nm with the Debye-Scherrer equation.
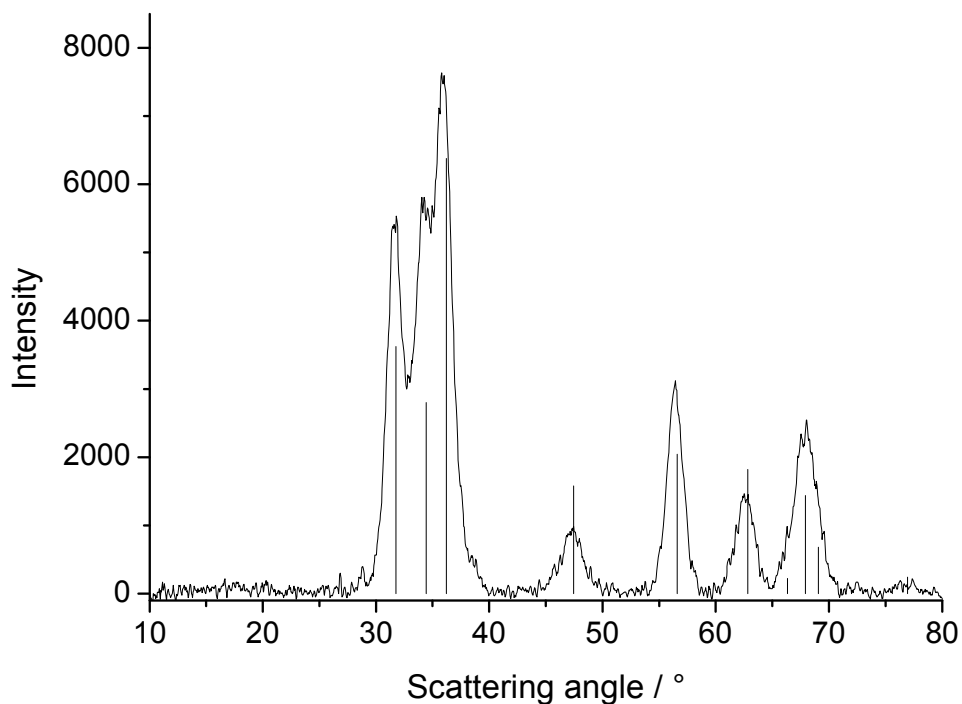
Figure 2.14 Powder diffraction patterns as measured after heating of [ZnEt(O$_2$CN(iPr)$_2$)]$_4$ to 300°C with a heating rate of 5°C min^{-1}. The inserted lines are taken from the database for ZnO

These results are furthermore confirmed[110] by a statistical evaluation from the TEM measurements giving a mean particle size of 9.3 (1.6) nm with a maximum in the particle size distribution at about 9.5 nm (see **Figure 2.15**).
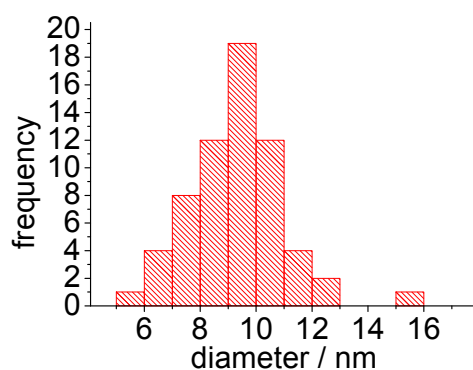
Figure 2.15 Plot of the particle size distribution

41

This value is in good to excellent agreement with the results for the particle size determination of 10.4 nm obtained from BET measurements (BET surface: 102.7 $m^2 g^{-1}$, density of ZnO: 5.6 g cm^{-3}).

In the high resolution TEM measurement (**Figure 2.16**), the crystalline nature of the material is, in addition to the XRD measurements, proven by the existence of crystal planes in the particles. The layers of the 1 0 0 (or 0 1 0) plane of ZnO with a corresponding plane to plane distance of 293(8) pm are resolved (expected 281 pm).
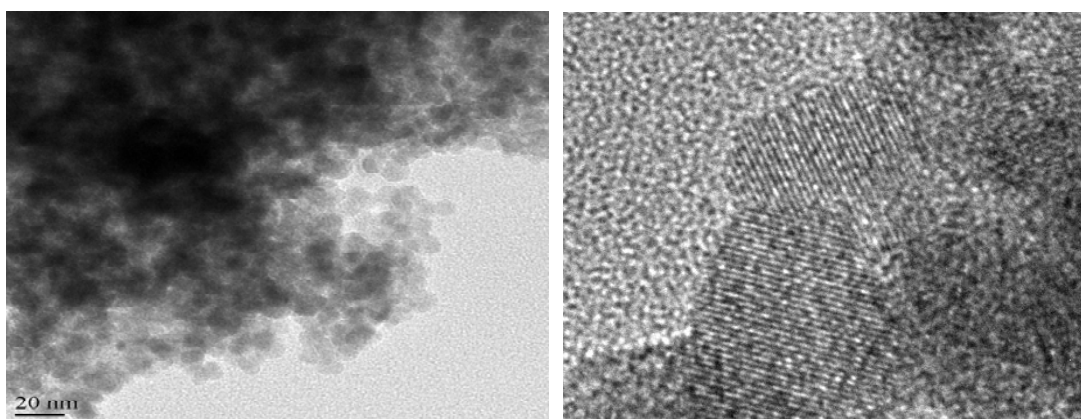
Figure 2.16 TEM image showing the ZnO nanoparticles formed by heating [ZnEt(O_2CN(iPr)$_2$)]$_4$ to 300°C (heating rate 5°C min^{-1})

An EDX analysis of the ZnO particles shows the presence of ca. 3% of carbon impurities which might be due to adsorbed solvent molecules. Solvent adsorption is found regularly for ZnO formation in polyol solvents.[111] All these results show that during the pyrolysis of **1** nanoparticles of definite shape and overall good particle size distribution are formed. This gives evidence that the pyrolysis proceeding at low temperatures of 200°C is finally a controlled process as otherwise not so well defined particles in terms of size and crystalline behaviour would be expected as the product.

2.2 Reactions between tetrameric alkylzinc carbamates and various nitrogen bases

The reaction between $[Zn(Et)NR_2]_n$ (R = *i*Pr and *i*Bu) and CO_2 results in the formation of the tetranuclear carbamate complex $[ZnEt(O_2CNR_2)]_4$.[112] This complex can subsequently be brought to reaction with a base to give in a directed synthesis mono-, di- and trinuclear complexes, depending on the base strength and the relative concentration of the two reactants. In the following part are presented the results obtained with pyridine, TMG and BTMGN (see **Scheme 2.2**).

| pyridine | TMG | BTMGN |
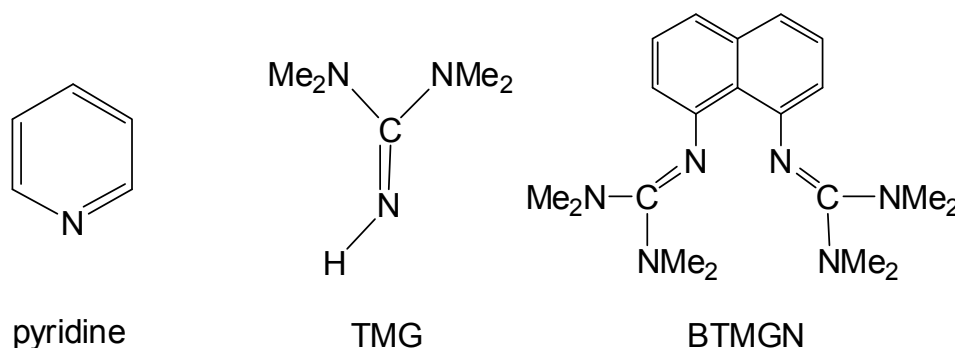
Scheme 2.2 Schematic structure of the nitrogen bases used in this work

2.2.1 Reaction of [ZnEt(O₂CN(*i*Pr₂))]₄ with pyridine

Reaction of $[ZnEt(O_2CN(iPr)_2)]_4$ with pyridine leads to formation of the dinuclear Zn-compound $[(py)ZnEt(O_2CN(iPr)_2)]_2$ (**4**) exhibiting a structure similar to that reported for $[(py)ZnMe(O_2CNR_2)]_2$ (R = *i*Pr and *i*Bu).[45]

Figure 2.17 illustrates the structure of one of the centrosymmetric molecules of **4** as obtained by X-ray diffraction.
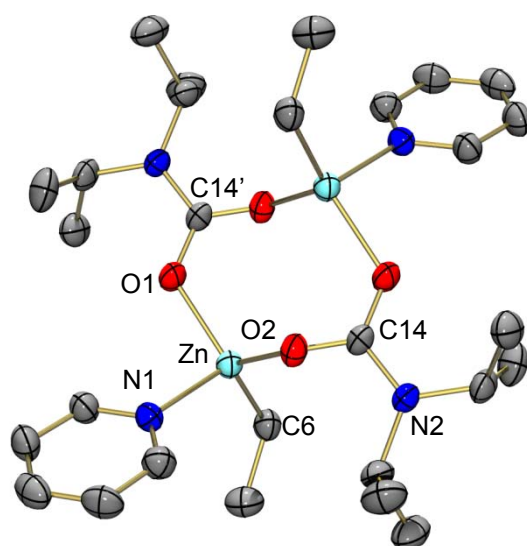
Figure 2.17 Molecular structure of **4**. Thermal ellipsoids are drawn at the 50% probability level; light-blue Zn, blue N, red O, grey C

The two carbamate ligands adopt a η^2-coordination mode leading to a puckered eight-membered $(ZnOCO)_2$ ring. Each Zn atom is thus bound to two O atoms, one ethyl C atom and a pyridine N atom. At 198.7(2) and 201.6(2) pm, the two Zn-O bond distances are slightly different. The bond angles around the Zn atoms deviate significantly from the 109.4° tetrahedral angles (see **Table 2.5** for more information about the structural parameters).

Table 2.5 Selected bond distances (in pm) and angles (in deg.) for **4** as determined by X-ray diffraction.

Zn-O1	198.7(2)	C6-Zn-N1	113.78(10)
Zn-O2	201.62)	O2-Zn-N1	94.20(8)
Zn-C6	198.8(3)	O1-Zn-C6	129.79(10)
Zn-N1	212.8(2)	O1-Zn-O2	107.69(8)
O1-C14'	127.6(3)	C6-Zn-O2	113.50(9)
O2-C14	127.3(3)	O1-Zn-N	89.85(8)
C14-N2	135.9(3)	C14'-O1-Zn	120.98(15)
C14-O2-Zn	125.98(15)		

In the Raman spectrum (**Figure 2.18**) the stretching modes ν(C-H) of the pyridine base at 3070 cm^{-1} are clearly separated from the stretching modes ν(C-H) of the alkyl groups (3000-2840 cm^{-1}), and a feature at 1456 cm^{-1} can be assigned to ν(CO$_2$).
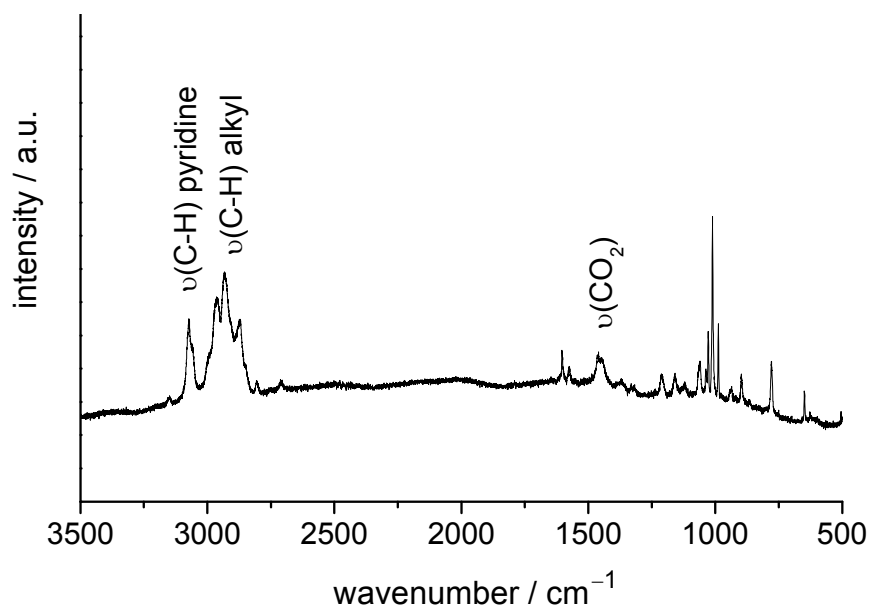
Figure 2.18 Raman spectra measured for **4**

The ^{1}H NMR (**Figure 2.19**) spectrum showed only one type of *iso*-propyl groups and pyridine groups, indicating that the two iso-propyl and respectively pyridine groups are identical with each other.
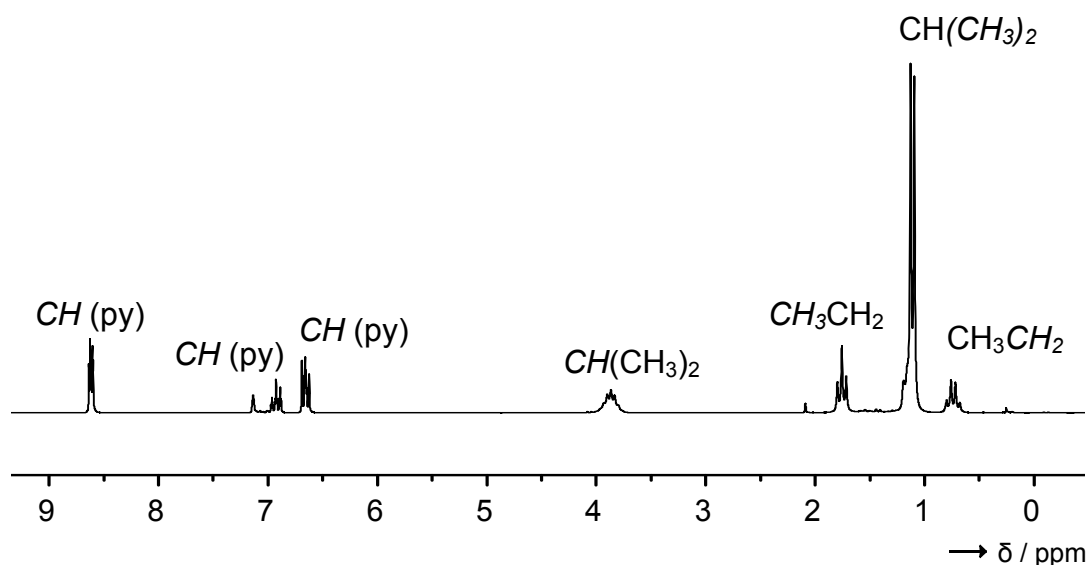
Figure 2.19 ^{1}H NMR spectrum (200 MHz, C$_6$D$_6$) for **4**

The ^{13}C NMR (**Figure 2.20**) spectrum shows the presence of carbamate units. The signals at δ = 163.31 ppm being assigned to the central C atom of the carbamate unit in complex **4**, [(py)ZnEt(O$_2$CN(iPr)$_2$)]$_2$.
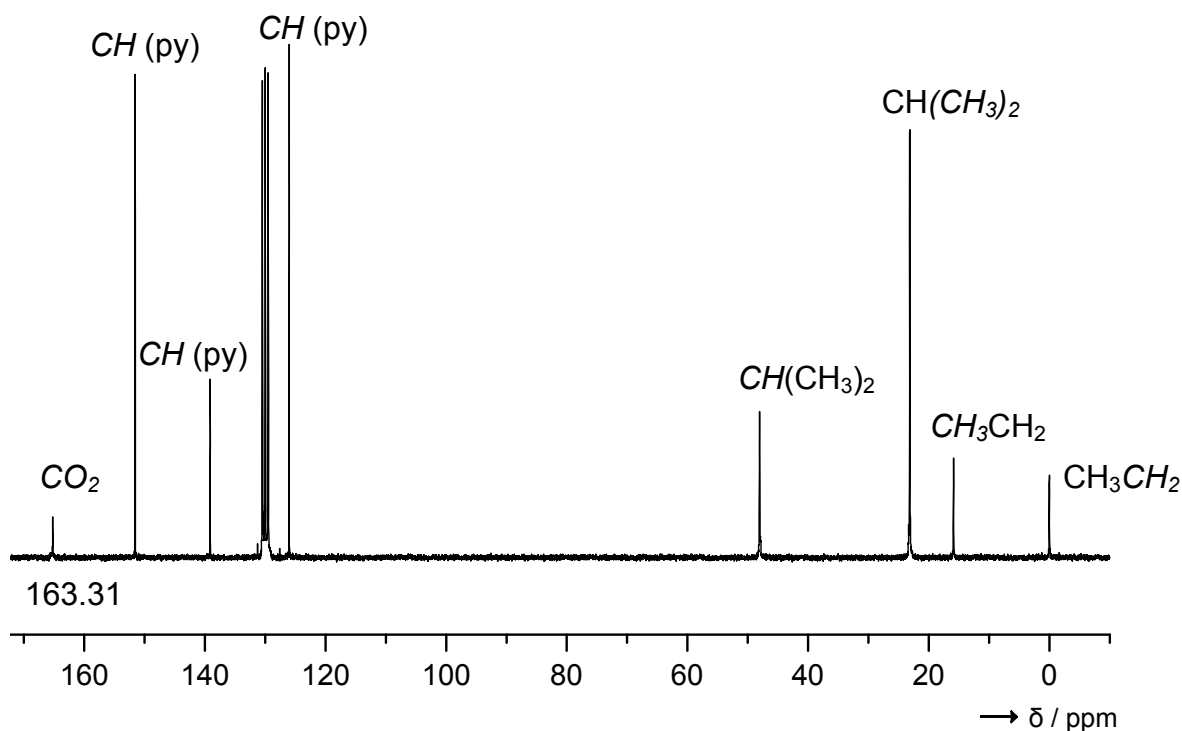
Figure 2.20 ^{13}C NMR spectrum (50.27 MHz, C$_6$D$_6$) for **4**

In contrast to the results obtained with guanidine derivatives (see below), no other product can be obtained (even with a very large excess of pyridine), especially no mono- or trinuclear species.

2.2.2 Reaction of [ZnEt(O$_2$CN(iPr)$_2$)]$_4$ with TMG

Reaction between [ZnEt(O$_2$CN(iPr)$_2$)]$_4$ and 4 equivalents of TMG yielded the dinuclear complex [(TMG)ZnEt(O$_2$CN(iPr)$_2$)]$_2$ (**5**). The structure of this species is displayed in **Figure 2.21**.

Again a puckered eight membered ring is formed and the two TMG ligands as well as the two ethyl groups adopt a *trans*-conformation.
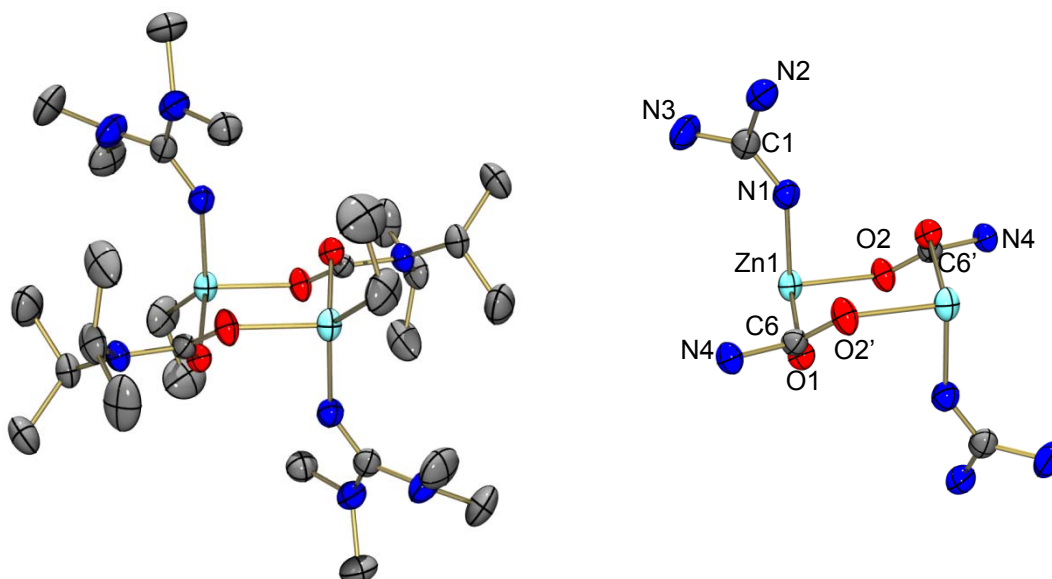
Figure 2.21 Molecular structure of **5**. Thermal ellipsoids are drawn at the 50% probability level; light-blue Zn, blue N, red O, grey C

At 202.8(3) pm the Zn-N distances from the Zn to the directly bound N atom of the TMG ligand in **5** are significantly shorter than the Zn-N distances from the Zn to the pyridine N atoms in **4** (see **Table 2.6** for selected structural parameters). In contrast, the Zn-O distances are shorter in **4** than in **5**. The two complexes also differ in the O-Zn-O angles, in **4** this angle measures 108.11(6)° while in **5** it is only 99.88(8)°. These structural differences are clearly a consequence of the stronger basicity of TMG with respect to pyridine.

Table 2.6 Selected bond distances (in pm) and angles (in deg.) for **5** as determined by X-ray diffraction.

| Zn1-O1	205.55(18)	Zn1-O2	203.31(19)
Zn1-N1	202.8(3)	Zn1-C	197.5(3)
C1-N1	129.9(4)	C1-N2	137.9(4)
C1-N3	136.6(4)	C6-N4	136.8(3)
C6-O1	127.7(3)	C6-O2	126.4(3)

N1-Zn1-O1	97.82(9)	N1-Zn1-O2	95.47(9)
C-Zn-O1	112.13(14)	C-Zn-O2	111.89(13)
O1-Zn1-O2	99.88(8)	Zn1-O1-C6	126.05(17)
Zn1-O2-C6'	125.52(17)	Zn1-N1-C1	144.2(2)
O1-C6-O2	123.8(2)	N1-C1-N2	122.4(3)
N1-C1-N3	122.1(3)	N2-C1-N3	115.5(3)
O1-C6-N4	118.2(2)		

The ^{1}H NMR spectrum for the complex $[(TMG)ZnEt(O_2CN(iPr)_2)]_2$ (**Figure 2.22**), like in the case of compound **4**, presents only one type of isopropyl groups.
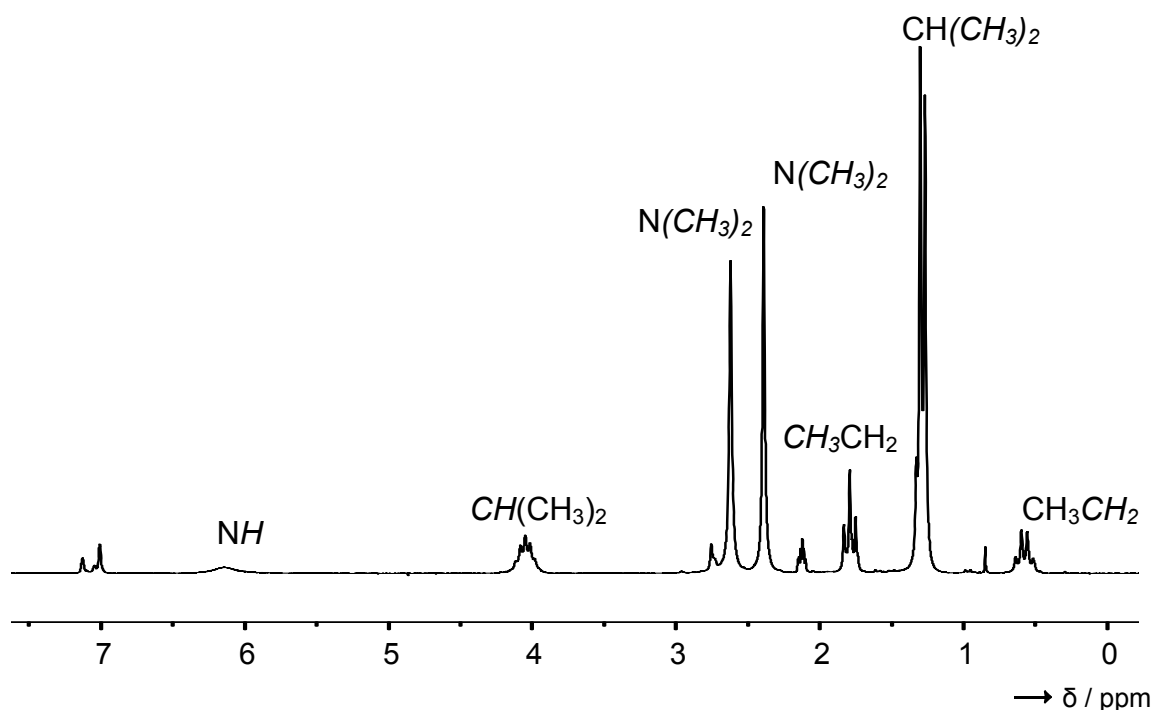
Figure 2.22 ^{1}H NMR spectrum (200 MHz, toluene d_8) for **5**

The ^{13}C NMR (**Figure 2.23**) spectrum shows the presence of carbamate units. The signals at δ = 163.27 ppm can be assigned to the central C atom of the carbamate unit in complex **5**, $[(TMG)ZnEt(O_2CN(iPr)_2)]_2$.

48
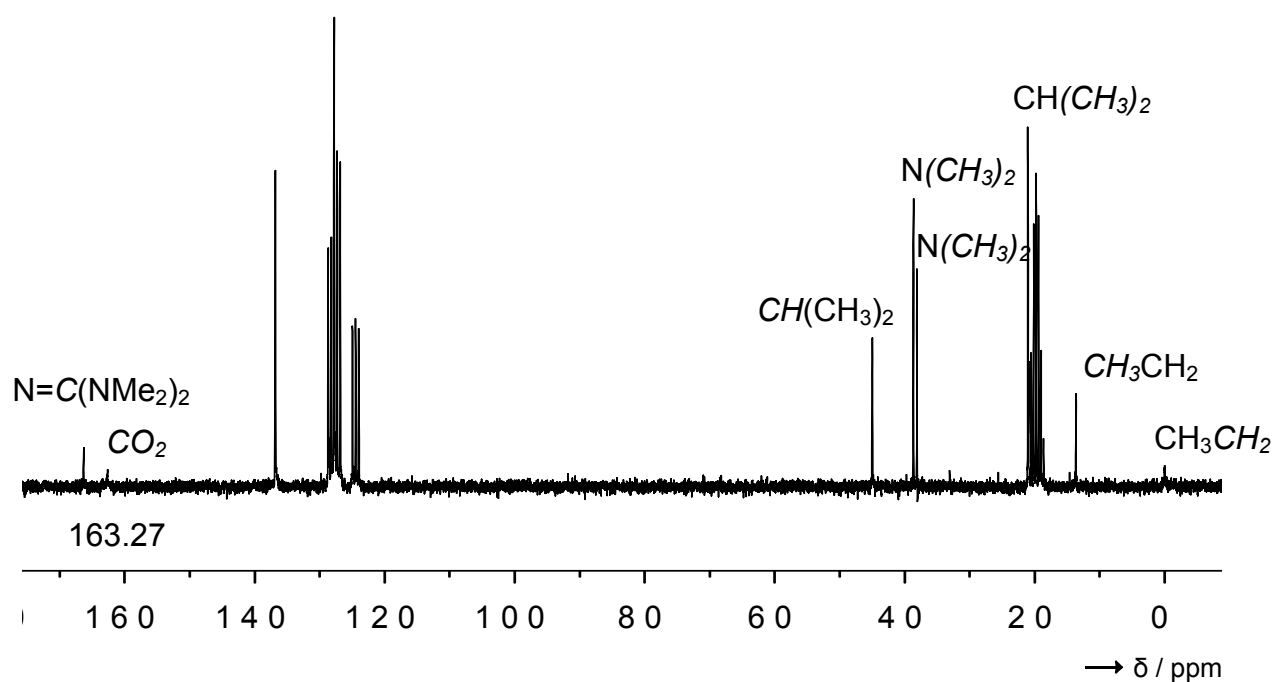
Figure 2.23 ^{13}C NMR spectrum (50.27 MHz, toluene d$_8$) for **5**

In contrast, the reaction between [ZnEt(O$_2$CN(iPr)$_2$)]$_4$ and 8 equivalents of TMG proceeded to the mononuclear bis-carbamate complex [(TMG)$_2$Zn(O$_2$CN(iPr)$_2$)$_2$] (**6**). The molecular structure as derived from an analysis of the X-ray diffraction data is visualized in **Figure 2.24**.
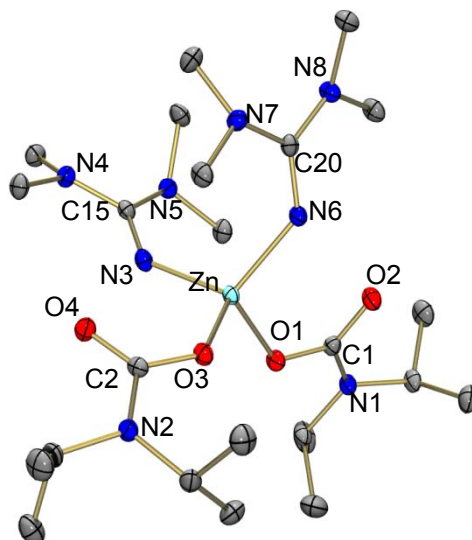
Figure 2.24 Molecular structure of **6**. Thermal ellipsoids are drawn at the 50% probability level; light-blue Zn, blue N, red O, grey C

The two carbamato ligands are η^1-coordinated. At 196.3 and 195.3 pm, the Zn-O1 and Zn-O3 bond distances are relatively short. The Zn···O2 and Zn···O4 separations amount to 313.4 and 322.5 pm and show that no significant bonds are established between these atoms. Other structural parameters can be found in **Table 2.7**.

Table 2.7 Selected bond distances (in pm) and angles (in deg.) for **6** as determined by X-ray diffraction.

Zn-O1	1.9628(11)	Zn-O3	1.9533(11)
Zn···O2	313.4(2)	Zn···O4	322.5(2)
Zn-N3	1.9974(14)	Zn-N6	1.9867(13)
O1-C1	1.2971(18)	O3-C8	1.2935(18)
C1-O2	1.2474(18)	C8-O4	1.2468(19)
C1-N1	1.3774(19)	C8-N2	1.3786(19)
N3-C15	1.302(2)	N6-C20	1.3029(19)
C15-N4	1.3690(19)	C20-N7	1.3735(19)
C15-N5	1.3755(19)	C20-N8	1.362(2)
O1-Zn-O3	106.87(5)	N3-Zn-N6	114.58(6)
O1-Zn-N3	111.02(5)	O3-Zn-N3	104.72(5)
O1-Zn-N6	107.80(5)	O3-Zn-N6	111.61(5)
O1-C1-O2	124.68(14)	O3-C8-O4	125.10(14)
O1-C1-N1	116.05(13)	O3-C8-N2	114.63(13)
Zn-N3-C15	136.61(11)	Zn-N6-C20	131.89(11)
N3-C15-N4	123.32(14)	N6-C20-N7	120.40(14)
N3-C15-N5	121.43(14)	N6-C20-N8	123.90(14)
N4-C15-N5	115.25(13)	N7-C20-N8	115.69(13)

The ^{1}H NMR spectrum is different than in the case of the complex [(TMG)ZnEt(O$_2$CN(iPr)$_2$)]$_2$ where the two isopropyl groups were identical. In contrast with the previous case, the ^{1}H NMR spectrum (**Figure 2.25**) shows two sets of signals assigned to the isopropyl groups, at 1.23 and 1.40 ppm two doublets for the two *(CH$_3$)$_2$*CH- groups and at 3.95 and 4.2 ppm two multiplets for the -C*H*(CH$_3$)$_2$ groups, indicating that this isopropyl groups are not anymore identical because of the rotation around the C - N amide bond.
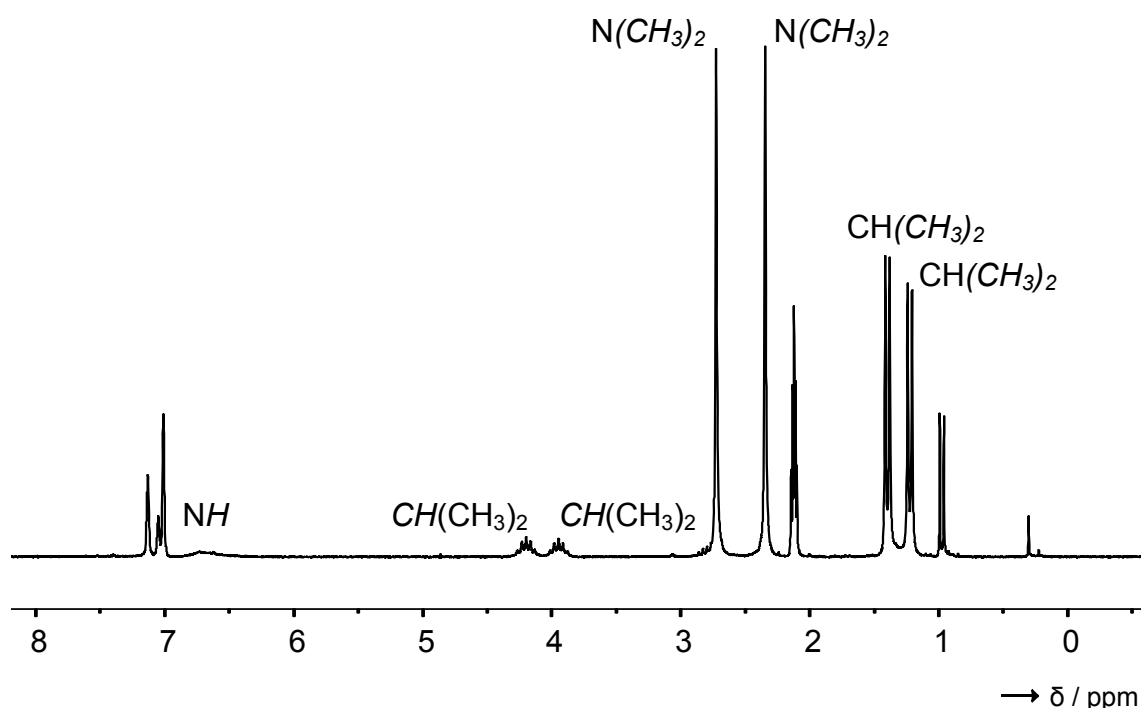

Figure 2.25 ^{1}H NMR spectrum (200 MHz, toluene d$_8$) for **6**

The ^{13}C NMR (**Figure 2.26**) spectrum shows the presence of carbamate units. The signals at δ = 163.15 can be assigned to the central C atom of the carbamate unit in complex **6**, [(TMG)$_2$Zn(O$_2$CN(iPr)$_2$)$_2$].

N=C(NMe$_2$)$_2$

CO_2

163.15

N$(CH_3)_2$ N$(CH_3)_2$

CH(CH$_3$)$_2$

CH$(CH_3)_2$

160   140   120   100   80   60   40   20

⟶ δ / ppm
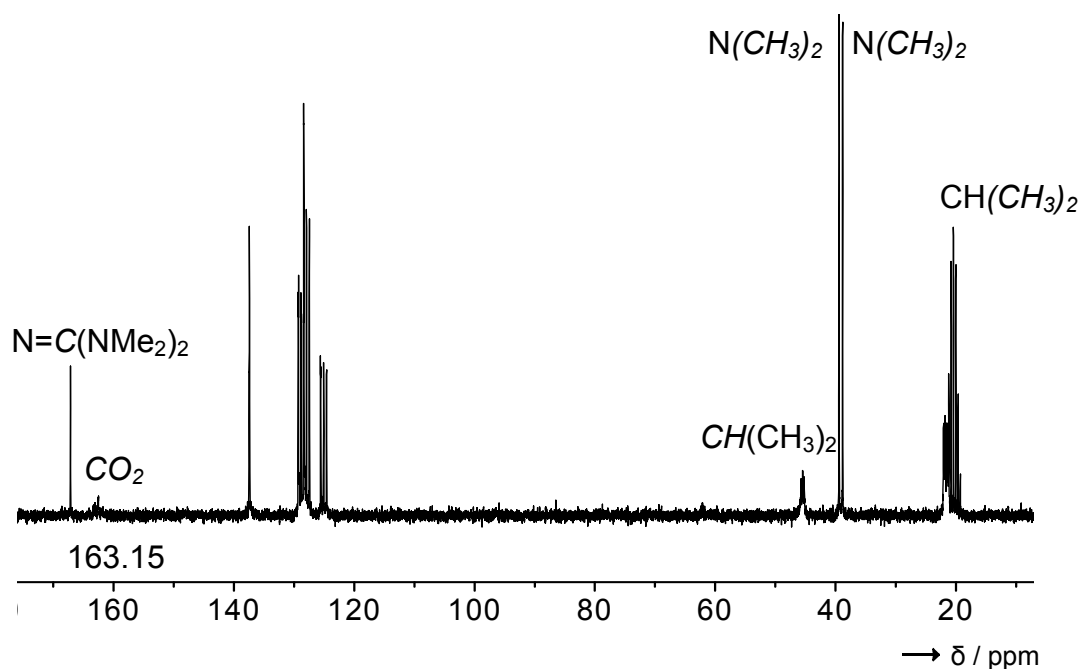
Figure 2.26 ^{13}C NMR spectrum (50.27 MHz, toluene d$_8$) for **6**

The first structurally characterized mononuclear biscarbamate complex of Zn with η[1]-coordinated carbamate ligands can be prepared by reaction between [ZnEt(O$_2$CN(iPr)$_2$]$_4$ and a guanidine base. The increased available (ligand-induced) charge density at the metal center is presumably responsible for the bonding mode change. The change from η[2]-coordination in [(TMEDA)Zn(O$_2$CNEt$_2$)$_2$][45] to η[1]-coordination in [(TMG)$_2$Zn(O$_2$CN(iPr)$_2$)$_2$] (see **Figure 2.27**) can be achieved by replacing the chelating TMEDA base by two moieties of the stronger base TMG.
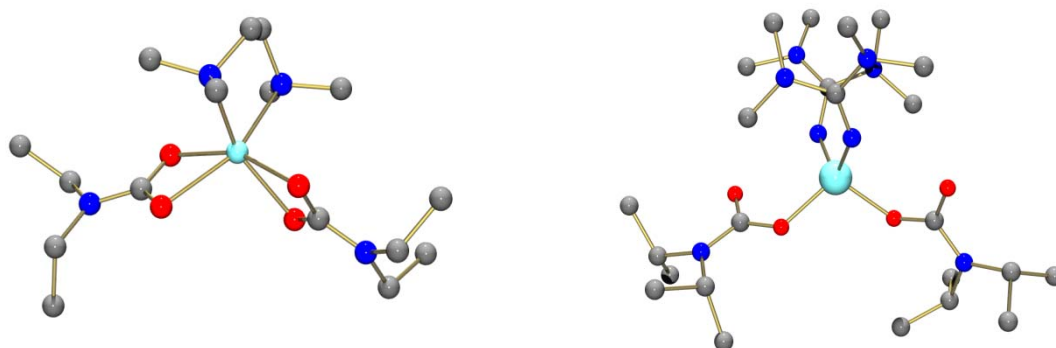
Figure 2.27 Schematic structure of η[2] (left side) and η[1](right side) coordination mode

The difference in the coordination mode highlights the basicity difference between amine and guanidine bases (the pK(BH$^+$) value in MeCN for TMG is 23.3 and 13.6 in H$_2$O[113,114]). There is, however, the possibility of further stabilisation of this structure by N-H⋯O=C interactions between the carbonyl O atom of the carbamato groups and the H atom attached to the imine N atom in the TMG ligands. According to the X-ray diffraction analysis, these H⋯O contacts measure ca. 214-215 pm in **6**. Hydrogen bonds are not responsible for the η^1-coordination mode and further in this work are presented experimental evidence which clearly show that the electron density accumulation due to the guanidine ligands is the decisive effect.

2.2.3 Reaction of [ZnEt(O$_2$CN(*i*Pr)$_2$)]$_4$ with BTMGN

Further experiments were carried out with the chelating bisguanidine BTMGN. Reaction between [ZnEt(O$_2$CN(*i*Pr)$_2$)]$_4$ and 4 equivalents of BTMGN leads to the mononuclear complex [(BTMGN)ZnEt(O$_2$CN(*i*Pr)$_2$)] (**7**). Crystals suitable for X-ray diffraction were grown from toluene solutions at -20°C. **Figure 2.28** displays the obtained molecular structure (see **Table 2.8** for selected structural parameters).
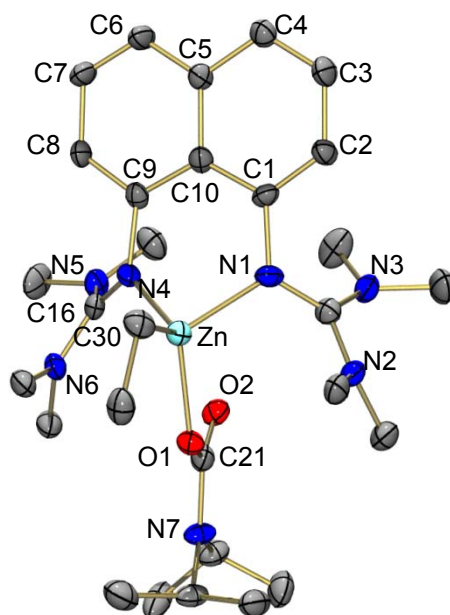
Figure 2.28 Molecular structure of **7**. Thermal ellipsoids are drawn at the 50% probability level; light-blue Zn, blue N, red O, grey C

Table 2.8 Selected bond distances (in pm) and angles (in deg.) for **7** as determined by X-ray diffraction.

C1-N1	1.417(10)	C8-N2	1.421(10)
N1-C11	1.325(11)	N2-C16	1.307(10)
C11-N3	1.379(11)	C16-N5	1.368(11)
C11-N4	1.336(11)	C16-N6	1.346(11)
Zn-N1	2.060(7)	Zn-N2	2.074(7)
Zn-C21	2.004(7)	Zn-O1	1.987(4)
C21-C22	1.518(9)	O1-C23	1.280(8)
C23-O2	1.237(8)	C23-N7	1.399(8)
Zn⋯O2	309.5		
N1-Zn-N2	86.1(2)	O1-Zn-C21	110.4(2)
N1-Zn-O1	107.5(2)	N2-Zn-O1	110.0(2)
N1-Zn-C21	121.4(3)	N2-Zn-C21	119.0(3)
Zn-O1-C23	120.4(4)	O1-C23-O2	125.7(6)
Zn-N1-C1	117.6(5)	Zn-N2-C8	116.2(5)
Zn-N1-C11	123.6(6)	Zn-N2-C16	125.1(6)
C1-N1-C11	118.7(7)	C8-N2-C16	118.7(7)
N1-C11-N3	123.5(8)	N2-C16-N5	124.5(8)
N1-C11-N4	121.4(8)	N2-C16-N6	120.1(8)
N3-C11-N4	115.1(7)	N5-C16-N6	115.3(7)
N1-C1-C10	120.8(7)	N2-C8-C10	121.4(7)

Most importantly, the carbamate ligand is η^1-coordinated, like in complex **6**. In this case there is no possibility for hydrogen bonding from the guanidine ligand to the carbonyl O atom of the carbamate ligand. The structure thus confirms that indeed the stronger basicity of the guanidine is responsible for the change in the carbamato coordination mode. The Zn-O distance in **7** [198.7(4) pm] is slightly larger than the Zn-O distances in **6** [196.3(1) and 195.3(1) pm]. As already observed in the case of complexes of group 10 metals with BTMGN ligand,[115] the metal is not located in the plane defined by the naphthalene aromatic system. Hence in **7**, the Zn atom is 122.0 pm above this plane.

However, in contrast to the Pd and Pt complexes [(BTMGN)PdCl$_2$] and [(BTMGN)PtCl$_2$] the naphthyl system in **7** remains planar. At 206.0(7) and 207.4(7) pm, the two Zn-N distances from the Zn to the directly bound N atoms of the BTMGN ligand are relatively large. For comparison, the two Zn-N distances from the Zn to the two directly bound N atoms of the TMG ligands in **6** are below 200 pm [199.7.4(1) and 198.7(1) pm].

At first glance it is surprising that no disproportionation and formation of [(BTMGN)Zn(O$_2$CNR$_2$)$_2$] is observed, in sharp contrast to the reaction with TMG. The BTMGN ligand is less flexible than the two TMG ligands, so that steric constraints are most likely the reason for this difference. The carbamato ligand is sterically more demanding than the ethyl group. It is, however, noteworthy in this context that in the crystalline phase the carbamate unit and not the ethyl group is located between the two guanidine units of the BTMGN ligand (see **Figure 2.29**).

Figure 2.29 Molecular structure of **7**. Thermal ellipsoids are drawn at the 50% probability level; light-blue Zn, blue N, red O, grey C
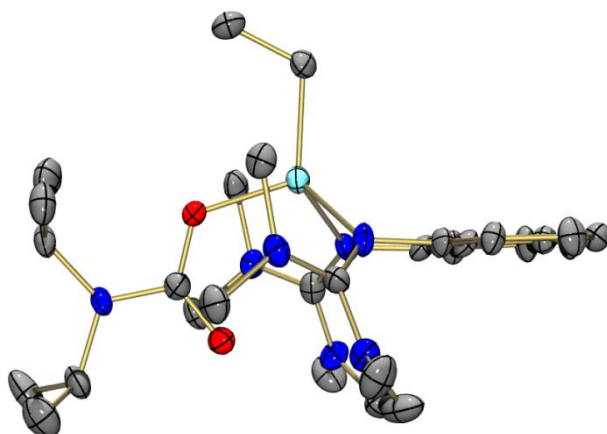
The complex [(BTMGN)ZnEt(O$_2$CN(*i*Pr)$_2$)] represents the first example of a structurally characterized monomeric alkylzinc carbamate. These species usually tend to form oligomers, like the [ZnEt(O$_2$CNR$_2$)]$_4$ tetramers (R = *i*Pr and *i*Bu) used in

this work. The complex is also quite stable compared to the related [(BTMGN)ZnEt$_2$] complex.[116]

Finally, it was obtained the trinuclear species [(BTMGN)Zn$_3$Et$_3$(O$_2$CN(*i*Pr)$_2$)$_3$] (**8**), by reaction of [ZnEt(O$_2$CN(*i*Pr)$_2$)]$_4$ with 2 equivalents of BTMGN. **Figure 2.30** displays its molecular structure.
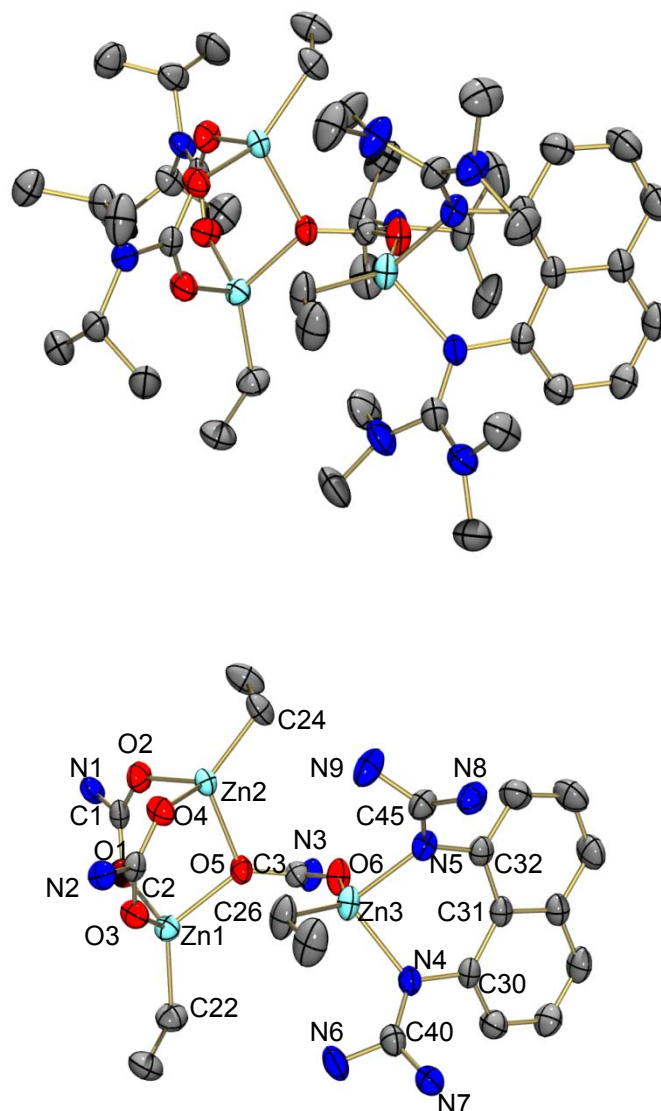

Figure 2.30 Molecular structure of **8**. Thermal ellipsoids are drawn at the 50% probability level; light-blue Zn, blue N, red O, grey C

Selected structural parameters are listed in **Table 2.9**. The complex can be described as a Lewis acid-base complex between [ZnEt(O$_2$CN(*i*Pr)$_2$)]$_4$ and **7**.

Complex [(BTMGN)Zn$_3$Et$_3$(O$_2$CN(iPr)$_2$)$_3$] (**8**) it is therefore most likely formed by reaction between **7** and remaining oligonuclear ethyl zinc carbamate species in the solution. To test this hypothesis compound **7** was treated with [ZnEt(O$_2$CN(iPr)$_2$)]$_4$ in a 2:1 molar ratio. The NMR spectra indeed indicated formation of **8**. Similar to the situation in **7**, the Zn atom is disploacted (by 85.5 pm in this case) from the plane defined by the naphthalene aromatic system. The carbamate unit connecting the mononuclear part with the dinuclear part of the complex adopts a η^{1,2}O-η^{3}O' coordination mode. As anticipated, the Zn3-O6 bond is significantly shorter than the Zn1-O5 and Zn2-O5 bonds, in agreement with the bonding situation in [ZnEt(O$_2$CN(iPr)$_2$)]$_4$, also featuring η^{1,2}O-η^{3}O' coordinated carbamato ligands.

Table 2.9 Selected bond distances (in pm) and angles (in deg.) for **8** as determined by X-ray diffraction.

Zn1-O1	199.0(2)	Zn2-O2	201.6(2)
Zn1-O3	195.80(19)	Zn2-O4	197.8(2)
Zn1-O5	208.5(2)	Zn2-O5	208.57(19)
Zn1-C22	198.9(3)	Zn2-C24	198.3(3)
Zn3-O6	199.6(2)	Zn3-C26	197.5(3)
Zn3-N4	205.2(3)	Zn3-N5	207.1(2)
C1-O1	125.9(4)	C1-O2	126.9(4)
C2-O3	127.5(3)	C2-O4	126.3(3)
C3-O5	129.4(3)	C3-O6	125.2(3)
C1-N1	137.2(4)	C2-N2	136.8(3)
C3-N3	135.5(4)	C30-N4	142.1(4)
C32-N5	141.1(3)	C45-N5	132.7(4)
C45-N8	136.0(4)	C45-N9	135.1(4)
C40-N4	132.2(4)	C40-N6	135.3(4)
O1-Zn1-O3	99.95(9)	O1-Zn1-O5	99.29(9)
O3-Zn1-O5	98.13(8)	O1-Zn1-C22	107.39(11)
O3-Zn1-C22	133.34(12)	O5-Zn1-C22	113.41(12)

O2-Zn2-O4	108.40(9)	O2-Zn2-O5	97.88(9)
O4-Zn2-O5	94.18(8)	O2-Zn2-C24	114.66(12)
O4-Zn2-C24	114.54(12)	O5-Zn2-C24	124.24(12)
Zn1-O5-Zn2	104.27(8)	N4-Zn3-N5	87.14(9)
N4-Zn3-O6	99.91(10)	N4-Zn3-C26	116.64(14)
N5-Zn3-O6	99.59(9)	N5-Zn3-C26	114.78(13)
O6-Zn3-C26	129.68(12)	Zn3-N4-C40	119.2(2)
Zn3-N5-C45	116.93(19)	Zn3-N4-C30	122.25(19)
Zn3-N5-C32	123.95(18)	N5-C45-N8	124.1(3)
N5-C45-N9	119.4(3)	N8-C45-N9	116.4(3)
N4-C40-N6	119.5(3)	N4-C40-N7	124.2(3)
N6-C40-N7	116.2(3)	O1-C1-O2	124.9(3)
O3-C2-O4	125.2(2)	O5-C3-O6	123.3(2)

2.3 Synthesis and thermal decomposition of oligonuclear mixed Zn/Co carbamates

2.3.1 Synthesis of some new $CoCl_2$ complexes

The reaction of $EtZnN(iPr)_2$ (or a $Et_2Zn/HN(iPr)_2$ mixtures) with CO_2 to give the tetranuclear complex $[ZnEt(O_2CN(iPr)_2)]_4$, was already presented in the previous part. This carbamate is easy to synthesize in high yield and was therefore used to accomplish the next step of the precursor synthesis, together with the methyl derivative $[ZnMe(O_2CN(iPr)_2)]_4$.[43] It has been shown before [117,118] that N-bases could break up these tetrameric carbamate units to give (in dependence of the reaction conditions and the specific base) tris-, bis- or mononuclear carbamates. Therefore the initial idea was to attach an N-base to the neutral ligands L in Co^{II} halide complexes of the general formula L_2CoCl_2. To this end were synthesized three different $CoCl_2$ complexes and tested their reaction with the tetrameric carbamate, namely the tetrahedral complexes $[CoCl_2(MAP)_2]$ (**9**), $[CoCl_2(MAEP)]$ (**10**), as well as the octahedral complex $[CoCl_2(MAEP)_2]$ (**11**) (see **Scheme 2.4**).
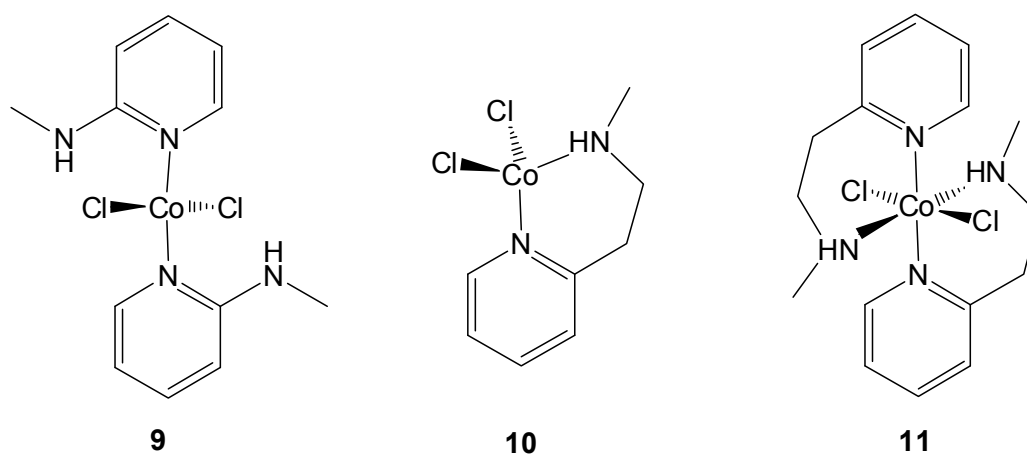
Scheme 2.4 Schematic structure of the CoCl$_2$ complexes

The crystal structures of these three complexes, which were not reported up to date, are shown in **Figure 2.31** and **Figure 2.32**. In complexes **10** and **11**, but not in **9**, the amino arms of the pyridine ligands coordinate to the Co atom.
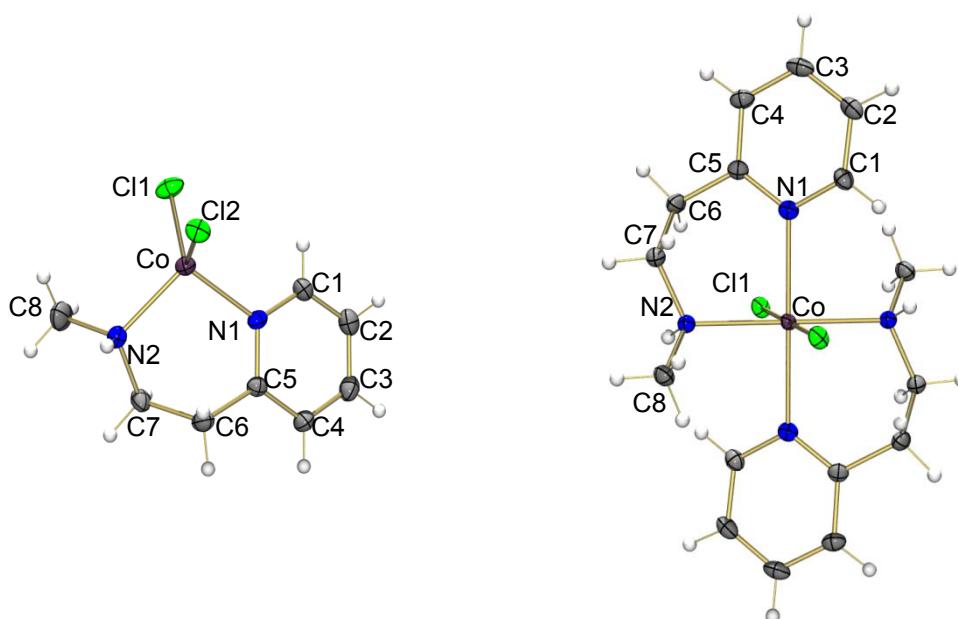
Figure 2.31 Molecular structure of **10** left and **11** right side.

Thermal ellipsoids are drawn at the 50% probability level;

purple Co, blue N, grey C, green Cl, white H
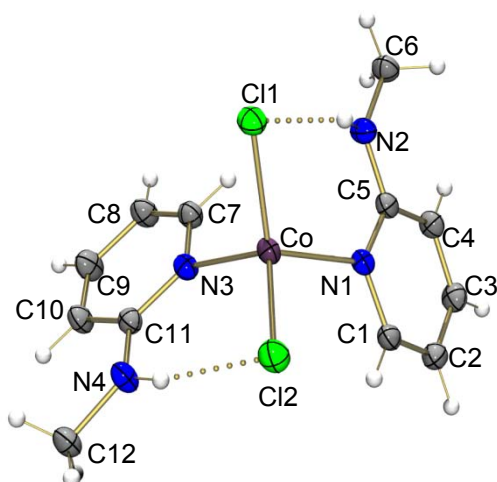
Figure 2.32 Molecular structure of **9**.

Thermal ellipsoids are drawn at the 50% probability level;

purple Co, blue N, grey C, green Cl, white H

An interesting and possibly important structural detail to appreciate the reactivity of this complex (see discussion below) is the presence of H⋯Cl bonding in **9**, leading to a slight weakening of the Co-Cl bond. Structural parameters for all three complexes are provided in **Tables 2.10**, **Table 2.11** and **Table 2.12**.

Table 2.10 Selected bond distances (in pm) and bond angles (in deg.) as measured for **9** as determined by X-ray diffraction.

Co-Cl1	224.93(6)	Co-Cl2	224.35(6)
Co-N1	204.86(14)	Co-N3	204.21(14)
N3-C11	136.0(2)	N1-C5	135.50(19)
C11-N4	135.1(2)	C5-N2	134.9(2)
N4-C12	145.3(2)	N2-C6	145.2(2)
N3-C7	135.9(2)	N1-C1	135.7(2)
C7-C8	136.8(2)	C1-C2	136.4(2)
C8-C9	140.0(2)	C2-C3	140.4(2)
C9-C10	136.7(2)	C3-C4	136.9(2)
C10-C11	141.0(2)	C4-C5	140.9(2)

N2-H…Cl1	244.9(3)	N4-H…Cl2	251.1(3)
Cl1-Co-Cl2	113.67(2)	N1-Co-N3	102.36(5)
N1-Co-Cl1	113.36(4)	N1-Co-Cl2	106.57(4)
N3-Co-Cl1	106.71(4)	N3-Co-Cl2	113.73(4)

Table 2.11 Selected bond distances (in pm) and bond angles (in deg.) as measured for **10** as determined by X-ray diffraction.

Co-Cl1	223.40(8)	Co-Cl2	224.88(10)
Co-N1	203.4(2)	Co-N2	204.2(2)
N1-C1	134.8(4)	N1-C5	135.8(4)
C8-N2	148.2(3)	C7-N2	148.4(4)
C1-C2	137.2(4)	C2-C3	139.8(4)
C3-C4	137.3(4)	C4-C5	138.2(4)
C5-C6	150.1(4)	C6-C7	152.8(4)
N2-H…Cl1	423.10(13)	N2-H…Cl2	322.75(8)
Cl1-Co-Cl2	118.38(3)	N1-Co-N2	100.11(9)
N1-Co-Cl1	106.50(7)	N1-Co-Cl2	111.39(7)
N2-Co-Cl2	106.49(8)	N2-Co-Cl1	112.50(7)

Table 2.12 Selected bond distances (in pm) and bond angles (in deg.) as measured for **11** as determined by X-ray diffraction.

Co-Cl1	247.78(6)	Co-Cl1'	247.78(6)
Co-N1	223.69(16)	Co-N2	217.94(16)
N1-C1	134.4(2)	N1-C5	135.1(2)
C8-N2	148.2(2)	C7-N2	148.2(2)
C1-C2	138.6(3)	C2-C3	138.1(3)
C3-C4	139.1(3)	C4-C5	139.5(2)
C5-C6	150.1(3)	C6-C7	152.8(3)
N2-H…Cl1	293.58(8)		

Cl1-Co-Cl1'	180.0	N1-Co-N1'	180.0
N2-Co-N2'	180.0		
N2-Co-N1'	91.27(6)	N2'-Co-N1	91.27(6)
N2'-Co-N1'	88.73(6)	N2-Co-N1	88.73(6)
N2-Co-Cl1'	90.64(4)	N2'-Co-Cl1	90.63(4)
N2'-Co-Cl1'	89.37(4)	N2-Co-Cl1	89.36(4)
N1'-Co-Cl1'	93.50(4)	N1-Co-Cl1	93.50(4)
N1-Co-Cl1'	86.50(4)	N1'-Co-Cl1	86.50(4)

2.3.2 Reaction between CoCl$_2$ complexes and tetrameric zinc carbamate

Interestingly, complexes **10** and **11** showed no sign of reaction with [ZnEt(O$_2$CN(iPr)$_2$)]$_4$. On the other hand, reaction of complex **9** with [ZnEt(O$_2$CN(iPr)$_2$)]$_4$ in toluene solution yielded a new Co and Zn containing, intensively purple-coloured product **12** in 34 % yield. The UV/Vis spectrum of a solution of **12** in toluene is displayed in **Figure 2.33**, together with that of **9**.
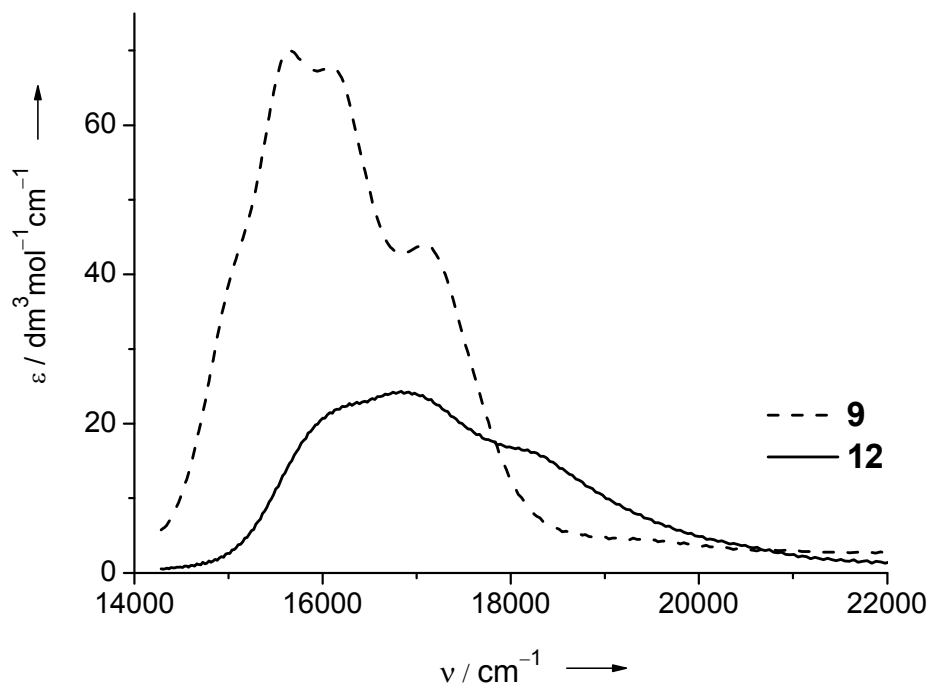
Figure 2.33 UV/Vis spectrum of **12** in toluene. For comparison the UV/Vis spectrum of the starting Co complex **9** is also displayed

Both spectra feature at least three absorptions with maxima of intensity at 15640, 16100 and 17100 cm^{-1} for **9** and ca. 16200, 16900 and 18200 cm^{-1} for **12**. The spectrum of **12** can also be compared with that obtained previously for the Co carbamate complex $[Co(O_2C(NEt_2)_2)]_6$,[41] and proves the presence of Co atoms in product **12**.

AAS measurements returned an average Zn : Co molar ratio of 2.5 : 1.5 for **12**. Crystals of **12** were grown from toluene solutions at -20°C. The X-ray diffraction analysis of these crystals showed the presence of tetranuclear clusters of the general formula $[M_4Et_2(O_2CN(iPr)_2)_6]$ (M = Co or Zn atoms), in which the four metal ions are connected through bridging carbamate units. As anticipated, it was not possible to distinguish unambiguously between Zn and Co atoms purely on the basis of the structure derived from X-ray diffraction.

Two of the metal ions carry terminal ethyl ligands and were therefore tentatively assigned to Zn. Because the ethyl groups were attached to Zn atoms in the reactant $[ZnEt(O_2CN(iPr)_2)]_4$, it is likely that these metals are also Zn atoms in the product **12**.

On the basis of the AAS studies, in half of the complexes the two remaining metal sites are occupied by Co, and in the other half by one Zn and one Co. Thus the crystal should consist of an equimolar mixture of the two complexes $[Zn_2Co_2Et_2(O_2CN(iPr)_2)_6]$ and $[Zn_3CoEt_2(O_2CN(iPr)_2)_6]$. The molecular structure as derived from X-ray diffraction is presented in **Figure 2.34**. Selected structural parameters are listed in **Table 2.13**.

For the two sites which are occupied either by Zn or Co atoms, the shortest metal-oxygen bond distance measures 195.5(2) pm (Zn/Co-O2) and the largest 237.3(2) pm (Zn/Co-O4). The coordination around the metal atoms can be compared with that in $[Co_6(O_2CNEt_2)_{12}]$,[41] for which variations between 197 and 215 pm were measured for the Co-O bond distances. The variations in the EtZn-O bond distances are smaller (194.3(2) – 207.56(19) pm).

Like in $[Co_6(O_2CNEt_2)_{12}]$[41], the O-M-O (M = Zn/Co) angles cover a large range from 59.96(8)° (O3-Zn/Co-O4) to 163.93(7)° (O4-Zn/Co-O6). For comparison, the O-Co-O bond angles in $[Co_6(O_2CNEt_2)_{12}]$ fall in the range 78.4(6)° - 171.1(6)°.

Figure 2.34 Molecular structure of **12**. Thermal ellipsoids are drawn at the 50% probability level, purple Zn/Co; light-blue Zn, blue N, red O, grey C

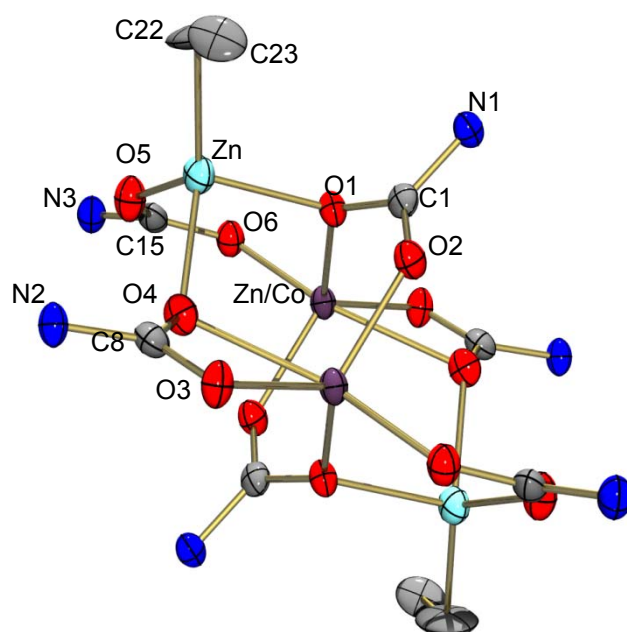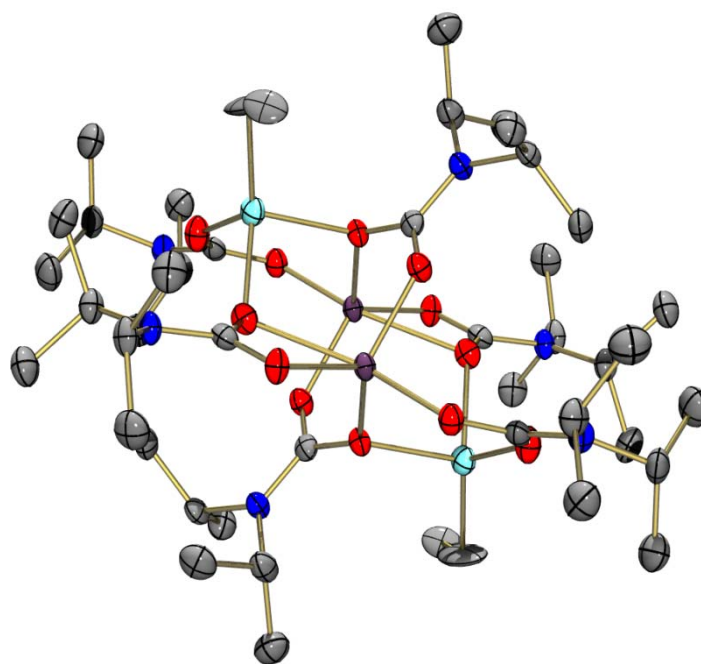**Table 2.13** Selected bond distances (in pm) and bond angles (in deg.) as measured for **12** as determined by X-ray diffraction.

Zn-O1	207.56(19)	Zn-O5	194.3(2)
Zn-O4	203.2(2)	Zn-C22	205.9(2)
Zn/Co-O1	199.5(2)	Zn/Co-O2	195.5(2)
Zn/Co-O3	198.78(19)	Zn/Co-O4	237.3(2)
Zn/Co-O6	196.3(2)		
O1-Zn-O5	100.98(8)	O4-Zn-O1	93.33(8)
O4-Zn-O5	99.48(9)		
C22-Zn-O4	120.99(9)	C22-Zn-O5	125.34(11)
C22-Zn-O1	110.70(8)		
O1-Zn/Co-O2	113.55(8)	O1-Zn/Co-O3	118.22(8)
O1-Zn/Co-O4	87.94(8)	O1-Zn/Co-O6	97.74(9)
O2-Zn/Co-O3	120.52(9)	O2-Zn/Co-O4	95.95(8)
O2-Zn/Co-O6	95.52(9)	O3-Zn/Co-O4	59.96(8)
O3-Zn/Co-O6	104.36(8)	O4-Zn/Co-O6	163.93(7)
Zn-O1-Zn/Co	110.25(9)	Zn-O4-Zn/Co	111.73(9)
Zn/Co-O2-Zn/Co	0.00(2)	Zn/Co-O3-Zn/Co	0.00(3)
Zn/Co-O4-Zn/Co	0.000(18)	Zn/Co-O6-Zn/Co	0.00(5)
O1-C1-O2	121.4(3)	O3-C8-O4	118.1(3)
O5-C15-O6	123.8(3)		

During the refinement of the structure a disorder of the Et groups was detected. A problem which remained was the high rest electron density near the Zn atoms. The rest electron density can be explained by the presence of some molecules in which instead of Et groups Cl is connected to the zinc atom (in average every fourth Et group is replaced by Cl).

SQUID data for complex **12** were also recorded. **Figure 2.35** and **Figure 2.36** show the dependence of the magnetic susceptibility on the temperature for **12** as derived from SQUID measurements. With 2.35 K cm^3 mol^{-1}, the χT value at 300 K is as expected slightly lower than the spin only value for 1.5 N$_A$ magnetically non-coupled Co atoms in one mole substance (2.81 K cm^3 mol^{-1}).
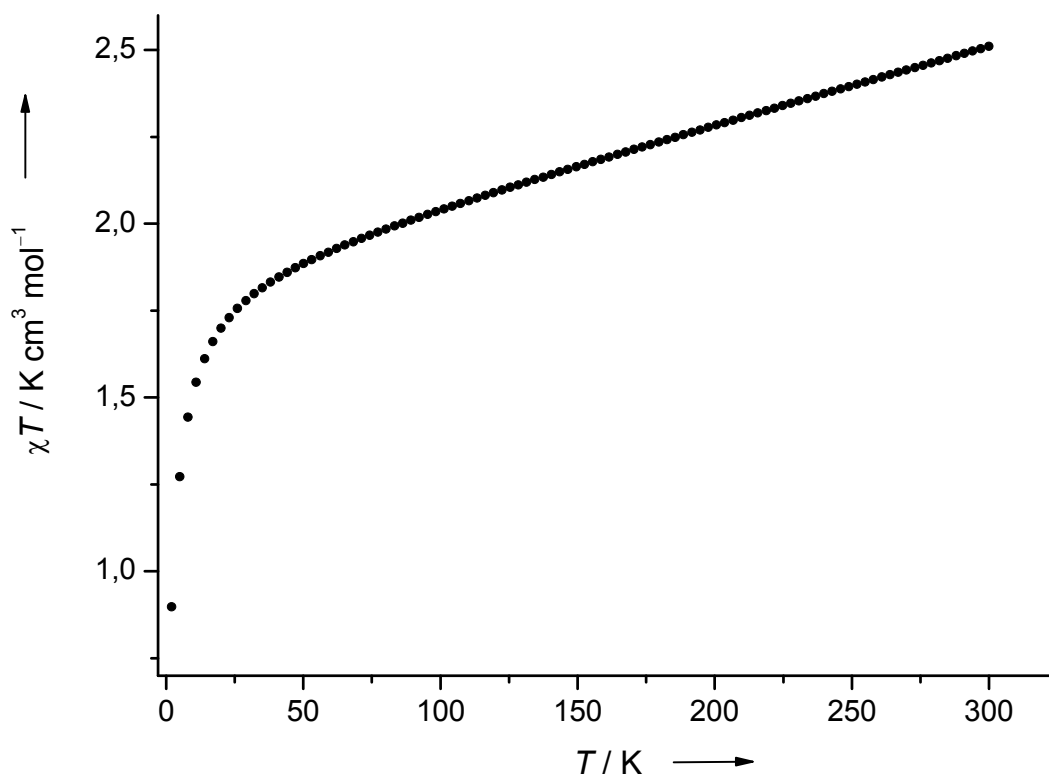
Figure 2.35 The χT vs T plot from SQUID measurements (at 500 Oe) as recorded for **12**

The χ^{-1}-T curve shown in **Figure 2.36** follows for temperatures above 50 K the Curie-Weiss law with a Weiss temperature Θ of -16.1 K and a Curie constant C of 0.40 cm^3 K mol^{-1}. As anticipated, the $\chi T - T$ curve indicates weak antiferromagnetic coupling of the Co^{II} ions in [Zn$_{2.5}$Co$_{1.5}$Et$_2$(O$_2$CN(*i*Pr)$_2$)$_6$].
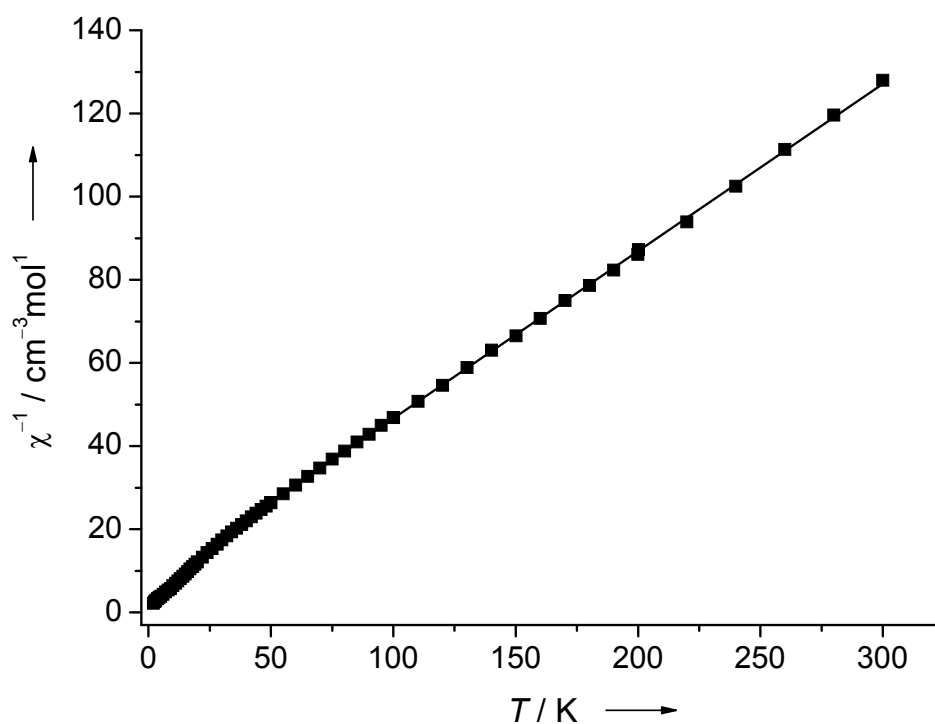
Figure 2.36 The χ^{-1} vs *T* plot from SQUID measurements (at 500 Oe) as recorded for **12**

The complex **12** turned out to be extremely reactive. Thus from solutions of **12** in hexane a new carbamate complex was crystallized, which turned out to be an octanuclear complex featuring two oxygen atoms in the center but no more ethyl groups, namely [$M_8(\mu_4\text{-O})_2(O_2CN(i\text{Pr})_2)_{12}$] (M = Zn or Co) (**13**) with an average Zn:Co ratio of 5:3. The molecular structure is visualized in **Figure 2.37**. Structural parameters are provided in **Tables 2.14**.
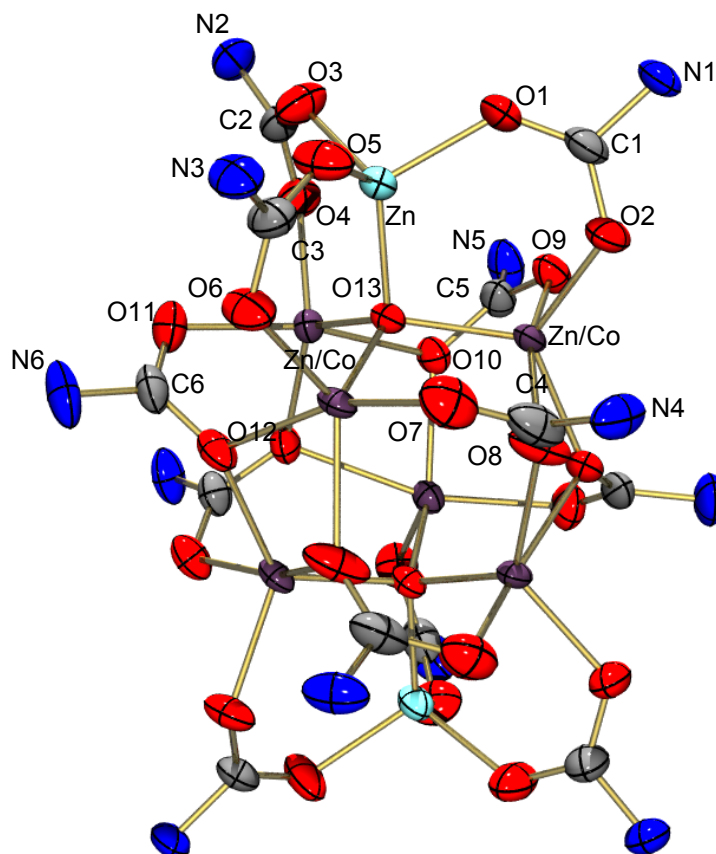
Figure 2.37 Molecular structure of **13**.

Thermal ellipsoids are drawn at the 50% probability level;

purple Zn/Co, light-blue Zn, blue N, red O, grey C, isopropyl groups not shown

The structure of this complex can be compared directly with that of the Zn complex [$Zn_8(\mu_4\text{-}O)_2(O_2CN(iPr)_2)_{12}$], which has previously been synthesized.[53]

Table 2.14 Selected bond distances (in pm) and bond angles (in deg.) as measured for **13** as determined by X-ray diffraction.

|			
Zn-O1	193.7(8)	Zn-O3	195.5(7)
Zn-O5	196.3(8)	Zn-O13	194.5(7)
Zn/Co-O2	195.5(8)	Zn/Co-O13	196.8(7)
Zn/Co-O7	203.8(8)	Zn/Co-O12	203.8(8)
Zn/Co-O9	216.2(8)	Zn/Co-O4	196.8(8)

Zn/Co-O8	207.8(8)	Zn/Co-O11	217.1(8)
Zn/Co-O6	196.4(8)	Zn/Co-O10	209.2(7)
O1-Zn-O13	115.5(3)	O1-Zn-O3	104.9(3)
O1-Zn-O5	104.6(4)	O5-Zn-O13	113.8(3)
O3-Zn-O5	104.1(3)	O3-Zn-O13	112.9(3)
O13-Zn/Co-O2	113.8(3)	O2-Zn/Co-O7	123.0(3)
O13-Zn/Co-O7	123.0(3)	O2-Zn/Co-O12	91.8(3)
O13-Zn/Co-O12	96.2(3)	O7-Zn/Co-O12	86.0(3)
O2-Zn/Co-O9	89.7(3)	O13-Zn/Co-O9	92.4(3)
O7-Zn/Co-O9	84.7(3)	O12-Zn/Co-O9	169.7(3)
Zn/Co-O4-Zn/Co	0.00(9)	Zn/Co-O2-Zn/Co	0.00(6)
Zn/Co-O6-Zn/Co	0.00(7)	Zn/Co-O7-Zn/Co	0.00(11)
Zn/Co-O8-Zn/Co	0.00(8)	Zn/Co-O9-Zn/Co	0.00(7)
Zn/Co-O10-Zn/Co	0.00(4)	Zn/Co-O11-Zn/Co	0.00(9)
Zn/Co-O12-Zn/Co	0.00(6)	Zn/Co-O13-Zn/Co	0.00(6)
O1-C1-O2	123.0(10)	O3-C2-O4	125.7(9)
O5-C3-O6	124.5(10)	O7-C4-O8	123.0(10)
O9-C5-O10	121.8(8)	O11-C6-O12	122.6(10)

From solutions of **12** in CH_3CN the tetranuclear complex $[M_4(\mu_4\text{-}O)(O_2CN(i\text{Pr})_2)_6]$ (M = Zn or Co) (**14**) was crystallized, with one oxygen atom in its center. Like in **12**, the Zn:Co ratio amounts to 2.5:1.5. The molecular structure is visualized in **Figure 2.38**. Structural parameters are provided in **Tables 2.15**.

The structure is similar to those reported previously for a number of $[Zn_4(\mu_4\text{-}O)(O_2CNR_2)_6]$ complexes (e.g. R = iPr or Et).[53]
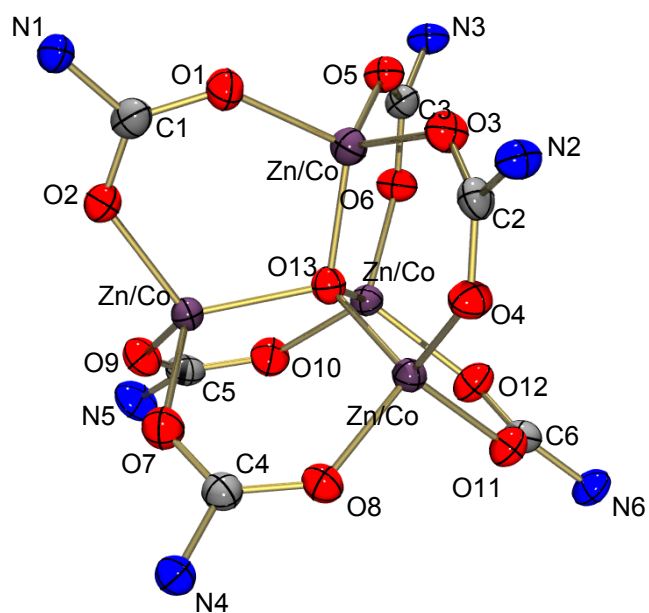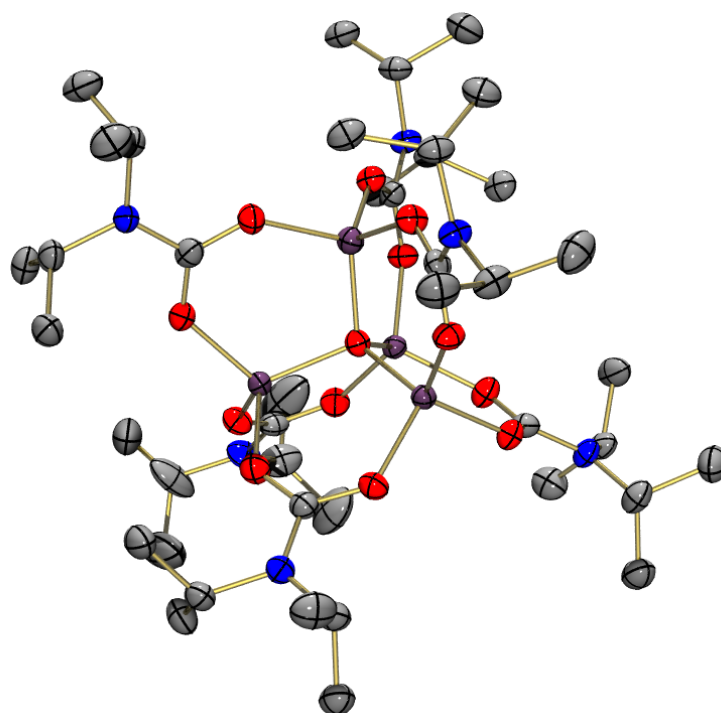
Figure 2.38 Molecular structure of **14**. Thermal ellipsoids are drawn at the 50% probability level; purple Zn/Co, blue N, red O, grey C

Table 2.15 Selected bond distances (in pm) and bond angles (in deg.) as measured for **14** as determined by X-ray diffraction.

Zn/Co-O1	194.9(3)	Zn/Co-O3	193.2(3)
Zn/Co-O5	193.3(3)	Zn/Co-O2	194.9(3)
Zn/Co-O9	193.7(3)	Zn/Co-O7	194.4(3)
Zn/Co-O10	195.2(3)	Zn/Co-O13	194.5(3)
Zn/Co-O11	195.5(3)	Zn/Co-O4	195.1(3)
Zn/Co-O8	196.5(3)	Zn/Co-O6	193.6(3)
Zn/Co-O12	192.9(3)		
O3-Zn/Co-O5	113.82(12)	O3-Zn/Co-O13	110.09(12)
O5-Zn/Co-O13	111.60(11)	O3-Zn/Co-O1	100.46(12)
O5-Zn/Co-O1	110.39(12)	O13-Zn/Co-O1	109.93(11)
O9-Zn/Co-O7	105.20(12)	O9-Zn/Co-O13	111.16(12)
O7-Zn/Co-O13	109.18(12)	O9-Zn/Co-O2	109.20(12)
O7-Zn/Co-O2	106.91(12)	O13-Zn/Co-O2	114.68(11)

Lamb *et al.* also reported already on the isolation of tetranuclear or octanuclear complexes in dependence of the solvent used for recrystallization $[Zn_4(\mu_4\text{-}O)(O_2CN(iPr)_2)_6]$ isolated e.g. from CH_3CN solutions and $[Zn_8(\mu_4\text{-}O)_2(O_2CN(iPr)_2)_{12}]$ isolated from alkane solutions.[53] Thus it is likely that **13** is formed by dimerization from **14**. All precautions were taken to avoid the presence of a significant amount of water in the solvents. It is not yet clear if reactions with traces of water are responsible for the presence of the central oxygen atoms in **13** and **14**, or if the oxygen is delivered by the carbamate groups. The possibility of oxygen delivery by the carbamate groups finds support by the relatively high yield of more than 10 % for product **13**, and by the decomposition experiments in which oxygen atoms are also eliminated from the carbamate groups.

For complex **14** were recorded high resolution mass spectra. The M$^+$ group of peaks is visualized in **Figure 2.39** together with a simulated pattern including the complexes with four, three, two and one Co atom.
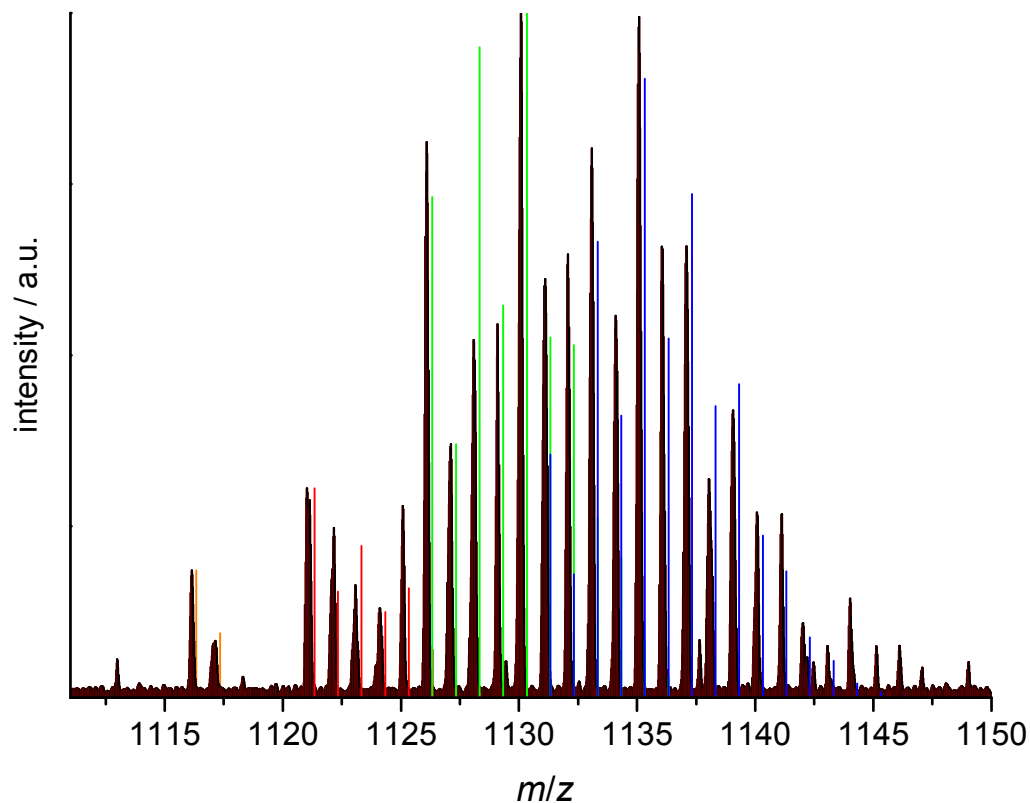
Figure 2.39 FD+ spectrum of **14** in solution measured spectrum (black trace) and a simulation of the most intense isotopic peaks: orange [Co$_4$(μ_4-O)(O$_2$CN(iPr)$_2$)$_6$], red [ZnCo$_3$(μ_4-O)(O$_2$CN(iPr)$_2$)$_6$], green [Zn$_2$Co$_2$(μ_4-O)(O$_2$CN(iPr)$_2$)$_6$], blue [Zn$_3$Co(μ_4-O)(O$_2$CN(iPr)$_2$)$_6$]

It can be seen that the complexes with one [Zn$_3$Co(μ_4-O)(O$_2$CN(iPr)$_2$)$_6$] (blue trace) or two [Zn$_2$Co$_2$(μ_4-O)(O$_2$CN(iPr)$_2$)$_6$] (green trace) Co atoms contribute most to the pattern. This two complexes have a 1:1 contribution while the other two complexes are only in small traces. This 1:1 contribution of the [Zn$_3$Co(μ_4-O)(O$_2$CN(iPr)$_2$)$_6$] and [Zn$_2$Co$_2$(μ_4-O)(O$_2$CN(iPr)$_2$)$_6$] is in good agreement with the result obtained from the AAS measurements, showing that the ratio Zn : Co in these complexes is 2.5 : 1.5.

In another series of experiments was synthesized [Zn$_{2.5}$Co$_{1.5}$Me$_2$(O$_2$CN(iPr)$_2$)$_6$] (**15**) (similar to **12**, but with Me groups in place for the Et groups) from reaction between [ZnMe(O$_2$CN(iPr)$_2$)]$_4$ and [CoCl$_2$(MAP)$_2$] (**9**). The molecular structure for this molecule, which is as anticipated similar to **12**, is displayed in the **Figure 2.40**. Structural parameters are provided in **Tables 2.16**.
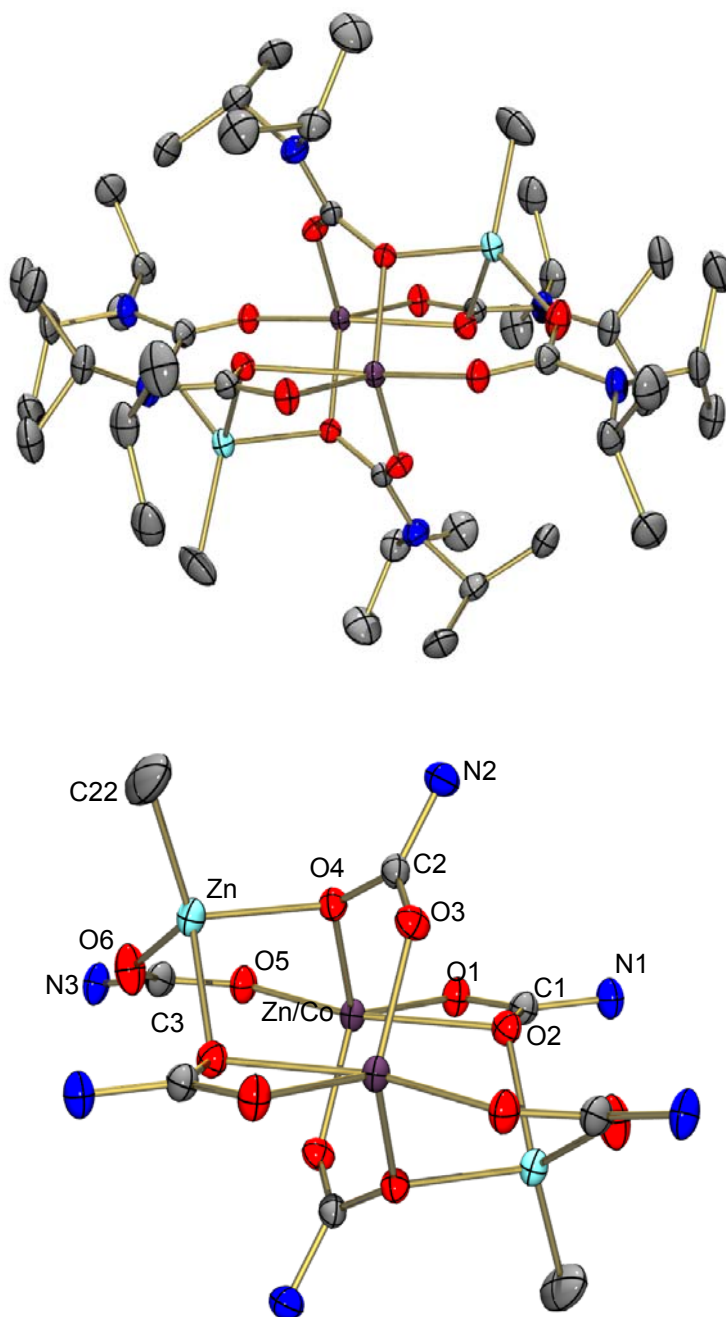
Figure 2.40 Molecular structure of **15**. Thermal ellipsoids are drawn at the 50% probability level; purple Co/Zn, light-blue Zn, blue N, red O, grey C

Table 2.16 Selected bond distances (in pm) and bond angles (in deg.) as measured for **15** as determined by X-ray diffraction.

Zn-O2	203.10(18)	Zn-O6	192.97(19)
Zn-O4	207.14(18)	Zn-C22	208.05(15)
Zn/Co-O1	200.92(18)	Zn/Co-O2	231.29(18)
Zn/Co-O3	196.72(18)	Zn/Co-O4	201.20(17)
Zn/Co-O5	196.63(18)		
O2-Zn-O6	99.07(8)	O4-Zn-O6	102.15(7)
O4-Zn-O2	93.51(7)	C22-Zn-O4	111.52(7)
C22-Zn-O6	124.84(8)	C22-Zn-O2	120.20(8)
C22-Zn-O2	120.20(8)	O4-Zn/Co-O3	119.40(7)
O1-Zn/Co-O4	114.40(8)	O3-Zn/Co-O5	97.10(8)
O2-Zn/Co-O4	87.70(7)	O5-Zn/Co-O4	96.74(8)
O1-Zn/Co-O3	118.11(8)	O1-Zn/Co-O2	60.66(7)
O2-Zn/Co-O3	92.85(7)	O2-Zn/Co-O5	165.30(7)
O1-Zn/Co-O5	104.91(7)	Zn-O4-Zn/Co	108.02(8)
Zn-O2-Zn/Co	113.46(8)	Zn/Co-O2-Zn/Co	0.000(19)
Zn/Co-O1-Zn/Co	0.000(18)	Zn/Co-O4-Zn/Co	0.00(3)
Zn/Co-O3-Zn/Co	0.00(3)		

The purpose of these experiments was to solve the disorder problem in the case of the Zn/Co mixed carbamate complex **12**. However, the problem with the rest electron density remained. The rest electron density can be explained by the presence of some molecules in which instead of Me groups Cl is connected to the zinc atom. In addition, new problem arises due to the disorder of the solvent molecules in the crystal.

### 2.3.3 Thermal decomposition of the mixed Zn/Co carbamate

Furthermore was studied thermal decomposition of the fully characterized molecular precursor **12**. The TG curve is plotted in **Figure 2.51** for three different heating rates (2, 5 and 10°C min^{-1}). It can be seen that the compound loses for all heating rates 76% of its initial mass, in pleasing agreement with the theoretical weight loss of 77% for decomposition to give $Zn_{2.5}Co_{1.5}O_4$.
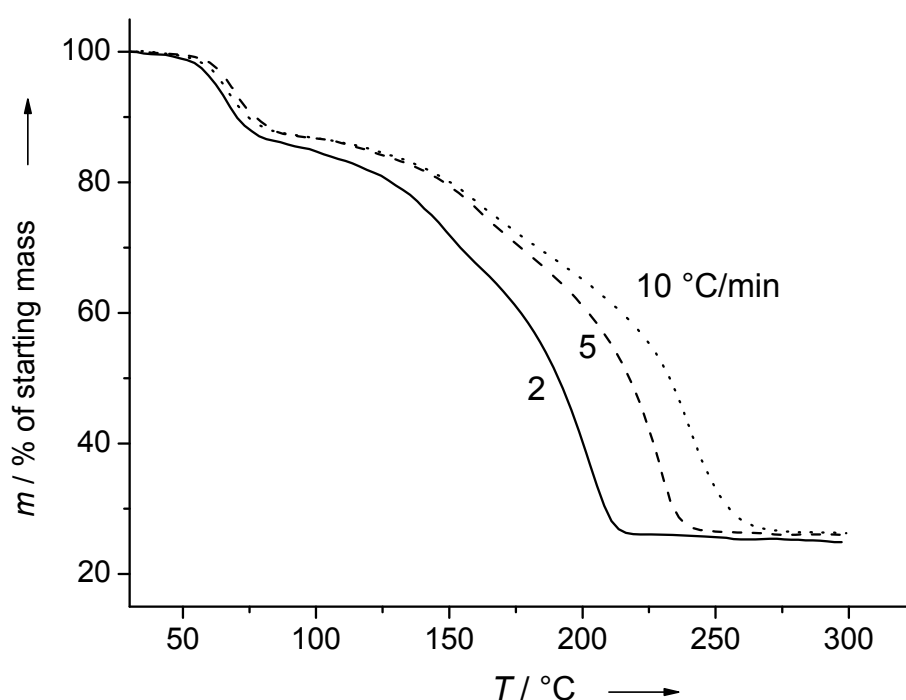
Figure 2.51 TG curve as recorded for **12** at different heating rates (2, 5, and 10°C min^{-1})

The process is finished at T = 205°C for a heating rate of 2°C min^{-1}, but requires temperatures of more than 250°C if the heating rate is increased to 10°C min^{-1}. This behaviour indicates kinetic control for high heating rates implying that decomposition is a relatively slow process. A similar behaviour was observed for decomposition of $[ZnEt(O_2CN(iPr)_2)]_4$ to give ZnO. The TG curves recorded for decomposition of **15** to yield $Zn_{2.5}Co_{1.5}O_4$ are virtually identical to those recorded for **12**.

A typical powder diffractogram after heating **12** with a heating rate of 5°C min^{-1} to an end temperature of 300°C is displayed in **Figure 2.52**. It shows the presence of two phases: a wurtzite (ZnO) phase and a distorted sodium chloride (CoO) phase. The presence of two phases has also been observed in other ZnO-CoO solid solutions. For example, hydrolysis of zinc and cobalt salts in polyol medium was shown to lead to a similar two-phase system.[102]
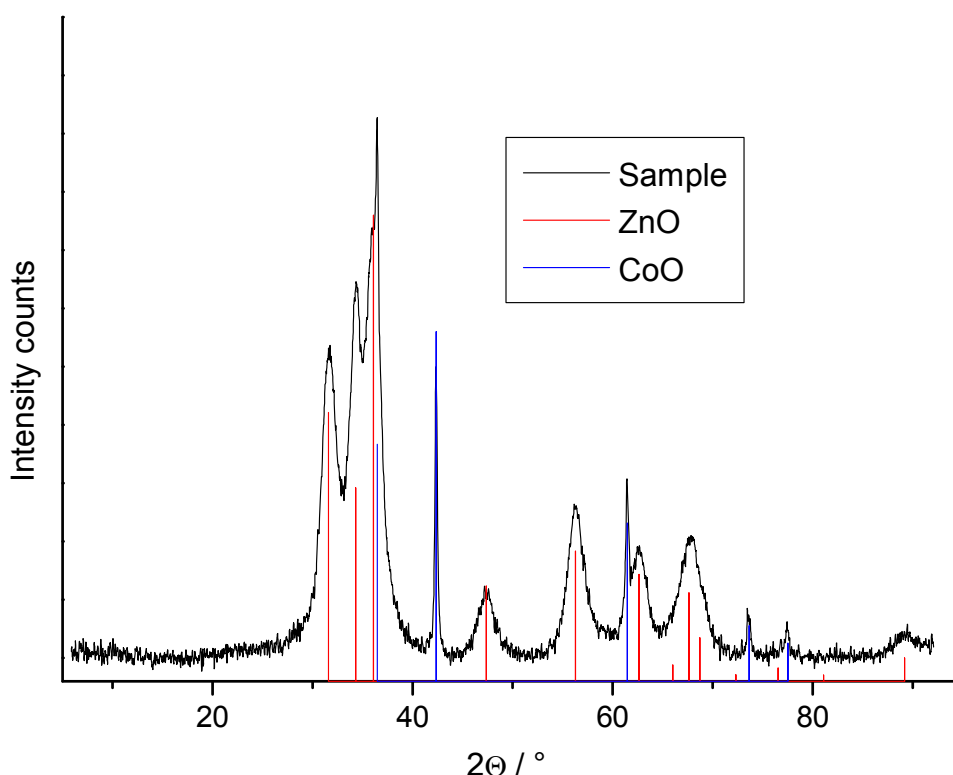
Figure 2.52 Powder diffraction patterns (black trace) as measured after heating of **12** to 300°C with a heating rate of 5°C min^{-1}. The inserted lines are taken from the database for ZnO (red trace) and CoO (blue trace)

The mean particle size was calculated, based on the Debye-Scherrer equation, from the line broadening in the diffractogramme. For CoO the particle size is ca. 47.7 nm based on the peak at 42.3 degrees. For ZnO the particle size is calculated to be 7.24 and 7.96 nm respectively (7.7 ± 0.4 nm) and is based on two peaks at 47.37 and 56.35 degrees.

These results are furthermore confirmed by a statistical evaluation from the TEM measurements (see **Figure 2.53**) giving a mean particle size of 25±1 nm. This value is in good to excellent agreement with the results for the particle size determination obtained from BET measurements (BET surface: 37.2 m^2 g^{-1}).
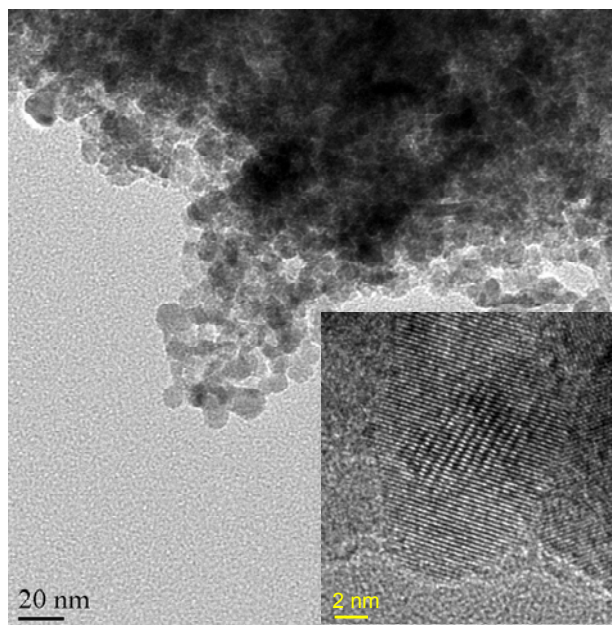

Figure 2.53 TEM image showing the Zn/Co oxide nanoparticles formed by heating **12** to 300°C (heating rate 5°C min^{-1})

An EDX analysis of the Zn/Co oxide particles (**Figure 2.54**) shows the presence of ca. 1.8% of carbon impurities which might be due to adsorbed solvent molecules. Solvent adsorption is found regularly for ZnO formation in polyol solvents. All these results show that during the pyrolysis of **12** nanoparticles of definite shape and overall good particle size distribution are formed. This gives evidence that the pyrolysis proceeding at low temperatures of 200°C is finally a controlled process as otherwise not so well defined particles in terms of size and crystalline behaviour would be expected as the product.
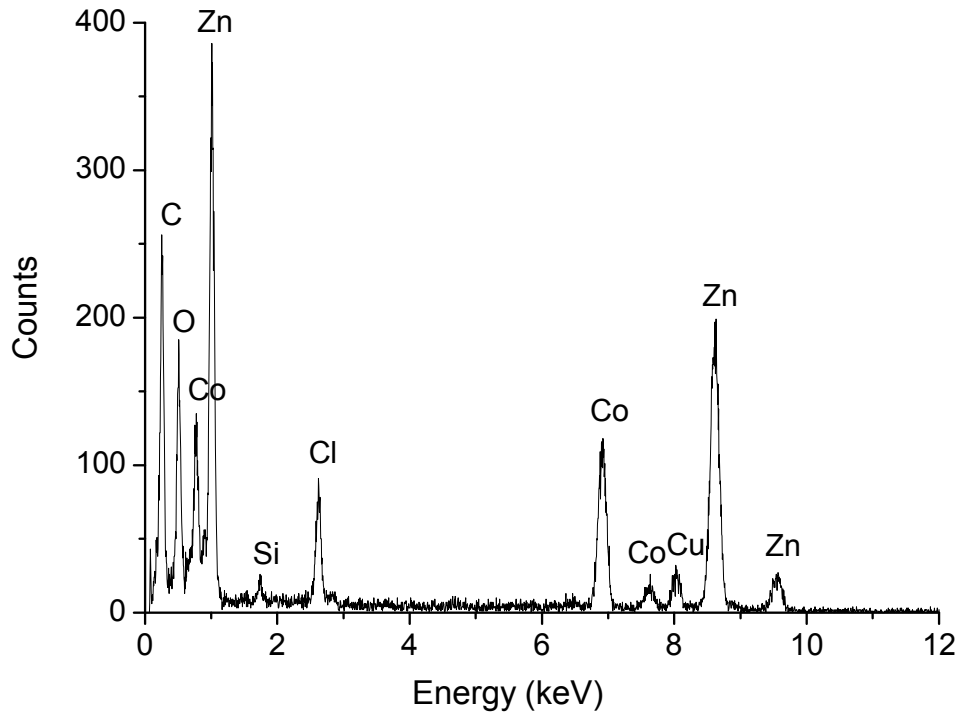
**Figure 2.54** EDX analysis of the Zn/Co oxide particles

The photocatalytic activity of the Zn/Co mixed oxide particles was tested by degrading methylene blue solution (see **Figure 2.55**) under UV illumination (254 nm). The results indicate that this compound has no photocatalytic activity.
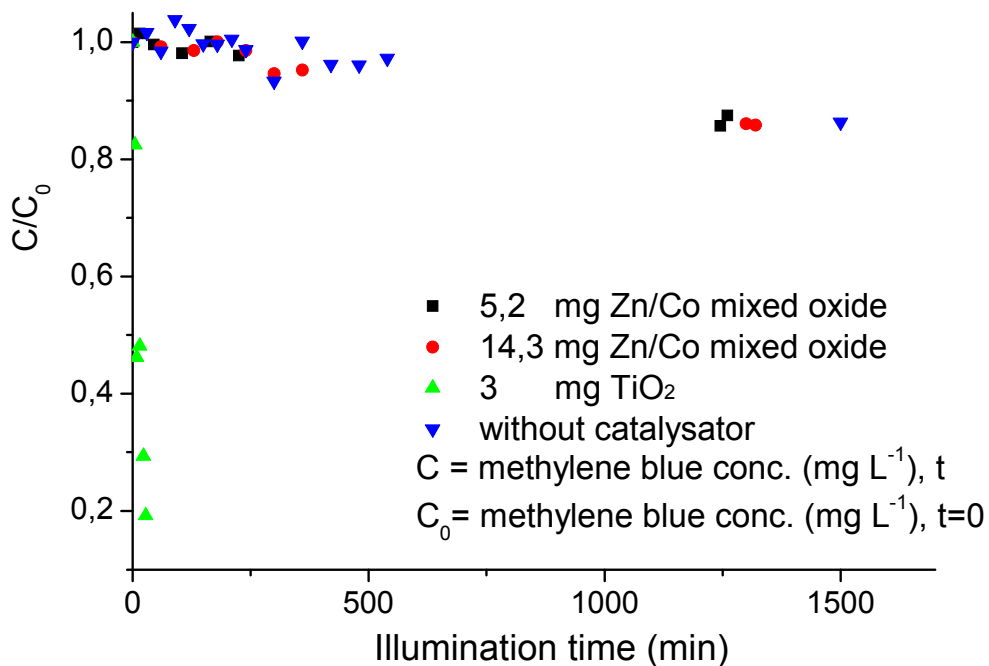
Figure 2.55 Photocatalytic investigation of the Zn/Co mixed oxide

2.4 Synthesis and thermal decomposition of oligonuclear mixed Zn/Mn carbamates

As already presented in the previous part, the fragmentation of the tetranuclear Zn carbamate complex $[ZnEt(O_2CN(iPr)_2)]_4$ by N-bases was studied. Motivated by these studies, the purpose was to synthesize new mixed carbamates by reaction of this tetramer with a transition metal complex to which ligands with secondary amine groups are attached. The base fulfils two tasks: first it should break up the tetrameric unit, and secondly it should provide protons for ethane abstraction. Therefore were synthesized three Mn(II) dichloride complexes, containing as ligands the bases pyridine, MAP or MAEP (see **Scheme 2.5**).

py   MAP   MAEP
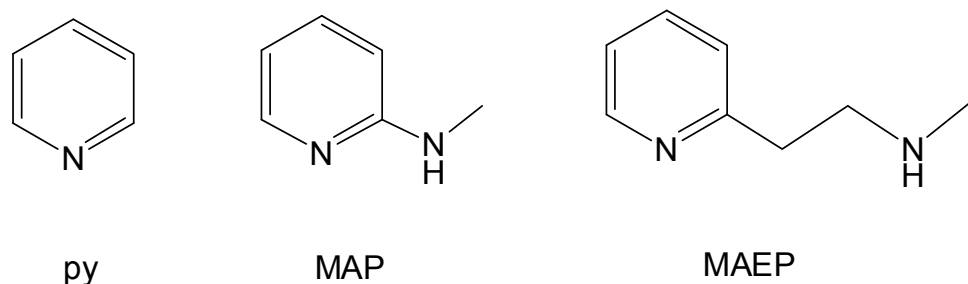
Scheme 2.5 Schematic structure of the bases pyridine, MAP or MAEP

2.4.1 Synthesis of some new MnCl$_2$ complexes

The structure of $[(py)_2MnCl_2]$ (**16**) in the solid state was already determined previously and shown to consist of linear chains of octahedrally coordinated Mn(II) centers, in which all chlorides adopt bridging positions.[119] On the other hand, the structure of the complex $[MnCl_2(MAEP)]_n$ (**17**) was previously unknown. **Figure 2.56** displays the structure as determined from X-ray diffraction measurements. Again octahedral coordination is achieved, and both the pyridine N as well as the amino N atoms are bound to the Mn(II) centers. Linear chain as depicted in Figure 2.55 result. The Mn-Cl distances cover the range 253 – 261 pm, and the closest Mn$\cdots$Mn separations amount to 379.6(3) pm. Selected structural parameters are provided in **Tables 2.17**. In the case of the base MAP no crystal formation was monitored.
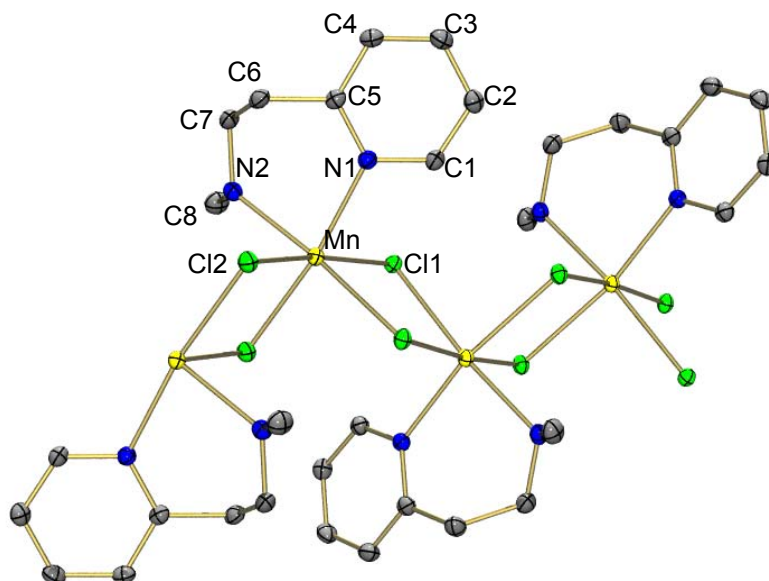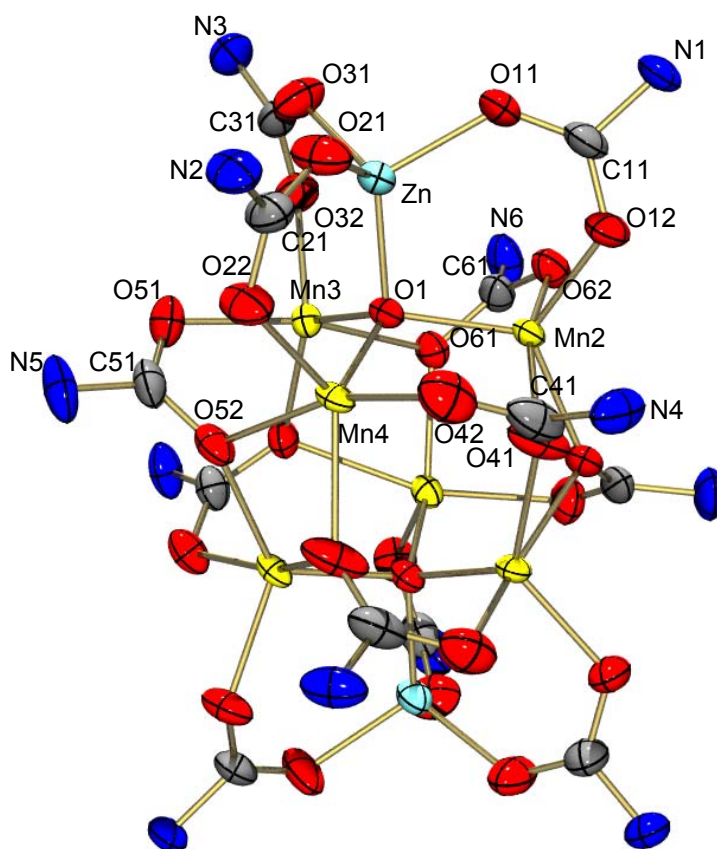
Figure 2.56 Molecular structure of **17**. Thermal ellipsoids are drawn at the 50% probability level; yellow Mn, green Cl, blue N, grey C

Table 2.17 Selected bond distances (in pm) and bond angles (in deg.) as measured for **17** as determined by X-ray diffraction.

Mn-N2	227.87(15)	Mn-N1	228.44(14)
Mn-Cl2	249.77(7)	Mn-Cl1	252.33(8)
N1-C1	134.4(2)	N1-C5	135.2(2)
N2-C8	147.5(2)	N2-C7	147.8(2)
N2-Mn-N1	88.63(5)	N2-Mn-Cl2	96.27(4)
N1-Mn-Cl2	94.68(4)	N2-Mn-Cl1	89.50(4)
N1-Mn-Cl1	87.44(3)	Cl1-Mn-Cl2	173.897(16)
C1-N1-C5	118.13(14)	C1-N1-Mn	114.90(10)
C8-N2-C7	111.21(13)	C5-N1-Mn	126.69(11)
C8-N2-Mn	115.31(10)	C7-N2-Mn	115.20(10)

2.4.2 Reaction between MnCl₂ complexes and tetrameric zinc carbamate

THF solutions of one of the three Mn complexes, formed from manganese dichloride and the ligand, were directly brought to reaction with a toluene solution of the zinc carbamate [ZnEt(O$_2$CN(iPr)$_2$)]$_4$. In the case of the ligands py and MAEP, the experiments gave no evidence for the formation of a mixed metal carbamate. On the other hand, reaction between [ZnEt(O$_2$CN(iPr)$_2$)]$_4$ and [(MAP)MnCl$_2$] (**18**) resulted in a solid product which was recrystallized from toluene to give colourless crystals of the octanuclear mixed metal carbamate [Zn$_2$Mn$_6$(μ_4-O)$_2$(O$_2$CN(iPr)$_2$)$_{12}$]. The molecular structure as derived from an X-ray analysis of the crystalline material is visualized in **Figure 2.57**. (see **Table 2.18** for selected structural parameters)

Figure 2.57 Molecular structure of **19**.

Thermal ellipsoids are drawn at the 50% probability level;

yellow Mn, light blue Zn, blue N, red O, grey C, isopropyl groups not shown

Table 2.18 Selected bond distances (in pm) and bond angles (in deg.) as measured for **19** as determined by X-ray diffraction.

Zn-O21	194.3(2)	Zn-O1	194.55(19)
Zn-O11	195.1(2)	Zn-O31	196.7(2)
Mn2-O1	204.9(2)	Mn2-O12	205.3(2)
Mn2-O62	211.4(2)	Mn2-O52	214.3(2)
Mn2-O41	222.7(2)	Mn3-O1	203.3(2)
Mn3-O32	204.5(2)	Mn3-O61	211.1(2)
Mn3-O51	212.0(2)	Mn4-O42	206.3(3)
Mn4-O1	206.76(19)	Mn4-O22	206.8(2)
Mn4-O52	219.9(2)		
O21-Zn-O1	113.05(9)	O21-Zn-O11	103.99(12)
O11-Zn-O1	114.78(10)	O21-Zn-O31	104.80(12)
O31-Zn-O1	116.80(9)	O11-Zn-O31	101.91(11)
O12-Mn2-O1	107.90(9)	O62-Mn2-O1	105.64(8)
O12-Mn2-O62	92.34(9)	O52-Mn2-O1	123.42(8)
O12-Mn2-O52	125.53(9)	O41-Mn2-O1	89.69(9)
O1-Mn3-O32	107.91(9)	O1-Mn3-O61	125.39(8)
O32-Mn3-O61	123.32(9)	O1-Mn3-O51	102.30(9)
O32-Mn3-O51	94.49(10)	O51-Mn3-O61	91.95(9)
O42-Mn4-O1	106.10(10)	O42-Mn4-O22	89.81(11)
O22-Mn4-O1	106.09(9)	O1-Mn4-O52	90.47(8)
O41-Mn4-O1	123.39(8)		

The structure can be described as follows. The six Mn atoms are arranged in the form of a highly distorsed trigonal antiprism. The trigonal faces are capped by OZn units. Three carbamate ligands on each side of the complex connect the Zn(II) with the Mn(II) centers in a μ^2 bonding mode. The two trigonal Mn3 units of the central trigonal antiprism are connected by additional six carbamate ligands with a μ_3 bonding mode. One of the carbamate oxygen atoms is bound to only one manganese ion, while the other carbamate oxygen is bound to one manganese ion of

the same trigonal face and in addition to one manganese ion from the other trigonal face of the Mn6 trigonal antiprism. The structure thus resembles the structures of the previously characterized octanuclear carbamate complexes [Zn$_8$(μ_4-O)$_2$(O$_2$CN(iPr)$_2$)$_{12}$][51], [Co$_8$(μ_4-O)$_2$(O$_2$CN(iPr)$_2$)$_{12}$][53], [Fe$_8$(μ_4-O)$_2$(O$_2$CN(iPr)$_2$)$_{12}$][120], [Zn$_2$Ni$_6$(μ_4-O)$_2$(O$_2$CN(iPr)$_2$)$_{12}$][54] and [Zn$_{8-n}$Mg$_n$(μ_4-O)$_2$(O$_2$CN(iPr)$_2$)$_{12}$].[57]

The magnetic curve of [Zn$_2$Mn$_6$(μ_4-O)$_2$(O$_2$CN(iPr)$_2$)$_{12}$] derived from SQUID measurements is presented in **Figure 2.58**.
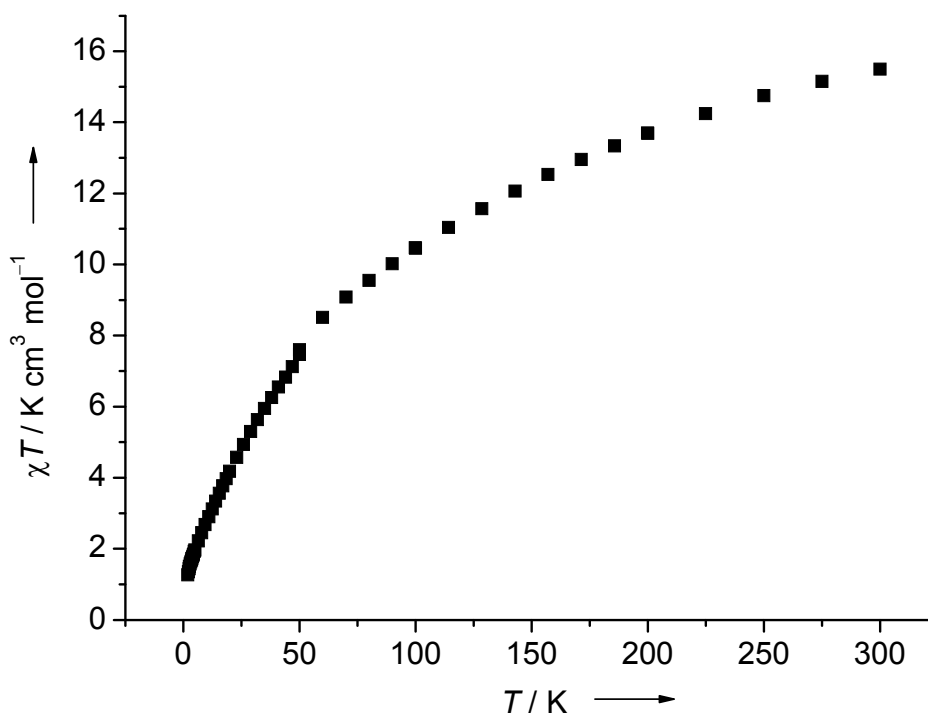

Figure 2.58 χT-T plot from SQUID measurements (at 500 Oe) as recorded for **19**

At 300 K, the χT value was found to be 15.6 K cm^3 mol^{-1}. In the absence of magnetic coupling between the Mn(II) centers and high spin configuration of each Mn(II) (S = 5/2), the maximum χT value for the 6 x 5 spins can be estimated to be 26.26 K cm^3 mol^{-1} (if g = 2 and spin-orbit coupling can be neglected). As anticipated, antiferromagnetic coupling between the spin centers reduces the χT value considerably. The behaviour at lower temperatures is in line with antiferromagnetic coupling resulting in a singlet ground electronic state.

The X-band EPR spectrum of the crystalline material [Zn$_2$Mn$_6$(μ_4-O)$_2$(O$_2$CN(iPr)$_2$)$_{12}$] at 295 K consists of a single broad signal, **Figure 2.59**, which is

consistent with weakly antiferromagnetically coupled Mn^{2+} ions (a similar spectrum was also observed in the case of the Mn carbamate $[Mn_6(O_2CNEt_2)_{12})]$[52]).
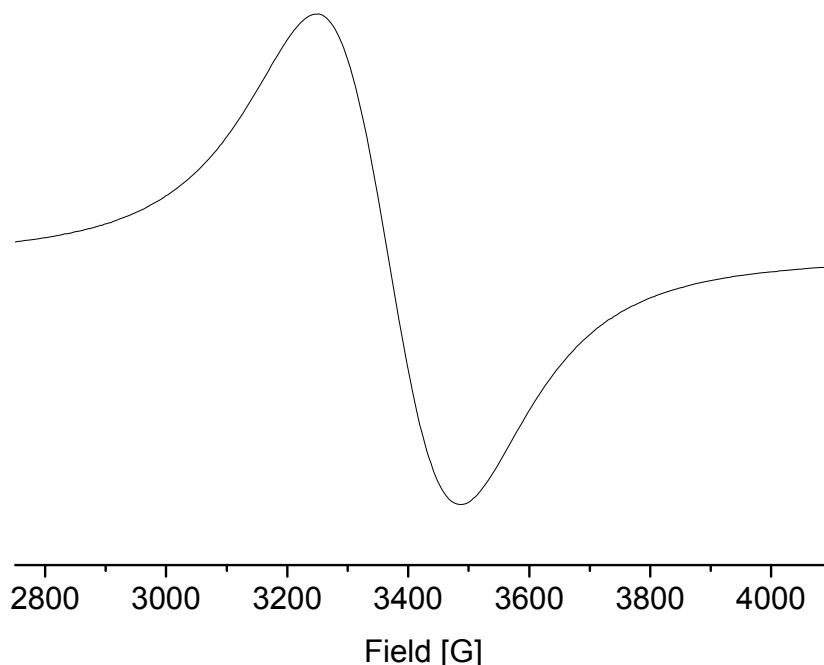

Figure 2.59 EPR spectrum of $[Zn_2Mn_6(\mu_4\text{-O})_2(O_2CN(i\text{Pr})_2)_{12}]$

Generally, the μ_4-O atoms in carbamate clusters arise from water which is added after carbamate formation to the solution. For example, $[Zn_4(\mu\text{-O})(O_2CNEt_2)_6]$ was prepared by addition of H_2O to a reaction mixture of $ZnEt_2$, $HNEt_2$ and CO_2.[51] In this case, no extra water was added in the synthesis of $[Zn_2Mn_6(\mu_4\text{-O})_2(O_2CN(i\text{Pr})_2)_{12}]$. The water needed to form the complex stems from the manganese dichloride, which is highly hygroscopic.

The amount of water present in the $MnCl_2 \cdot xH_2O$ ($x \leq 1$) was determined with the help of the TG measurements. TG curve as recorded for $MnCl_2 \cdot xH_2O$ ($x \leq 1$) with a 10°C min^{-1} heating rate is plotted in **Figure 2.60**. It can be seen that the compound loses, in the interval 100-150°C, 2% of its initial mass which represents 0.22 molecules H_2O. The H_2O can also be detected by IR spectroscopic measurements (see **Figure 2.61**).
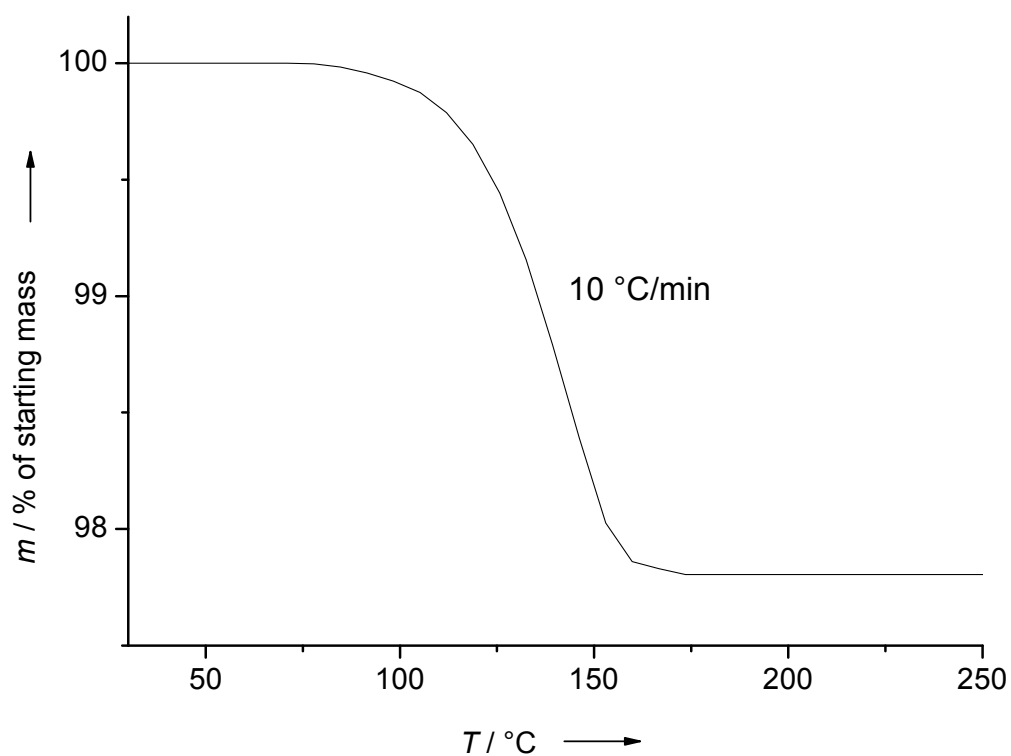
**Figure 2.60** TG curve as recorded for MnCl$_2$·xH$_2$O (x ≤ 1)
with a 10°C min^{-1} heating rate
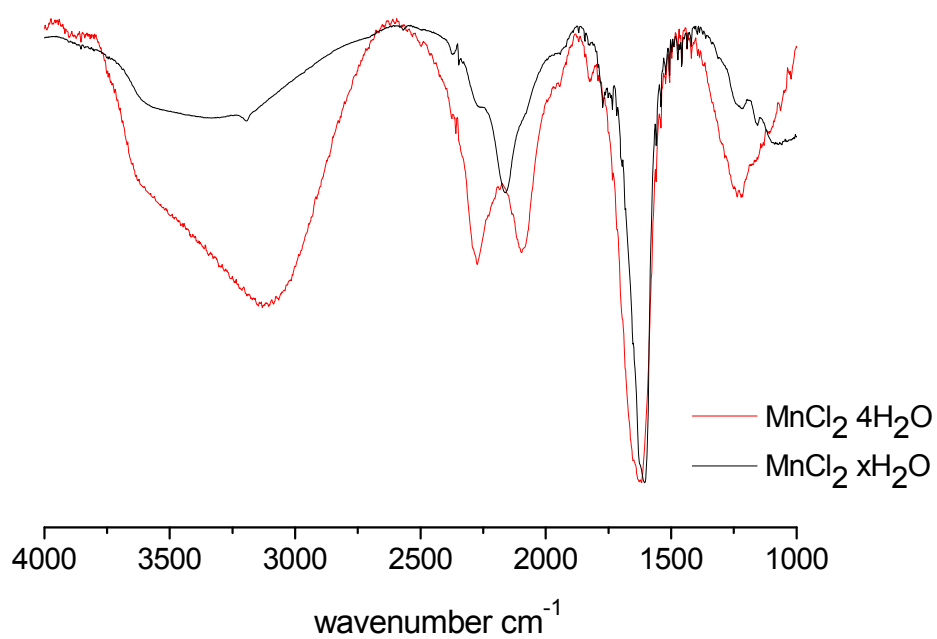
Figure 2.61 IR spectrum from MnCl$_2$·xH$_2$O (x ≤ 1) and MnCl$_2$·4H$_2$O

The amount of water is critical, and a larger excess of it reduces the yield. Hence if extra quantities of water were deliberately added ($MnCl_2 : H_2O$ = 1:2) to a mixture of the manganese dichloride, MAP and $[ZnEt(O_2CN(iPr)_2)]_4$, the only product isolated from the reaction mixture were the crystals of the salt $[(MAP)H]^+[(MAP)ZnCl_3]^-$ (**20**). The molecular structure as derived from an X-ray analysis of the crystalline material is visualized in **Figure 2.62**. Selected structural parameters are presented in **Table 2.19**.
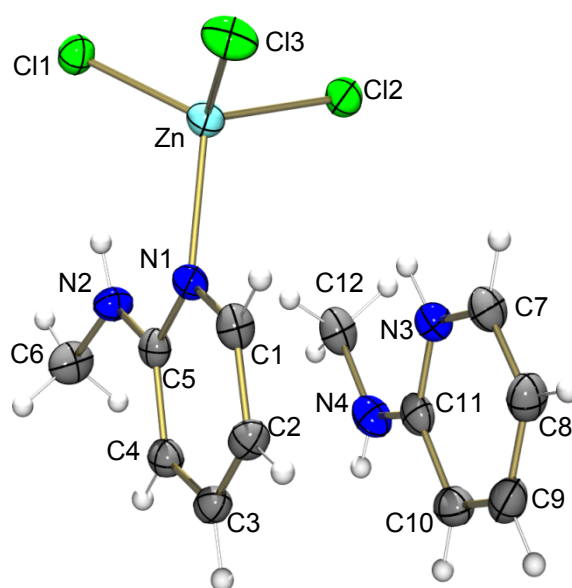

Figure 2.62 Molecular structure of **20**. Thermal ellipsoids are drawn at the 50% probability level; light blue Zn, blue N, green Cl, grey C and white H

Table 2.19 Selected bond distances (in pm) and bond angles (in deg.) as measured for **20** as determined by X-ray diffraction.

Zn-N1	205.2(2)	Zn-Cl2	224.72(7)
Zn-Cl3	225.72(8)	Zn-Cl1	227.64(8)
N1-C5	135.7(3)	N1-C1	135.9(3)
N2-C5	135.3(3)	N2-C6	145.6(3)
N2-H(N2)	83.(3)	N3-C11	134.6(3)
N3-C7	136.2(3)	N3-H(N3)	94.(3)

| N4-C11	133.0(4)	N4-C12	145.8(4)
N4-H(N4)	76.(3)		
N1-Zn-Cl1	106.85(6)	N1-ZnCl2	111.05(6)
N1-Zn-Cl3	106.34(6)	Cl2-Zn-Cl3	114.02(3)
Cl1-Zn-Cl2	109.39(3)	Cl1-Zn-Cl3	108.90(3)

When a solution of the carbamate $[Zn_2Mn_6(\mu_4\text{-}O)_2(O_2CN(iPr)_2)_{12}]$ was stirred under air, a colouring of the solution signals (partial) Mn(II) oxidation. First information about the product was derived from mass spectrometric data.
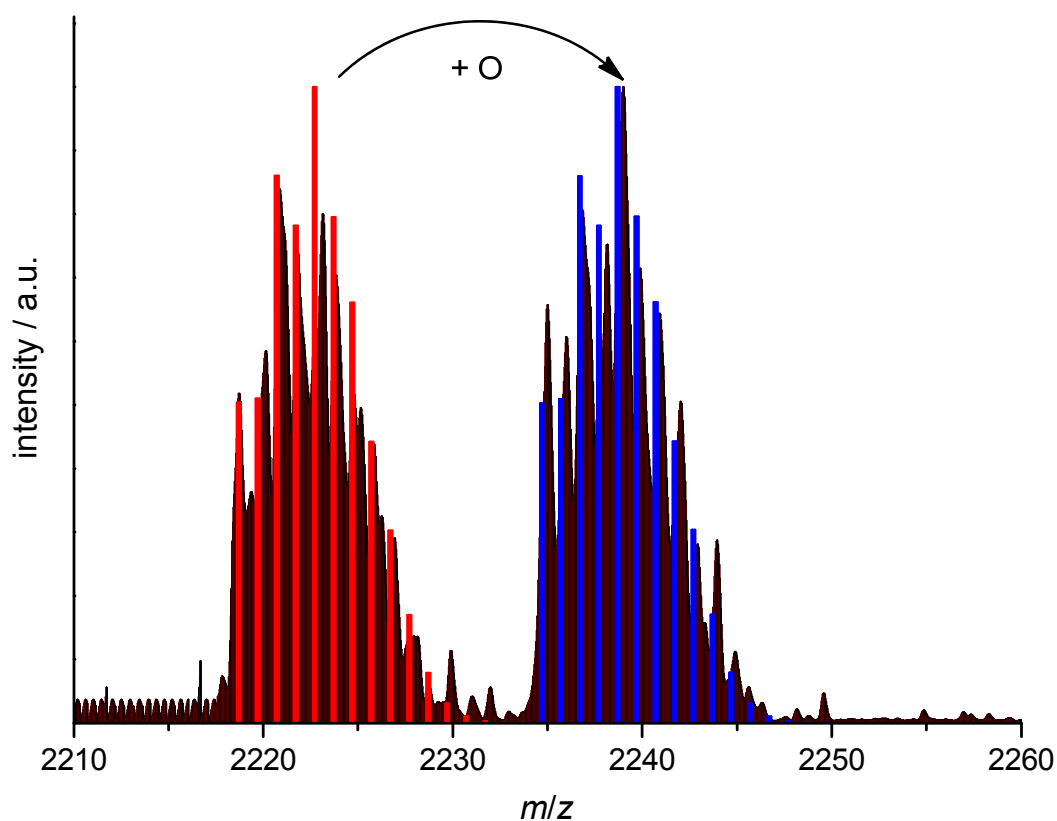
Figure 2.63 FD+ spectrum of $[Zn_2Mn_6(\mu_4\text{-}O)_2(O_2CN(iPr)_2)_{12}]$ in solution measured spectrum (black) and simulation of the most intense isotopic peaks: red $[Zn_2Mn_6(\mu_4\text{-}O)_2(O_2CN(iPr)_2)_{12}]$, blue $[Zn_2Mn_6(\mu_4\text{-}O)_2(\mu_3\text{-}O)(O_2CN(iPr)_2)_{12}]$

Figure 2.63 shows the region of the M^+ peak of $[Zn_2Mn_6(\mu_4\text{-}O)_2(O_2CN(iPr)_2)_{12}]$. The isotopic pattern fits nicely to the simulated pattern. In addition, a peak appears which can be explained by the uptake of one oxygen atom. After completion of the

oxidation process the peak due to [$Zn_2Mn_6(\mu_4\text{-}O)_2(O_2CN(iPr)_2)_{12}$] has disappeared completely (see **Figure 2.64**). The spectrum indicates that at this stage no product with two or more additional oxygen atoms is formed. It proved possible to crystallize the oxidation product, and **Figure 2.65** shows its molecular structure.
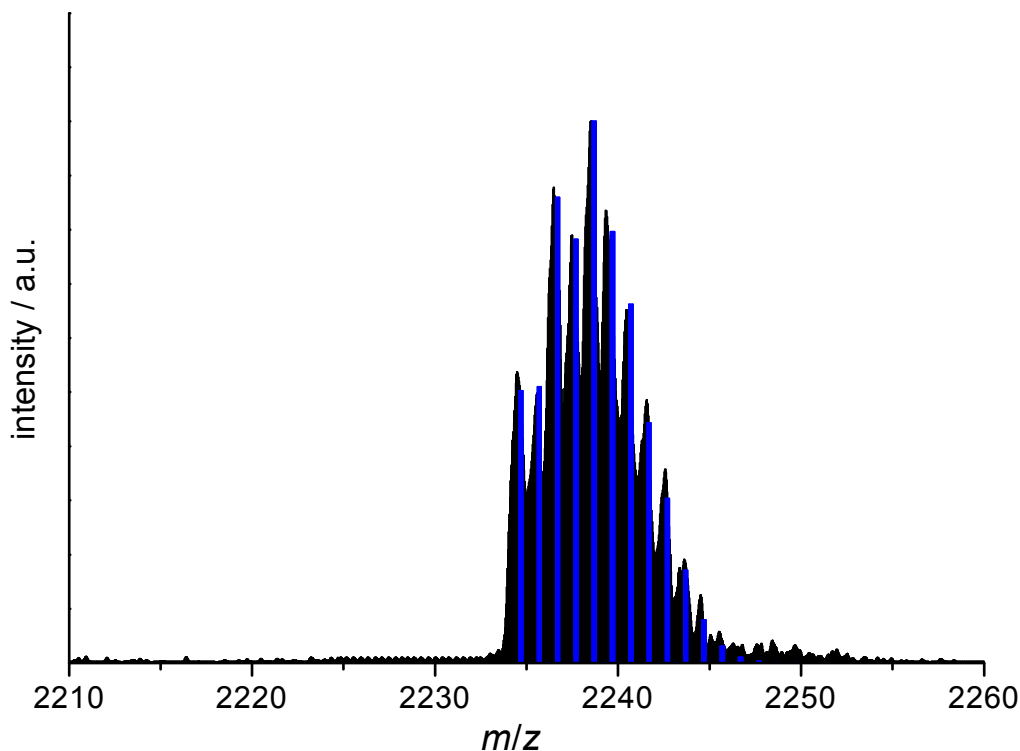
Figure 2.64 FD+ spectrum of [$Zn_2Mn_6(\mu_4\text{-}O)_2(\mu_3\text{-}O)(O_2CN(iPr)_2)_{12}$] in solution measured spectrum (black) and simulation of the most intense isotopic peaks (blue)

The void of the carbamate [$Zn_2Mn_6(\mu_4\text{-}O)_2(O_2CN(iPr)_2)_{12}$] is now filled with one oxygen atom, leading to the formula [$Zn_2Mn_6(\mu_4\text{-}O)_2(\mu_3\text{-}O)(O_2CN(iPr)_2)_{12}$]. The oxygen atom occupies two different sites in this void. Three of the six Mn atoms become sixfold coordinated by oxygen (distorted octahedral coordination mode). The six Mn atoms are now clearly arranged in a form of a trigonal antiprism. The six carbamate ligands bridging the two trigonal faces still adopt a μ_3-bonding mode. However, one of the carbamate oxygen atoms is now bound to two Mn centers of the same trigonal face of this antiprism, while the other oxygen atom is bound to only one

Mn ion of the other trigonal face. This change in the carbamate bonding mode relative to the situation before oxidation increases the void within the complex. **Figure 2.65** shows the molecular structure of $[Zn_2Mn_6(\mu_4\text{-}O)_2(\mu_3\text{-}O)(O_2CN(iPr)_2)_{12}]$ (**21**) determined from X-ray diffraction measurements. Selected structural parameters are presented in **Table 2.20**.
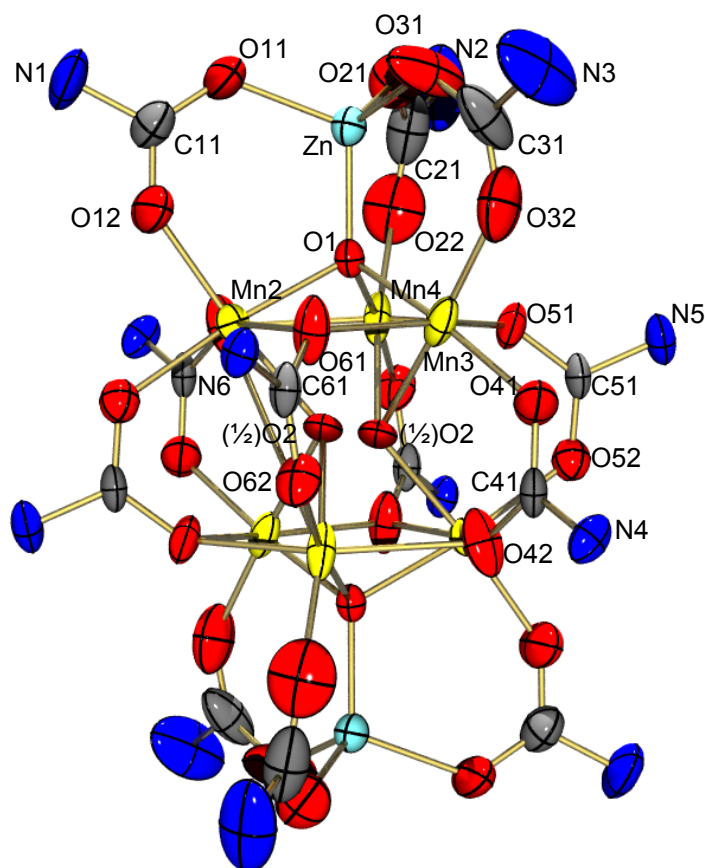
Figure 2.65 Molecular structure of **21**.

Thermal ellipsoids are drawn at the 50% probability level;

yellow Mn, light blue Zn, blue N, red O, grey C, isopropyl groups not shown

Table 2.20 Selected bond distances (in pm) and bond angles (in deg.) as measured for **21** as determined by X-ray diffraction.

Zn-O21	193.7(4)	Zn-O1	191.8(3)
Zn-O11	193.5(4)	Zn-O31	193.5(4)

Mn2-O1	198.6(3)	Mn2-O12	200.5(4)
Mn2-O61	228.8(3)	Mn2-O2	208.1(9)
Mn2-O41	218.6(3)	Mn3-O1	199.4(3)
Mn3-O32	201.2(5)	Mn3-O61	220.8(3)
Mn3-O51	229.2(3)	Mn3-O2	226.4(11)
Mn4-O1	200.0(3)	Mn4-O22	202.2(6)
Mn4-O51	218.1(3)	Mn4-O41	228.1(3)
Mn4-O2	247.1(11)	(½)O2-(½)O2	80.1(11)
O21-Zn-O1	112.40(15)	O21-Zn-O11	107.30(18)
O11-Zn-O1	111.22(14)	O21-Zn-O31	106.8(2)
O31-Zn-O1	111.77(14)	O11-Zn-O31	107.0(2)
O12-Mn2-O1	97.26(13)	O41-Mn2-O2	77.2(4)
O12-Mn2-O41	96.73(16)	O61-Mn2-O1	78.22(11)
O41-Mn2-O1	80.94(11)	O2-Mn3-O61	87.4(3)
O1-Mn3-O32	97.61(15)	O1-Mn3-O61	80.00(12)
O32-Mn3-O61	97.36(16)	O1-Mn3-O51	78.04(11)
O32-Mn3-O51	102.04(15)	O51-Mn3-O61	152.33(12)
O41-Mn4-O1	78.32(11)	O51-Mn4-O22	98.91(17)
O22-Mn4-O1	97.46(15)	O1-Mn4-O51	98.91(17)
O41-Mn4-O22	100.65(17)	O51-Mn3-O41	152.85(12)
O1-Mn4-O2	72.3(3)	O2-Mn4-O22	166.1(3)

The UV/Vis spectra recorded for $[Zn_2Mn_6(\mu_4\text{-}O)_2(\mu_3\text{-}O)(O_2CN(iPr)_2)_{12}]$ is compared to that of the initial $[Zn_2Mn_6(\mu_4\text{-}O)_2(O_2CN(iPr)_2)_{12}]$ complex in **Figure 2.66**. The main difference between the spectra before and after oxidation is the increase of the extinction coefficient upon oxidation. The $\chi T - T$ curve for $[Zn_2Mn_6(\mu_4\text{-}O)_2(\mu_3\text{-}O)(O_2CN(iPr)_2)_{12}]$ as derived from SQUID measurements is presented in **Figure 2.67**. As anticipated (simply on the basis of the reduced number of unpaired electrons), the χT value at room temperature (9.7 K cm^3 mol^{-1}) is smaller than that of the complex before oxidation (15.6 K cm^3 mol^{-1}).

90
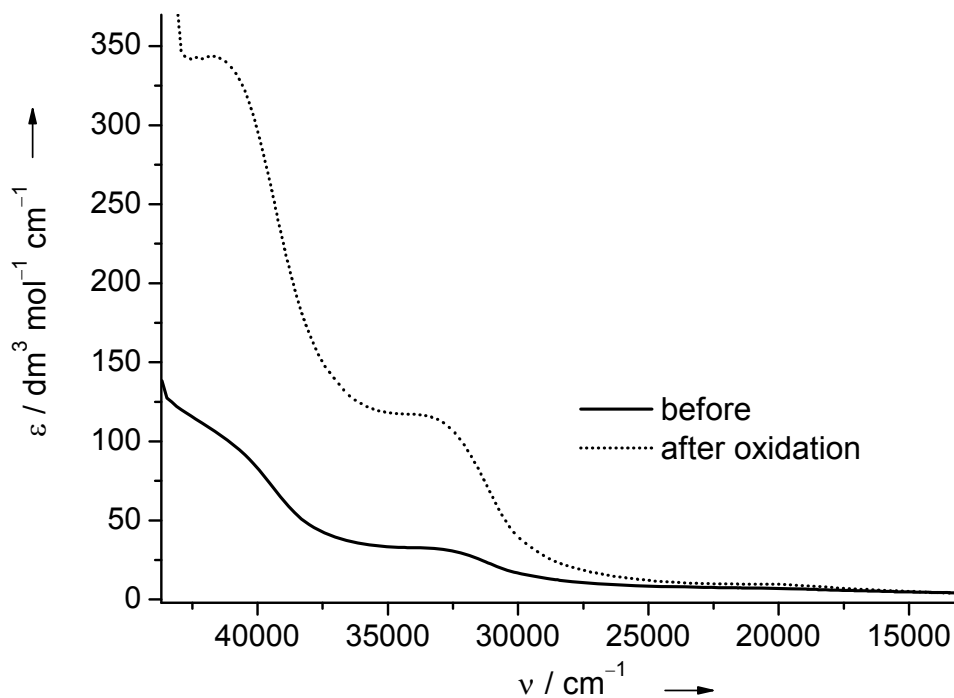
Figure 2.66 UV/Vis spectra as recorded for the carbamate complexes
before and after oxidation
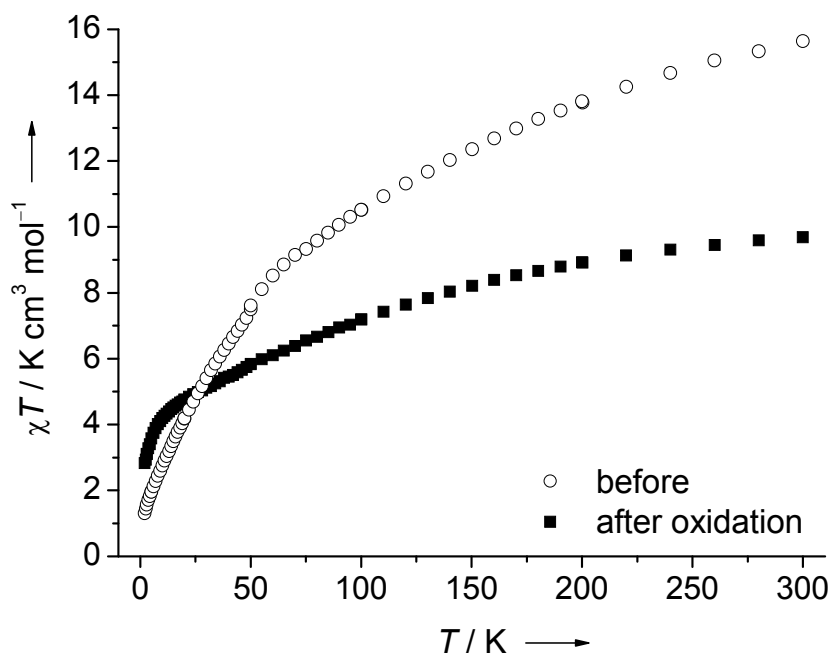
Figure 2.67 χT vs. T plots from SQUID measurements (at 500 Oe)
as recorded for the carbamate complexes before and after oxidation

### 2.4.3 Thermal decomposition of the mixed Zn/Mn carbamate

In line with other carbamates,[112] decomposition of $[Zn_2Mn_6(\mu_4\text{-}O)_2(O_2CN(iPr)_2)_{12}]$ occurs already at mild conditions. **Figure 2.68** shows the TG curves for three different heating rates (2, 5 and 10 °C min^{-1}). For all heating rates, the complex witnesses a similar loss of ca. 73% of its initial mass. This fits nicely to the theoretical mass loss of 74% for decomposition to give an oxide of the overall formula $ZnMn_3O_4$.
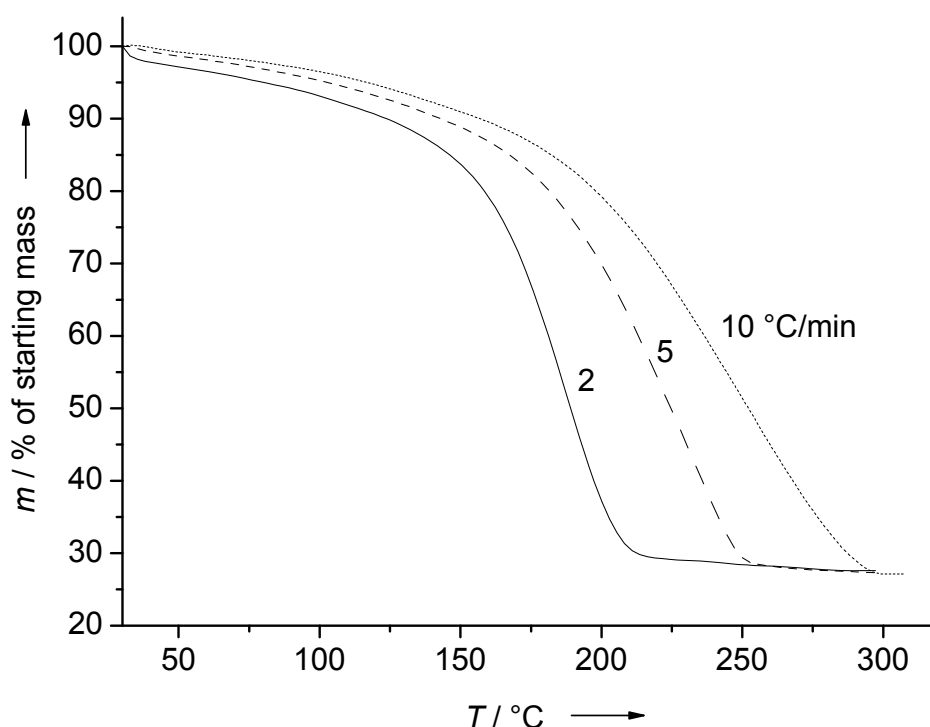
Figure 2.68 TG curve as recorded for $[Zn_2Mn_6(\mu_4\text{-}O)_2(O_2CN(iPr)_2)_{12}]$ at different heating rates (2, 5 and 10°C min^{-1})

The decomposition is completed at 210°C for a heating rate of 2°C min^{-1}, but requires temperatures of more than 270°C if the heating rate is increased to 10°C min^{-1}. This behaviour indicates kinetic control of the decomposition for high heating rates implying that decomposition is a relatively slow process. A similar behaviour was observed for decomposition of $[ZnEt(O_2CN(iPr)_2]_4$ to give ZnO.[112]

The decomposition product for a heating rate of 5°C min^{-1} was further analysed by X-ray powder diffraction. **Figure 2.69** displays a typical diffraction pattern, which cannot be explained by a single phase, but with respect to the results from the EDX analysis rather points to formation of MnO and $ZnMn_2O_4$ nanoparticles existing in a ratio of 1 to 2.5. This composition is in agreement with a ratio Mn:Zn of ca. 3:1, indicating that no additional amorphous particles are formed. For comparison, the characteristic lines of these two lattices are included in **Figure 2.69**. A Debye-Scherer analysis to estimate the particle sizes proved impossible due to peak overlapping. However, from the powder pattern it can be derived that the particles have to be small as otherwise sharper peaks would have been observed in the diffractogramms.
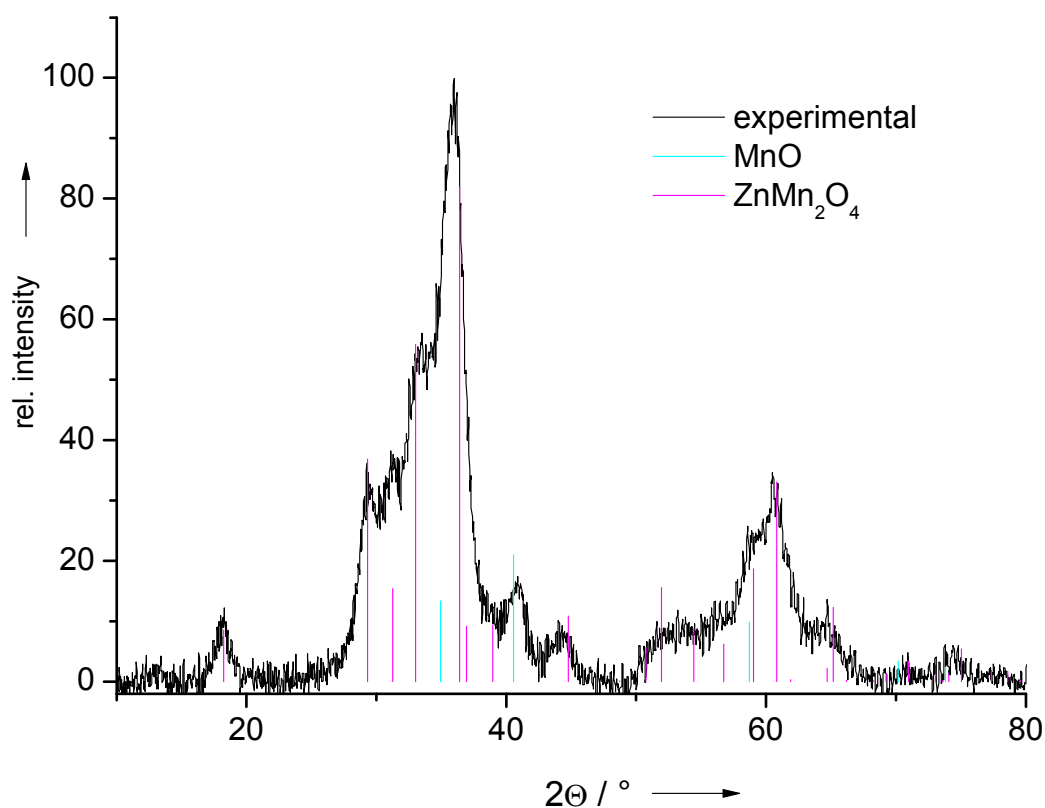

Figure 2.69 Powder diffraction patterns (black trace) as measured after heating of $[Zn_2Mn_6(\mu_4\text{-}O)_2(O_2CN(i\text{Pr})_2)_{12}]$ to 300°C with a heating rate of 5°C min^{-1}.
The inserted lines are taken from the database: MnO (light blue) and $ZnMn_2O_4$ (pink)

A particle size distribution (see **Figure 2.71**) determination based on the TEM images (see **Figure 2.70)**, supporting the results obtained from XRD analysis, shows that the particle size is ≤ 23.0 nm with a mean particle size of 9 nm.
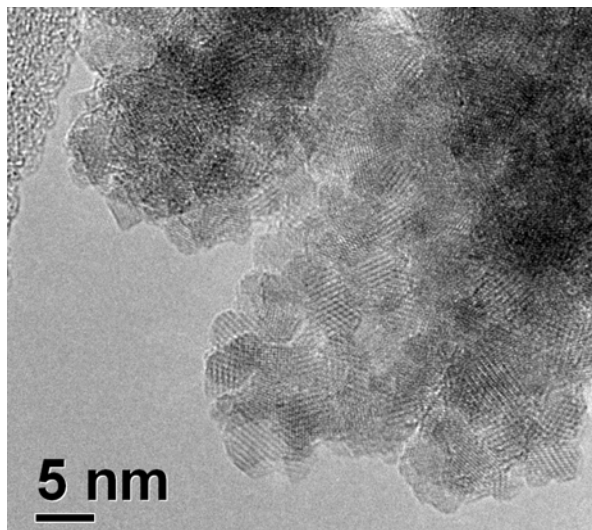
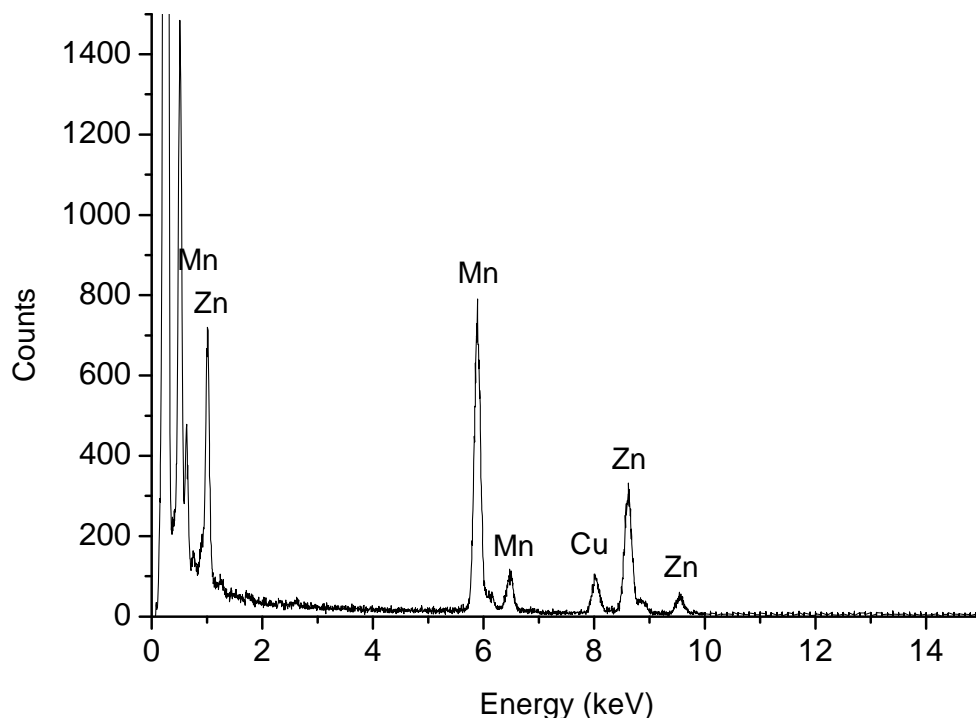**Figure 2.70** TEM image showing the Zn/Mn oxide nanoparticles formed by heating [$Zn_2Mn_6(\mu_4\text{-}O)_2(O_2CN(iPr)_2)_{12}$] to 300°C (heating rate 5°C min^{-1})
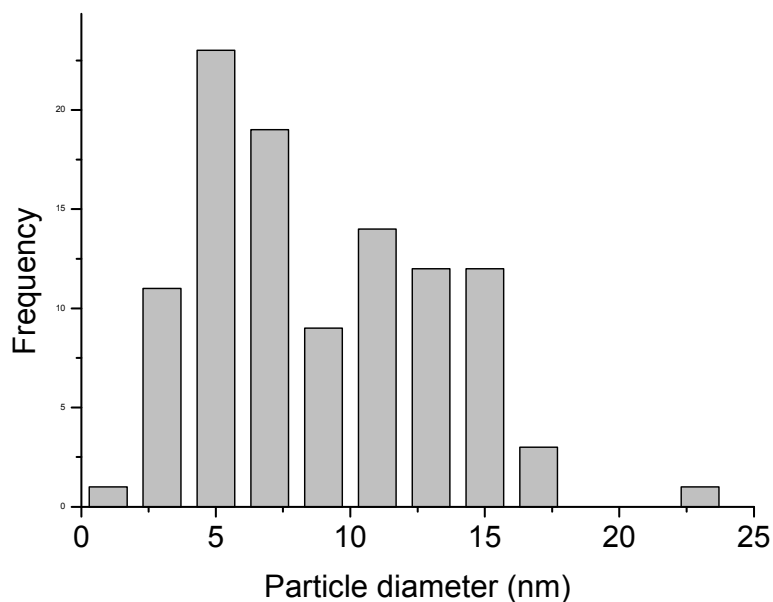
Figure 2.71 Plot of the particle size distribution

EDX measurements (see **Figure 2.72**) at different places of the sample show slight variations in the Mn:Zn ratio, which in average amounts to ca. 3:1, in line with the other analytical data.


Figure 2.72 EDX analysis of the Zn/Mn oxide particles formed by heating $[Zn_2Mn_6(\mu_4\text{-}O)_2(O_2CN(iPr)_2)_{12}]$ to 300°C (heating rate 5°C min^{-1})

The TG curves recorded for $[Zn_2Mn_6(\mu_4\text{-}O)_2(\mu_3\text{-}O)(O_2CN(iPr)_2)_{12}]$ are similar to those of $[Zn_2Mn_6(\mu_4\text{-}O)_2(O_2CN(iPr)_2)_{12}]$, showing the same dependence of the end-temperature for complete decomposition on the heating rate. An analysis of the TEM pictures might indicate a slightly more narrow particle size distribution. However, else wise the data obtained for the two carbamates are similar.

A typical powder diffractogram after heating $[Zn_2Mn_6(\mu_4\text{-}O)_2(\mu_3\text{-}O)(O_2CN(iPr)_2)_{12}]$ with a heating rate of 5°C min^{-1} to an end temperature of 300°C is displayed in **Figure 2.73**, which cannot be explained by a single phase, but rather points to formation of MnO and $ZnMn_2O_4$ nanoparticles existing in a ratio of 1 to 1.

This composition is in agreement with a ratio Mn:Zn of ca. 3:1. A Debye-Scherer analysis to estimate the particle sizes proved impossible due to peak overlapping.
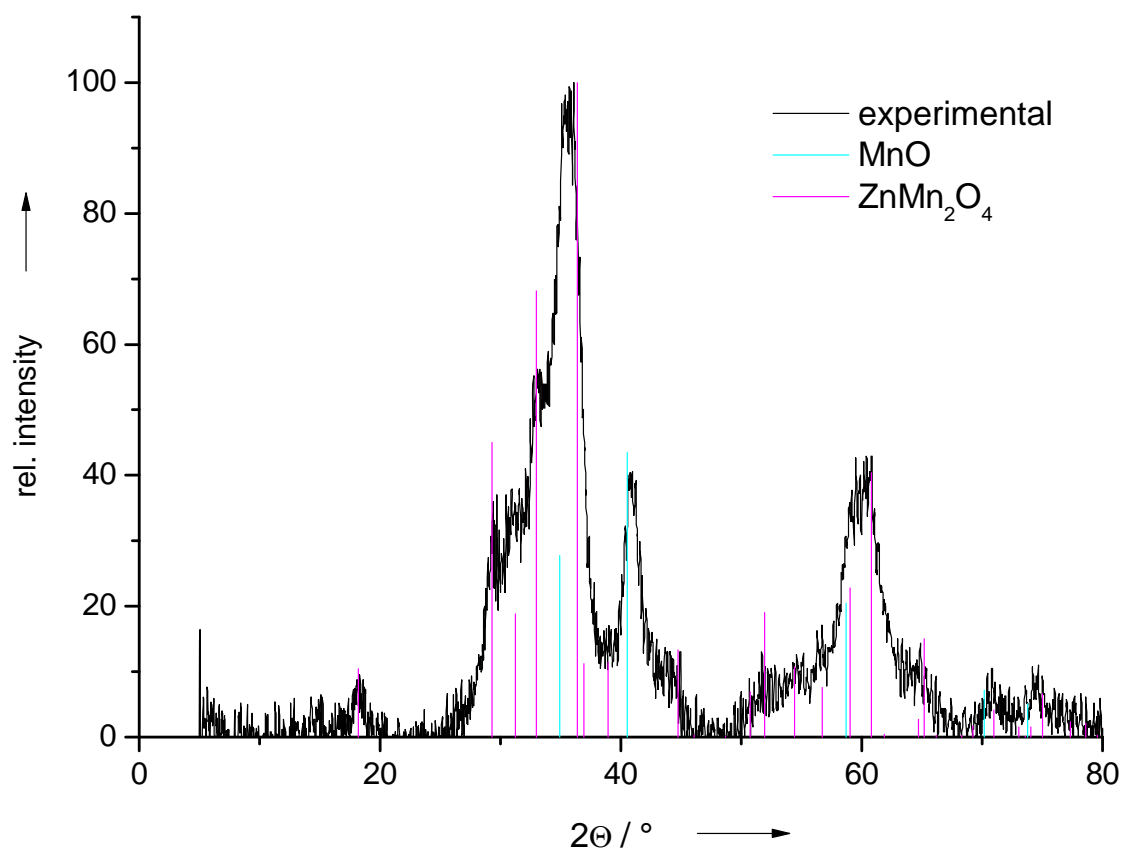
Figure 2.73 Powder diffraction patterns (black trace) as measured after heating of [Zn$_2$Mn$_6$(μ_4-O)$_2$(μ_3-O)(O$_2$CN(iPr)$_2$)$_{12}$] to 300°C with a heating rate of 5°C min^{-1}. The inserted lines are taken from the database: MnO (light blue) and ZnMn$_2$O$_4$ (pink)

A TEM image of the oxide particles obtained after decomposition of [Zn$_2$Mn$_6$(μ_4-O)$_2$(μ_3-O)(O$_2$CN(iPr)$_2$)$_{12}$] with a heating rate of 5°C min^{-1} to an end temperature of 300°C is visualised in **Figure 2.74**.

A particle size distribution (see **Figure 2.75**) determination, based on the TEM images, is difficult due to particle overlapping, it can approximately be estimated to be ≤ 18.2 nm (mean value of 8.4 nm).
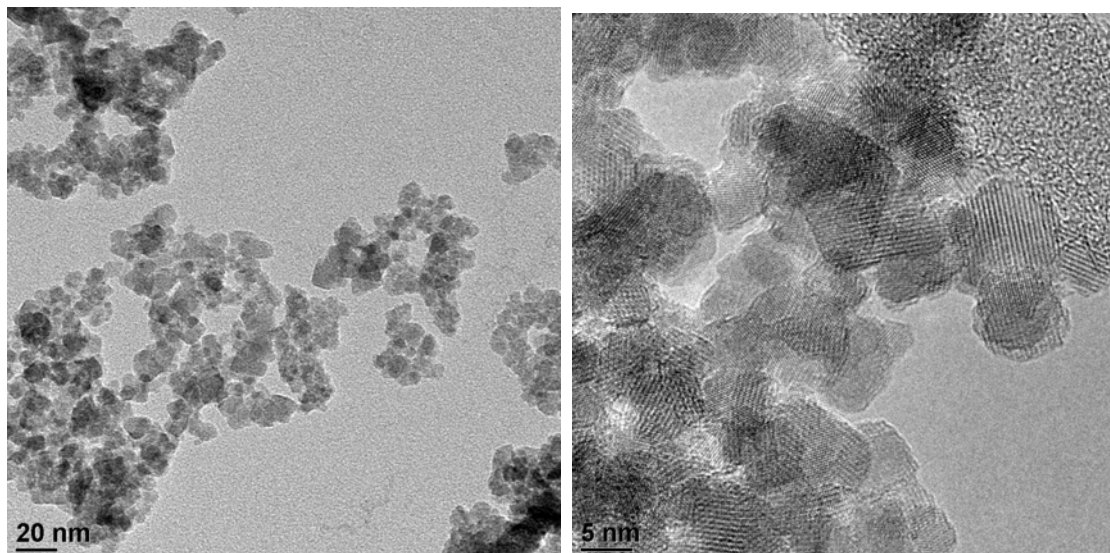
Figure 2.74 TEM image showing the Zn/Mn oxide nanoparticles formed by heating $[Zn_2Mn_6(\mu_4\text{-}O)_2(\mu_3\text{-}O)(O_2CN(i\text{Pr})_2)_{12}]$ to 300°C (heating rate 5°C min^{-1})
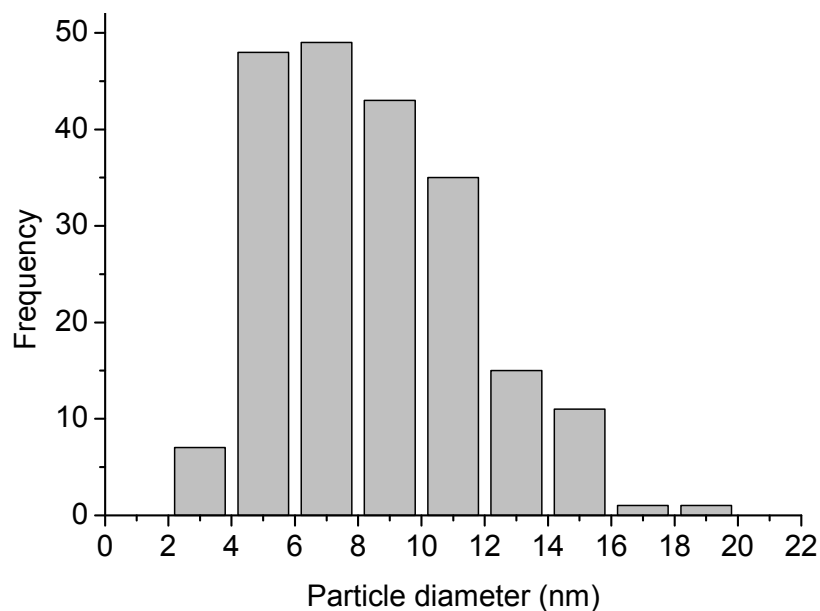
Figure 2.75 Plot of the particle size distribution

EDX measurements (see **Figure 2.76**) at different places of the sample show variations of the Mn:Zn ratio, which in average amounts to ca. 3:1, in line with the other analytical data.
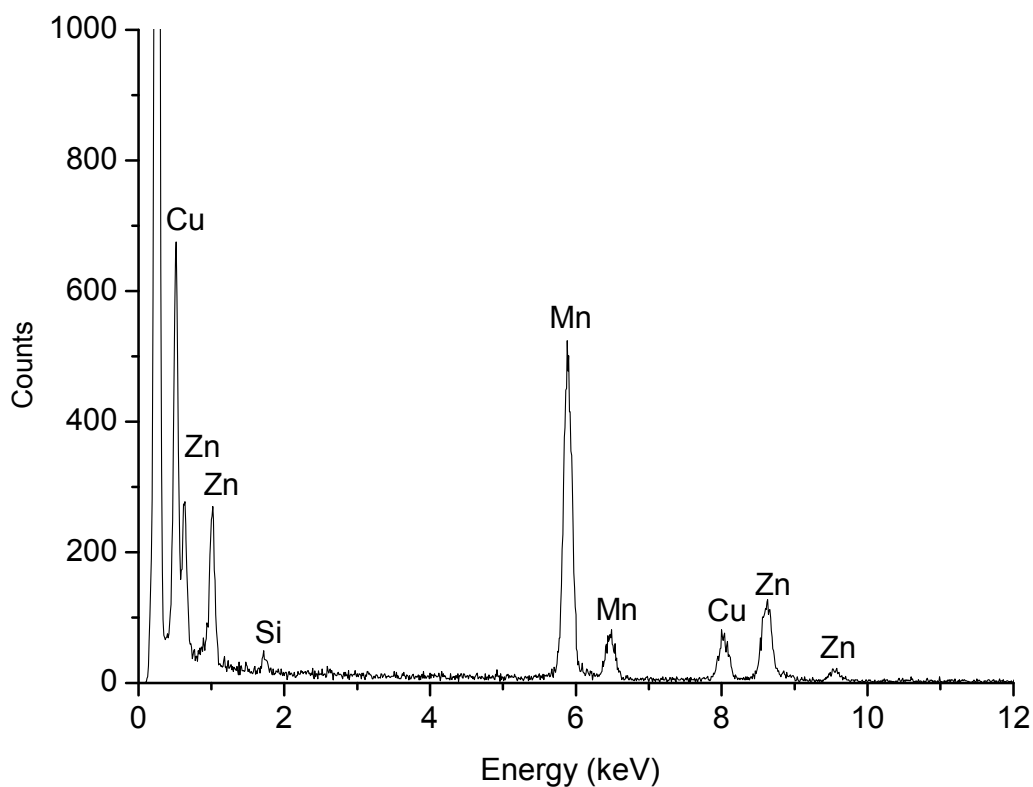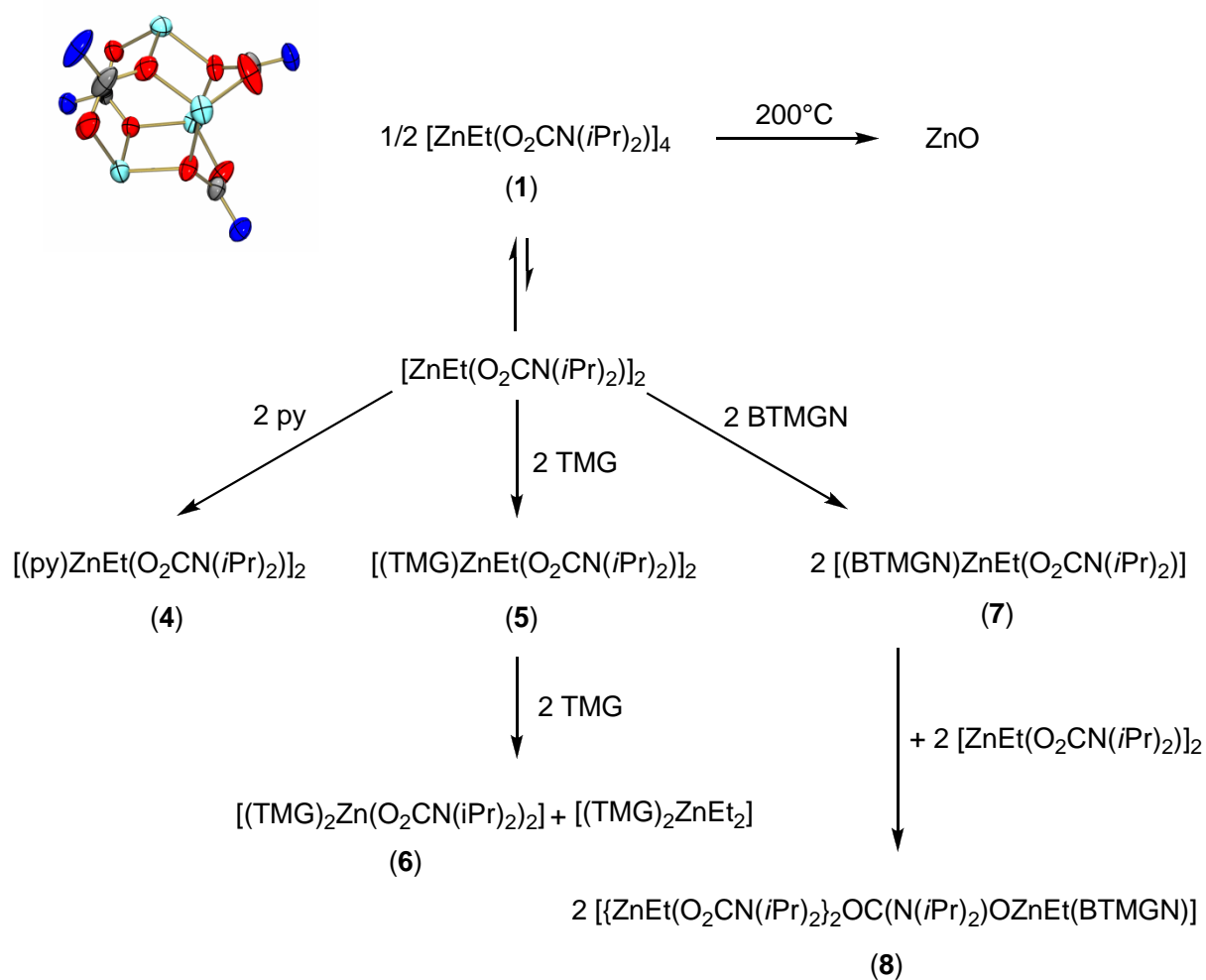

Figure 2.76 EDX analysis of the Zn/Mn oxide particles formed by heating [$Zn_2Mn_6(\mu_4\text{-}O)_2(\mu_3\text{-}O)(O_2CN(i Pr)_2)_{12}$] to 300°C (heating rate 5°C min^{-1})

3. Conclusions
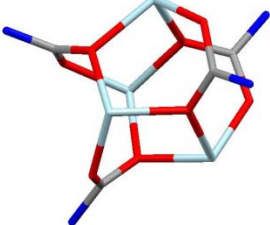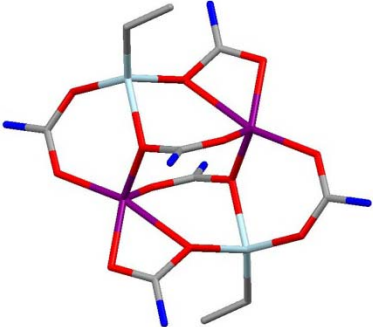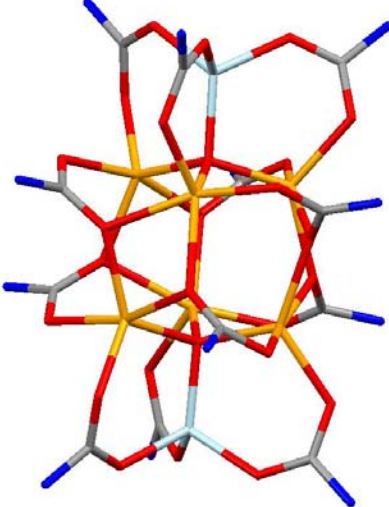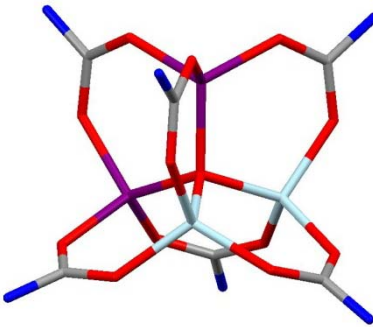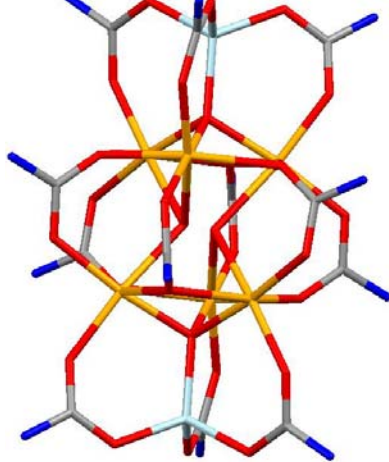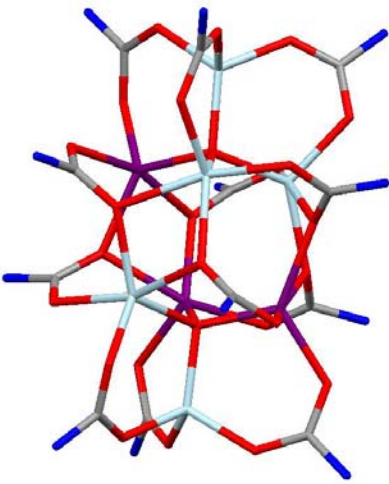
In this work a new method for the preparation of heterobimetallic carbamate complexes is described. As starting material the tetrameric zinc carbamate $[ZnEt(O_2CN(iPr)_2)]_4$ was used which was shown to break up in smaller units when brought to reaction with a nitrogen base (see **Scheme 3**).

$$1/2\ [ZnEt(O_2CN(iPr)_2)]_4 \xrightarrow{200°C} ZnO$$

(**1**)

$[ZnEt(O_2CN(iPr)_2)]_2$

2 py   2 TMG   2 BTMGN

$[(py)ZnEt(O_2CN(iPr)_2)]_2$ $[(TMG)ZnEt(O_2CN(iPr)_2)]_2$ $2\ [(BTMGN)ZnEt(O_2CN(iPr)_2)]$

(**4**)   (**5**)   (**7**)

2 TMG   + 2 $[ZnEt(O_2CN(iPr)_2)]_2$

$[(TMG)_2Zn(O_2CN(iPr)_2)_2] + [(TMG)_2ZnEt_2]$

(**6**)

$2\ [\{ZnEt(O_2CN(iPr)_2)\}_2OC(N(iPr)_2)OZnEt(BTMGN)]$

(**8**)

Scheme 3. Reaction pathway for reaction of tetranuclear alkylzinc carbamates with the three nitrogen bases pyridine, TMG and BTMGN

When the tetramer [ZnEt(O$_2$CN(iPr)$_2$)]$_4$ is brought to reaction with a CoCl$_2$ or MnCl$_2$ complex, featuring a pyridine ligand to which a secondary amine unit is attached (this amine unit fulfils two tasks: it splits up the tetrameric Zn carbamate and provides protons for alkane elimination), new tetra- and octanuclear carbamate complexes are formed.

Starting materials	CoCl$_2$(MAP)$_2$	MnCl$_2$(MAP)$_2$
[ZnEt(O$_2$CN(iPr)$_2$)]$_4$	[Zn$_{2.5}$Co$_{1.5}$Et$_2$(O$_2$CN(iPr)$_2$)$_6$] [Zn$_{2.5}$Co$_{1.5}$(μ_4-O)(O$_2$CN(iPr)$_2$)$_6$] [Zn$_5$Co$_3$(μ_4-O)$_2$(O$_2$CN(iPr)$_2$)$_{12}$]	[Zn$_2$Mn$_6$(μ_4-O)$_2$(O$_2$CN(iPr)$_2$)$_{12}$] [Zn$_2$Mn$_6$(μ_4-O)$_2$(μ_3-O)(O$_2$CN(iPr)$_2$)$_{12}$]

It was shown that these Zn/Co and Zn/Mn carbamates are suitable precursors for heterobimetallic oxide nanoparticles.

Advantages	Disadvantages
- mild conditions (ca. 200°C) - oxygen comes (at least partially) from CO_2 - clean process (3% of carbon impurities for ZnO and 1.8% for Zn/Co oxide) - narrow particle size distribution - generation of nanoparticles (mean particle size 10 nm for ZnO, 25 nm for Zn/Co oxide and 9 nm for Zn/Mn oxide)	- two phases for Zn/Co oxide: wurtzite (ZnO) and sodium chloride (CoO) phase - two phases for Zn/Mn oxide: MnO and $ZnMn_2O_4$

4. Experimental part

4.1. General comments

All reactions were carried out under a dry argon atmosphere using standard Schlenk techniques. All solvents were dried using standard methods followed by distillation and kept over 4Å molecular sieves in Schlenk flask under argon atmosphere.

NMR spectra

NMR spectra were recorded at room temperature using the following instruments:

^{1}H NMR	200 MHz	Bruker Avance AC200
	400 MHz	Bruker Avance II 400
^{13}C NMR	50.27 MHz	Bruker Avance AC200
	100.56 MHz	Bruker Avance II 400

EA

Elemental analyses were carried out at the Microanalytical Laboratory of the University Heidelberg.

IR Spectroscopy

Infrared spectra were recorded with a BIORAD Excalibur FTS 3000 spectrometer.

Thermogravimetric (TG) measurements

Thermogravimetric measurements were carried out on a Mettler TC15 under nitrogen atmosphere in a temperature range 30-600°C. The heating rate was varied between 2 and 10°C/min.

BET measurements

BET measurements were performed on a Quantachrome NOVA automated Gas adsorption system.

TEM experiments

TEM experiments were performed with a FEI Tecnai F20 TEM with field emission gun at 200 kV on carbon-coated 400 mesh copper grids.

Raman spectra

Raman spectra were recorded (without using a polarisator) on a Horiba JobinYvon Triple T64000 spectrometer equipped with a triple monochromator system and a CCD camera detector. The 514 nm line of an Ar^+ ion laser (500 mW) was used for excitation.

XRD measurement

The XRD measurements were performed on a Siemens D500 diffractogramme using Cu radiation and with a stepsize of 0.1° and an irradiation time of 2° min^{-1}. The data were evaluated with EVA (DIFFRACplus, EVA 9.0, XRD evaluation programme, Bruker AXS, 2003). The calculation of the particle size proceeded via the Debye-Scherrer equation.[121]

UV/VIS

UV-visible spectra were obtained using a Varian Cary 5000 Win UV-vis-NIR spectrophotometer.

Mass spectrometry

LIFDI and FD+ mass spectra were measured on a JeolJMS-700 spectrometer. Low resolution mass spectra were recorded on a Finnigan MAT 8200 spectrometer.

EPR

The EPR spectra were recorded on a Bruker Elexsys E 500 spectrometer.

SQUID

The magnetic properties were investigated using a super-conducting quantum interference device Quantum Design MPMS-XL-5.

X-ray crystalographic study

Suitable crystals were taken directly out of the mother liquor, immersed in perfluorinated polyether oil, and fixed on top of a glass capillary. Measurements were made at low temperature (200 and 100K) on a Nonius-Kappa CCD and Bruker AXS Smart 1000 diffractometers (Mo-K$_\alpha$ radiation, graphite-monochromator, λ = 0.71073Å) The data collected were processed using the standard Nonius [122] and Bruker software[123,124]. All calculations were performed using the SHELXT-PLUS software package. Structures were solved by direct methods with the SHELXS-97 program and refined with the SHELXL-97 program.[125,126,127] Graphical handling of the structural data during solution and refinement was performed with XPMA.[128] Structural representations were generated using Winray 32.[129] The structures have been produced and visualized using Ortep3v2[130] and POVRay.[131] Atomic coordinates and anisotropic thermal parameters of non-hydrogen atoms were refined by full-matrix least-squares calculations.

Reagents and solvents

CO_2	Linde
Diethylzinc 1.5 M solution in toluene	Acros
Diisopropylamine	Aldrich
Diisobutylamine	Aldrich
Dimethylzinc 1.2 M solution in toluene	Acros
N,N,N',N'-tetramethylguanidine	Acros
bis-N,N,N',N'-tetramethylguanidine naphthalene	Acros
Pyridine	Acros
2-(Methylamino)pyridine (MAP)	Aldrich
2-[2-(Methylamino)-ethyl]-pyridine (MAEP)	Aldrich
$CoCl_2$ 97%	Acros
$MnCl_2$ 99%	Acros
Acetonitrile 99.9%	Acros
Hexane 96%	Acros
Methanol 99.8%	Acros
THF 99.5%	Acros
Toluene 99.8%	Acros

4.2 Synthesis and characterization of new zinc carbamate complexes formed by CO$_2$ fixation and their use as precursors for ZnO particles under mild conditions

4.2.1 Synthesis of EtZnN(*i*Pr)$_2$

$$C_{18}H_{48}N_2Zn_2$$
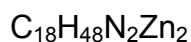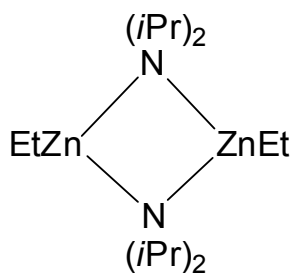
Mol. Wt. 415.28 g/mol

Materials

Et$_2$Zn	20 mL	30 mmol
HN(*i*Pr)$_2$	3.03 g	30 mmol
Toluene	50 mL	

Experimental

Diethylzinc (20 mL, 30 mmol) was reacted with 1 equiv of HN(*i*Pr)$_2$ (3.03 g, 30 mmol) in 50 mL toluene for 72 h at room temperature under argon. The solvent was evaporated completely leaving a colourless liquid.

^{1}H NMR (400 MHz, C$_6$D$_6$):

$δ$ = 0.33 (q, ^3J = 8.16 Hz, 2 H, CH$_3$*CH$_2$*Zn), 1.42 (t, ^3J = 8.15 Hz, 3 H, *CH$_3$*CH$_2$Zn), 0.92 (d, ^3J = 6.27 Hz, 12 H, *Me$_2$*CH-), 2.76 (m, 2 H, -*CH*Me$_2$) ppm.

^{13}C NMR (100.56 MHz, C$_6$D$_6$):

$δ$ = 6.27 (CH$_3$*CH$_2$*Zn), 11.97 (*CH$_3$*CH$_2$Zn), 22.99 (*Me$_2$*CH-), 45.65 (-*CH*Me$_2$) ppm.

4.2.2 Synthesis of [ZnEt(O$_2$CN(*i*Pr)$_2$)]$_4$

*i*Pr$_2$N

N*i*Pr$_2$

Zn

Zn

Zn

Zn

*i*Pr$_2$N

N*i*Pr$_2$

C$_{36}$H$_{76}$N$_4$O$_8$Zn$_4$
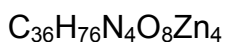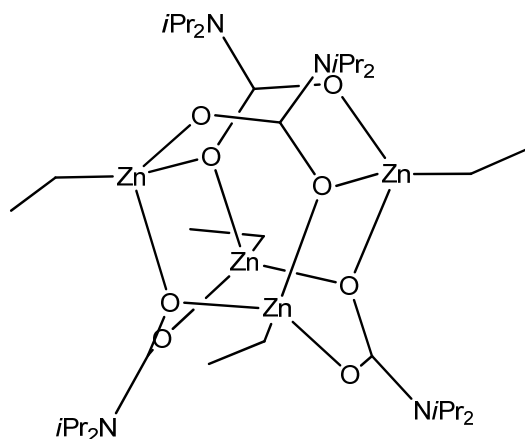
Mol. Wt. 954.53 g/mol

Materials

Et$_2$Zn	20 mL	30 mmol
HN(*i*Pr)$_2$	3.03 g	30 mmol
Toluene	50 mL	
CO$_2$		

Experimental

Diethylzinc (20 mL, 30 mmol) was reacted with 1 equiv of diisopropylamine (3.03 g, 30 mmol) in 50 mL toluene for 3 h at 70°C under argon. The resulting solution was cooled to room temperature and dry CO$_2$ gas bubbled through for 30 min. The solvent was removed in vacuum and the solid product recrystallized from toluene/hexane (6:1) at -20°C to give colourless cubic crystals.

Yield

82%	5.91 g	6.21 mmol

EA (C$_{36}$H$_{76}$N$_4$O$_8$Zn$_4$)

calcd.: C [%] 45.30, H [%] 8.03, N [%] 5.87

found: C [%] 43.69, H [%] 7.59, N [%] 5.96

¹H NMR (400 MHz, C₆D₆):

$δ$ = 0.66 (q, ^3J = 8.17 Hz, 2 H, CH₃*CH₂*Zn), 1.69 (t, ^3J = 8.12 Hz, 3 H, *CH₃*CH₂Zn), 1.13 (d, ^3J = 6.8 Hz, 12 H, *Me₂*CH-), 3.88 (m, 2 H, -*CH*Me₂) ppm.

¹³C NMR (100.56 MHz, C₆D₆):

$δ$ = -2.14 (CH₃*CH₂*Zn), 13.36 (*CH₃*CH₂Zn), 20.76 (*Me₂*CH-), 46.08 (-*CH*Me₂), 163.04 (*CO₂*) ppm.

4.2.3 Synthesis of [ZnEt(O₂CN(*i*Bu)₂)]₄

C₄₄H₉₂N₄O₈Zn₄
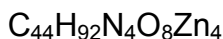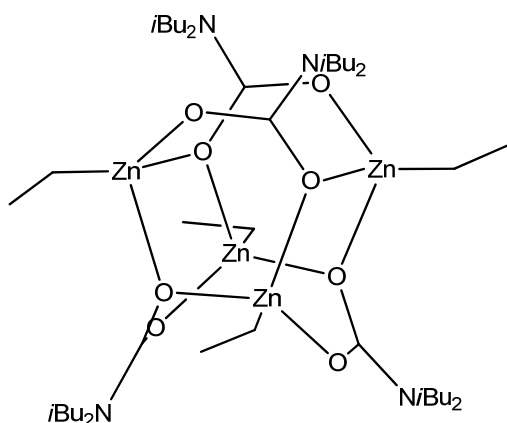
Mol. Wt. 1066.70 g/mol

Materials

Et₂Zn	20 mL	30 mmol
HN(*i*Bu)₂	3.87 g	30 mmol
Toluene	50 mL	
CO₂		

Experimental

Diethylzinc (20 mL, 30 mmol) was reacted with 1 equivalent of diisobutylamine (3.87 g, 30 mmol) in 50 mL toluene for 3 h at 70°C under argon. The resulting solution was cooled to room temperature and dry CO₂ gas bubbled through for 30 min. The solution was then evaporated to dryness and the solid product recrystallized from hexane at -20°C to give colourless cubic crystals.

Yield

79%   6.31 g   5.92 mmol

EA (C$_{44}$H$_{92}$N$_4$O$_8$Zn$_4$)

calcd.: C [%] 49.54, H [%] 8.69, N [%] 5.25

found: C [%] 46.35, H [%] 7.92, N [%] 5.22

^{1}H NMR (200 MHz, C$_6$D$_6$):

δ = 0.67 (q, ^3J = 7.08 Hz, 2 H, CH$_3$*CH$_2$*Zn), 1.71 (t, ^3J = 7.18 Hz, 3 H, *CH$_3$*CH$_2$Zn),
0.89 (d, ^3J = 7.12 Hz, 12 H, *Me$_2$*CHCH$_2$-), 1.99 (m, ^3J = 6.42 Hz, 2 H, Me$_2$*CH*CH$_2$-),
3.88 (d, ^3J = 6.52 Hz, 4 H, Me$_2$CH*CH$_2$*-) ppm.

^{13}C NMR (50.27 MHz, C$_6$D$_6$):

δ = -0.42 (CH$_3$*CH$_2$*Zn), 13.10 (*CH$_3$*CH$_2$Zn), 20.41 (*Me$_2$*CHCH$_2$-), 27.41 (Me$_2$*CH*CH$_2$-),
55.91 (Me$_2$CH*CH$_2$*-), 164.69 (*CO$_2$*) ppm.

4.2.4 Synthesis of [Zn$_4$(µ$_4$-O)(O$_2$CN(*i*Bu)$_2$)$_6$]

C$_{54}$H$_{108}$N$_6$O$_{13}$Zn$_4$
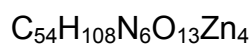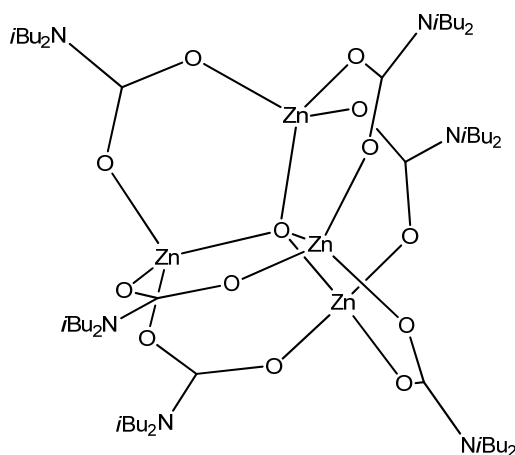
Mol. Wt. 1310.94 g/mol

The compound was obtained in the presence of small amounts of water in the
reaction mixture in which it was obtained the complex [ZnEt(O$_2$CN(*i*Bu)$_2$)]$_4$.

^{1}H NMR (200 MHz, C$_6$D$_6$):

$δ$ = 0.85 (d, ^3J = 6.67 Hz, 12 H, *Me*$_2$CHCH$_2$-), 1.97 (m, ^3J = 6.74 Hz, 2 H, Me$_2$*CH*CH$_2$-), 3.13 (d, ^3J = 7.44 Hz, 4 H, Me$_2$CH*CH$_2$*-) ppm.

^{13}C NMR (50.27 MHz, C$_6$D$_6$):

$δ$ = 20.42 (*Me*$_2$CHCH$_2$-), 27.63 (Me$_2$*CH*CH$_2$-), 55.42 (Me$_2$CH*CH$_2$*-), 164.69 (*CO$_2$*) ppm.

MS (LIFDI, c= 10^{-4} mol L^{-1} in toluene)

calcd. m/z (%) = 1311.07 (100)

found m/z (%) =1310.50 (100)

4.2.5 Synthesis of ZnO nanoparticles

Materials

[ZnEt(O$_2$CN(*i*Pr)$_2$)]$_4$	0.016 g	0.016 mmol

Experimental

[ZnEt(O$_2$CN(*i*Pr)$_2$)]$_4$ (0.016 g, 0.016 mmol) were filled in a platinum crucible. The compound was heated with different heating rates (2, 5 and 10°C min^{-1}) under nitrogen atmosphere with a flow rate of 150 mL min^{-1}. The starting temperature was settled at 30°C and the end temperature was fixed at 300°C. Decomposition of the [ZnEt(O$_2$CN(*i*Pr)$_2$)]$_4$ leads to the formation of ZnO nanoparticles.

Raman

literature values	E_2^{low} 99 cm^{-1}
	E_2^{high} 439 cm^{-1}[132]
experimental	E_2^{low} 98 cm^{-1}
	E_2^{high} 437 cm^{-1}

TEM

mean particle size	9.3 nm
maximum particle size	9.5 nm

BET

BET surface: 102.7 $m^2 g^{-1}$

density of ZnO: 5.6 g cm^{-3}

particle size: 10.4 nm

XRD

mean particle size   10.3 nm

4.3 Synthesis of trinuclear, dinuclear and mononuclear carbamato-zinc complexes from tetranuclear precursors

4.3.1 Synthesis of [(py)ZnEt(O$_2$CN(*i*Pr)$_2$)]$_2$

$C_{28}H_{48}N_4O_4Zn_2$
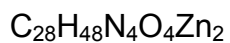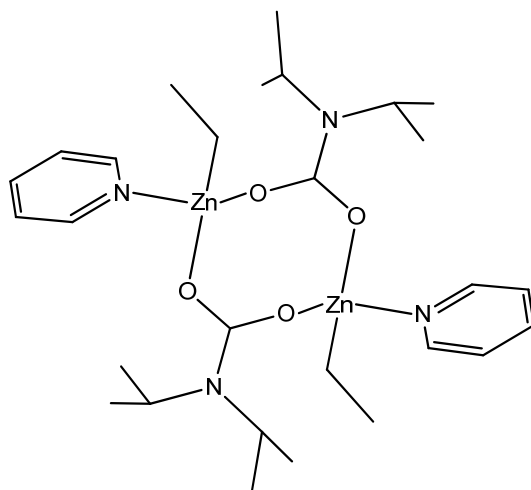
Mol. Wt. 635.44 g/mol

Materials

[ZnEt(O$_2$CN(*i*Pr)$_2$)]$_4$	2 g	2.1 mmol
pyridine	4 mL	50 mmol
Toluene	20 mL	

Experimental

[ZnEt(O$_2$CN(*i*Pr)$_2$)]$_4$ (2.0 g, 2.1 mmol) was dissolved in 20 mL of toluene, treated with an excess of pyridine (4 mL, 50 mmol) and stirred for 2 h. The solution was then evaporated to dryness and the solid product recrystallized from toluene/hexane 5 : 1 at room temperature to give colourless cubic crystals of [(py)ZnEt(O$_2$CN(*i*Pr)$_2$)]$_2$.

Yield

83%   1.11 g   1.75 mmol

EA (C$_{28}$H$_{48}$N$_4$O$_4$Zn$_2$)

calcd.: C [%] 52.92, H [%] 7.61, N [%] 8.82
found: C [%] 51.35, H [%] 7.21, N [%] 8.31

^{1}H NMR (200 MHz, C$_6$D$_6$):

δ = 0.74 (q, ^3J = 8.05 Hz, 2 H, CH$_3$*CH$_2$*Zn), 1.11 (d, ^3J = 6.8 Hz, 12 H, *Me*$_2$CH-), 1.76 (t, ^3J = 8.07 Hz, 3 H, *CH$_3$*CH$_2$Zn), 3.87 (m, ^3J = 6.62 Hz, 2 H, -C*H*Me$_2$), 6.66 (m, 2 H, *py*), 6.93 (m, 1 H, *py*), 8.61 (m, 2 H, *py*) ppm.

^{13}C NMR (50.27 MHz, C$_6$D$_6$):

δ = −1.94 (CH$_3$*CH$_2$*Zn), 13.93 (*CH$_3$*CH$_2$Zn), 21.18 (*Me*$_2$CH-), 46.09 (-*CH*Me$_2$), 124.12 (*py*), 137.20 (*py*), 149.63 (*py*), 163.31 (*CO$_2$*) ppm.

Raman

ν(C-H) py = 3070 cm^{-1}, ν(C-H) alkyl groups = 3000-2840 cm^{-1}, ν(CO$_2$) = 1456 cm^{-1}

4.3.2 Synthesis of [(TMG)ZnEt(O$_2$CN(*i*Pr)$_2$)]$_2$

C$_{28}$H$_{62}$N$_8$O$_4$Zn$_2$
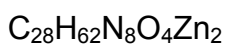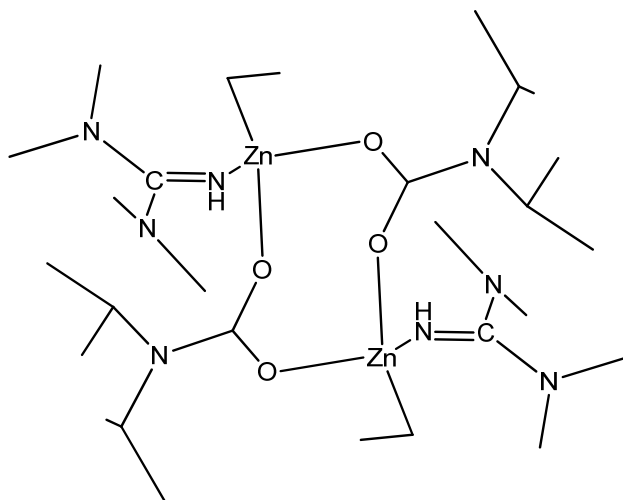
Mol. Wt. 705.64 g/mol

Materials

[ZnEt(O$_2$CN(*i*Pr)$_2$)]$_4$	1 g	1 mmol
TMG	0.51 mL	4 mmol
Toluene	10 mL	

Experimental

[ZnEt(O$_2$CN(*i*Pr)$_2$)]$_4$ (1 g, 1 mmol) was dissolved in 10 mL of toluene and reacted with 4 equivalents of TMG (0.51 ml, 4 mmol) for 2 h at room temperature under argon. The solution was then evaporated to dryness and the solid product recrystallized from toluene at 10°C to give colourless cubic crystals.

Yield

39%	0.55 g	0.78 mmol

EA (C$_{28}$H$_{62}$N$_8$O$_4$Zn$_2$)

calcd.: C [%] 47.66, H [%] 8.86, N [%] 15.88

found: C [%] 46.78, H [%] 8.87, N [%] 16.08

¹H NMR (200 MHz, toluene d₈):

δ = 0.58 (q, ³*J* = 8.08 Hz, 2 H, CH₃*CH₂*Zn), 1.79 (t, ³*J* = 8.02 Hz, 3 H, *CH₃*CH₂Zn), 1.28 (d, ³*J* = 6.71 Hz, 12 H, *Me₂*CH-), 2.39 (s, 6H, *Me₂*N-), 2.62 (s, 6H, *Me₂*N-), 4.05 (m, ³*J* = 6.63 Hz, 2 H, Me₂*CH*-), 6.15 (b, 1 H, *NH*) ppm.

¹³C NMR (50.27 MHz, toluene d₈):

δ = 0.62 (CH₃*CH₂*Zn), 14.26 (*CH₃*CH₂Zn), 21.65 (*Me₂*CH-), 38.73 (-N*Me₂*), 39.28 (-N*Me₂*), 45.59 (-*CH*Me₂), 163.27 (*CO₂*), 166.94 (N=*C*(NMe₂)₂) ppm.

IR (solid CsI):

3294 (w) ṽ(N-H); 2963 (m), 2870 (w) ṽ(C-H); 1605 (s), 1560 (s) ṽ(C=O); 1325 (s), 1223 (s), 1161(s), 1132 (s), 1065 (s) ṽ(C-N) cm⁻¹

4.3.3 Synthesis of [(TMG)₂Zn(O₂CN(*i*Pr)₂)₂]

C₂₄H₅₄N₈O₄Zn
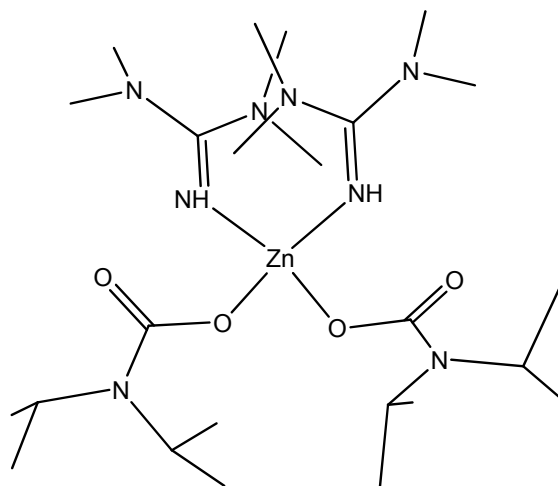
Mol. Wt. 584.12 g/mol

Materials

[ZnEt(O₂CN(*i*Pr)₂)]₄	0.6 g	0.63 mmol
TMG	0.65 mL	5.04 mmol
Toluene	5 mL	
Hexane	1 mL	

Experimental

[ZnEt(O$_2$CN(iPr)$_2$)]$_4$ (0.6 g, 0.63 mmol) was dissolved in 5 mL of toluene and 1 mL hexane and reacted with 8 equivalents of TMG (0.65 ml, 5.04 mmol) for 24 h at room temperature under argon. The solution was then evaporated to dryness and the solid product recrystallized from toluene/hexane (1:1) at 10°C to give colourless cubic crystals.

Yield

| 40% | 0.30 g | 0.51 mmol |

EA (C$_{24}$H$_{54}$N$_8$O$_4$Zn)

calcd.: C [%] 49.34, H [%] 9.34, N [%] 19.18

found: C [%] 48.19, H [%] 8.89, N [%] 17.68

^{1}H NMR (200 MHz, toluene d$_8$):

$δ$ = 1.23 (^3J = 6.77 Hz) 1.40 (^3J = 6.77 Hz) (d, 24 H, *Me$_2$*CH-), 2.35 (s, 12 H, *Me$_2$*N-) 2.73 (s, 12 H, *Me$_2$*N-), 3.95 (m, 2 H, -C*H*Me$_2$), 4.2 (m, 2 H, -C*H*Me$_2$), 6.73 (b, 2 H, *NH*) ppm.

^{13}C NMR (50.27, toluene d$_8$):

$δ$ = 21.33 (*Me$_2$*CH-), 38.86 (-N*Me$_2$*), 39.46 (-N*Me$_2$*), 45.86 (-*CH*Me$_2$), 163.15 (*CO$_2$*), 167.07 (N=*C*(NMe$_2$)$_2$) ppm.

IR (solid CsI):

3280 (w) $\tilde{υ}$(N-H); 2963 (m), 2881 (w) $\tilde{υ}$(C-H); 1603 (m), 1560 (m) $\tilde{υ}$(C=O); 1327 (s), 1221 (s), 1161(s), 1132 (s), 1067 (s) $\tilde{υ}$(C-N) cm^{-1}

4.3.4 Synthesis of [(BTMGN)ZnEt(O₂CN(*i*Pr)₂)]

$C_{29}H_{49}N_7O_2Zn$
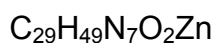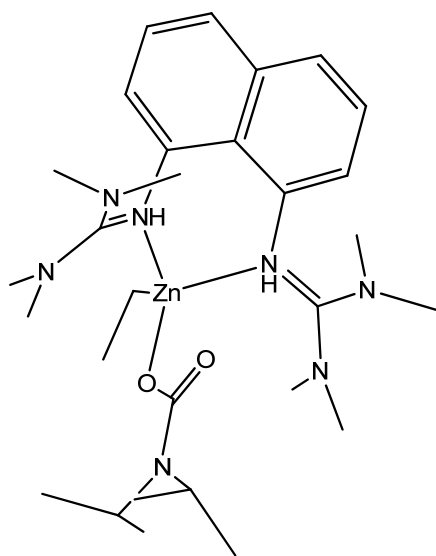
Mol. Wt. 593.12 g/mol

Materials

[ZnEt(O₂CN(*i*Pr)₂)]₄	0.1 g	0.1 mmol
BTMGN	0.142 g	0.4 mmol
Toluene	3 mL	

Experimental

[ZnEt(O₂CN(*i*Pr)₂)]₄ (0.1 g, 0.1 mmol) was dissolved in 3 mL of toluene and reacted with 4 equivalents of BTMGN (0.142 g, 0.4 mmol) for 24 h at room temperature under argon. The solution was then evaporated to dryness and the solid product recrystallized from toluene at -20°C to give colourless needles crystals.

Yield

19%	0.044 g	0.074 mmol

EA (C₂₉H₄₉N₇O₂Zn)

calcd.: C [%] 58.78, H [%] 8.28, N [%] 16.55

found. C [%] 58.82, H [%] 8.24, N [%] 16.48

^{1}H NMR (200 MHz, toluene d$_8$):

δ = 0.44 (q, ^3J = 8.09 Hz, 2 H, CH$_3$*CH$_2$*Zn), 1.36 (d, ^3J = 6.77 Hz, 12 H, *Me$_2$*CH-), 1.54 (t, ^3J = 8.09 Hz, 3 H, *CH$_3$*CH$_2$Zn), 2.22 / 2.26 (s, 12 H, *Me$_2$*N-), 2.75 / 3.21 (s, 12 H, *Me$_2$*N-), 4.15 (m, 2 H, -*CH*Me$_2$), 6.24 (dd, ^3J (H4H3) = 7.43 Hz, ^4J (H4H2) = 0.89 Hz, 2 H; H4,5), 7.19 (t, ^3J (H3H4) = 7.75 Hz, ^3J (H3H2) = 7.75 Hz, 2 H; H3,6), 7.41 (dd, ^3J (H2H3) = 8.19 Hz, ^4J (H2H4) = 0.89 Hz, 2 H; H2,7) ppm.

^{13}C NMR (50.27 MHz, toluene d$_8$):

δ = 1.15 (CH$_3$*CH$_2$*Zn), 14.81 (*CH$_3$*CH$_2$Zn), 22.57 (*Me$_2$*CH-), 39.34 (-N*Me$_2$*), 44.86 (-*CH*Me$_2$), 117.68, 122.70, 125.74, 148.21, 150.36 (aromat *C*), 160.96 (*C*O$_2$), 164.38 (N=*C*(NMe$_2$)$_2$) ppm.

IR (solid CsI):

3440 (w) ῦ(N-H); 2931 (m), 2881 (w) ῦ(C-H); 1591 (m), 1554 (m) ῦ(C=O); 1313 (s), 1215 (s), 1161(s), 1115 (s), 1054 (s) ῦ(C-N) cm^{-1}

4.3.5 Synthesis of [(BTMGN)Zn$_3$Et$_3$(O$_2$CN(*i*Pr)$_2$)$_3$]

C$_{47}$H$_{87}$N$_9$O$_6$Zn$_3$
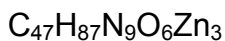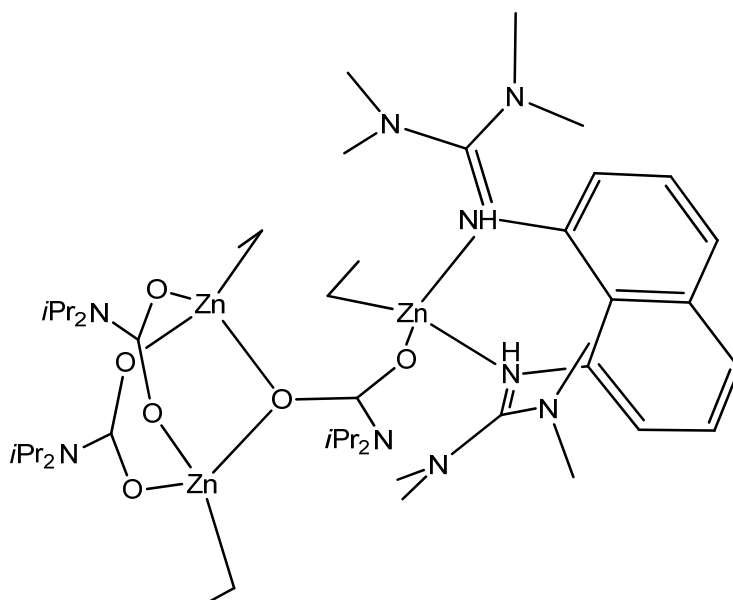
Mol. Wt. 1070.40 g/mol

Method A

Materials

[ZnEt(O$_2$CN(*i*Pr)$_2$)]$_4$	0.1 g	0.1 mmol
BTMGN	0.071 g	0.2 mmol
Toluene	3 mL	
Hexane	1 mL	

Experimental

[ZnEt(O$_2$CN(*i*Pr)$_2$)]$_4$ (0.1 g, 0.1 mmol) was dissolved in toluene (3 mL) and hexane (1 mL) and treated with 2 equivalents of BTMGN (0.071 g, 0.2 mmol) for 24 h at room temperature under argon. The solution was then evaporated to dryness and the solid product recrystallized from toluene/hexane 4:1 at 10°C to give colourless cubic crystals.

Yield

31%	0.07 g	0.061 mmol

Method B

Materials

[ZnEt(O$_2$CN(*i*Pr)$_2$)]$_4$	0.137g	0.143 mmol
[(BTMGN)ZnEt(O$_2$CN(*i*-Pr)$_2$)]	0.17 g	0.286 mmol
Toluene	3 mL	

Experimental

[ZnEt(O$_2$CN(*i*Pr)$_2$)]$_4$ (0.137 g, 0.143 mmol) was dissolved in toluene (3 mL) and treated with 2 equivalents of [(BTMGN)ZnEt(O$_2$CN(*i*Pr)$_2$)] (0.17 g, 0.286 mmol) for 2 h at room temperature under argon. The solution was then evaporated to dryness and the solid product recrystallized from toluene/hexane 4:1 at 10°C to give colourless cubic crystals.

Yield

29%	0.038 g	0.035 mmol

EA (C$_{47}$H$_{87}$N$_9$O$_6$Zn$_3$)

calcd.: C [%] 52.74, H [%] 8.19, N [%] 11.78

found: C [%] 49.25, H [%] 7.40, N [%] 9.07

^{1}H NMR (200 MHz, toluene d$_8$):

δ = –0.02 (q, ^3J = 7.76 Hz, 2 H, CH$_3$*CH$_2$*Zn), 0.45 (q, ^3J = 8.06 Hz, 4 H, CH$_3$*CH$_2$*Zn), 0.94 (t, ^3J = 7.20 Hz, 3 H, *CH$_3$*CH$_2$Zn), 1.18 (d, ^3J = 6.77 Hz, 27 H, *Me$_2$*CH-), 1.36 (d, ^3J = 6.78 Hz, 9 H, *Me$_2$*CH-), 1.45 (t, ^3J = 8.12 Hz, 6 H, *CH$_3$*CH$_2$Zn), 2.61 (s, 24 H, *Me$_2$*N-), 3.92 (m, ^3J = 6.78 Hz, 4 H, -*CH*Me$_2$), 4.06 (b, 2 H, -*CH*Me$_2$), 6.49 (dd, ^3J (H4-H3) = 7.24, ^4J (H4-H2) = 0.99 Hz, 2 H, H4,5), 7.31 (dd, ^3J (H3-H4) = 7.34, ^3J (H3-H2) = 8.01 Hz, 2 H, H3,6), 7.44 (dd, ^3J (H2-H3) = 8.18, ^4J (H2-H4) = 0.90 Hz, 2 H, H2,7) ppm.

^{13}C NMR (50.27 MHz, toluene d$_8$):

δ = 0.01 (CH$_3$*CH$_2$*Zn), 1.38 (CH$_3$*CH$_2$*Zn), 11.67 (*CH$_3$*CH$_2$Zn), 14.14 (*CH$_3$*CH$_2$Zn), 21.03 (*Me$_2$*CH-), 39.65 (-N*Me$_2$*), 46.09 (-*CH*Me$_2$), 115.79, 120.78, 126.03, 148.04, 153.96, 157.50 (*C* aromat), 162.84 (*C*O$_2$), 169.11 [N=*C*(NMe$_2$)$_2$] ppm.

IR (solid CsI):

3450 (w) $\tilde{\upsilon}$(N-H); 2966 (m), 2867 (w) $\tilde{\upsilon}$(C-H); 1558 (s), 1485 (s) $\tilde{\upsilon}$(C=O); 1354 (s), 1213 (s), 1161(s), 1066 (s), 1001 (s) $\tilde{\upsilon}$(C-N) cm^{-1}

4.4 Synthesis of new CoCl$_2$ complexes with different nitrogen bases

4.4.1 Synthesis of [CoCl$_2$(MAP)$_2$]

C$_{12}$H$_{16}$Cl$_2$CoN$_4$
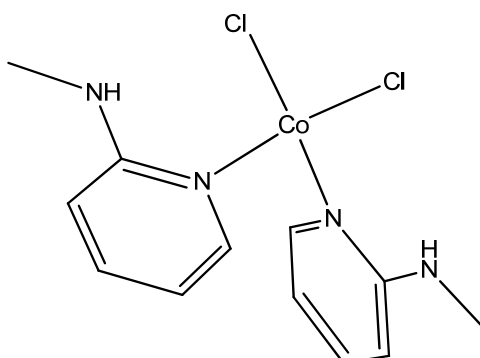
Mol. Wt. 346.12 g/mol

Materials

MAP	0.148 g	1.370 mmol
CoCl$_2$	0.089 g	0.685 mmol
Methanol	15 mL	

Experimental

2-(Methylamino)pyridine (MAP) (0.148 g, 1.37 mmol) in methanol (5 mL) was added to a methanol (10 mL) solution of CoCl$_2$ (0.089 g, 0.685 mmol). The solution was stirred at 60°C for 3 h. Then the solvent was removed in vacuum. Recrystallization from methanol at room temperature afforded the product in the form of blue crystals.

Yield

67%	0.159 g	0.459 mmol

EA (C$_{12}$H$_{16}$Cl$_2$CoN$_4$)

calcd.: C [%] 41.64, H [%] 4.66, N [%] 16.19

found: C [%] 41.04, H [%] 4.60, N [%] 15.95

UV/VIS (c=2.85*10^{-3} mol L^{-1} in toluene)

ν = 15640 cm^{-1} (λ_{max} = 639 nm), ε = 86 dm^3 mol^{-1} cm^{-1}

ν = 16100 cm^{-1} (λ_{max} = 621 nm), ε = 83 dm^3 mol^{-1} cm^{-1}

ν = 17100 cm^{-1} (λ_{max} = 585 nm), ε = 54 dm^3 mol^{-1} cm^{-1}

4.4.2 Synthesis of [CoCl$_2$(MAEP)]

$C_8H_{12}Cl_2CoN_2$
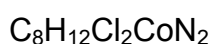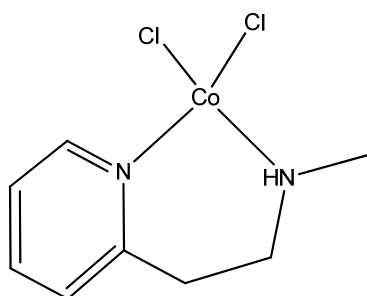
Mol. Wt. 266.03 g/mol

Materials

MAEP	0.74 g	5.42 mmol
CoCl$_2$	0.705 g	5.42 mmol
Methanol	50 mL	

Experimental

2-[2-(Methylamino)-ethyl]-pyridine (MAEP) (0.74 g, 5.42 mmol) in methanol (10 mL) was added to a methanol (40 mL) solution of CoCl$_2$ (0.705 g, 5.42 mmol). The reaction mixture was stirred at 60°C for 3 h. The solution was then evaporated to dryness and the solid product recrystallized from methanol at room temperature to give blue crystals.

Yield

65%	0.934 g	3.51 mmol

EA (C$_8$H$_{12}$Cl$_2$CoN$_2$)

calcd.: C [%] 36.12, H [%] 4.55, N [%] 10.53

found: C [%] 36.15, H [%] 4.47, N [%] 10.64

4.4.3 Synthesis of [CoCl$_2$(MAEP)$_2$]

C$_{16}$H$_{24}$Cl$_2$CoN$_4$
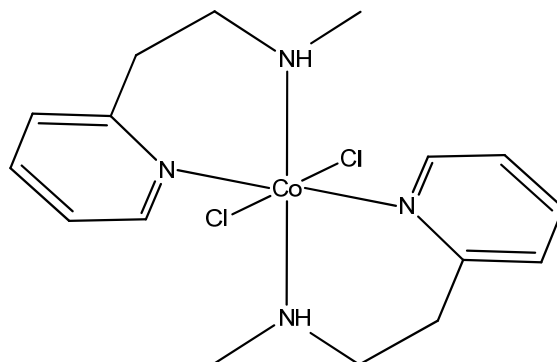
Mol. Wt. 402.23 g/mol

Materials

MAEP	0.618 g	4.54 mmol
CoCl$_2$	0.295 g	2.27 mmol
Methanol	25 mL	

Experimental

2-[2-(Methylamino)-ethyl]-pyridine (MAEP) (0.618 g, 4.54 mmol) in methanol (5 mL) was added to a methanol (20 mL) solution of CoCl$_2$ (0.295 g, 2.27 mmol). The reaction mixture was stirred at 60°C for 3 h. The solution was then evaporated to dryness and the solid product recrystallized from acetonitrile at room temperature to give pink crystals.

Yield

66%	0.599 g	1.49 mmol

EA (C$_{16}$H$_{24}$Cl$_2$CoN$_4$)

calcd. C [%] 47.78, H [%] 6.01, N [%] 13.93

found. C [%] 47.90, H [%] 5.99, N [%] 14.07

4.5 Synthesis of oligonuclear mixed Zn/Co carbamates as precursors to nanosized magnetic oxides under mild conditions

4.5.1 Synthesis of [Zn$_{2.5}$Co$_{1.5}$Et$_2$(O$_2$CN(iPr)$_2$)$_6$]

C$_{58.8}$H$_{107}$Cl$_{0.6}$Co$_{1.5}$N$_6$O$_{12}$Zn$_{2.5}$ [a]
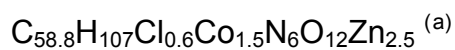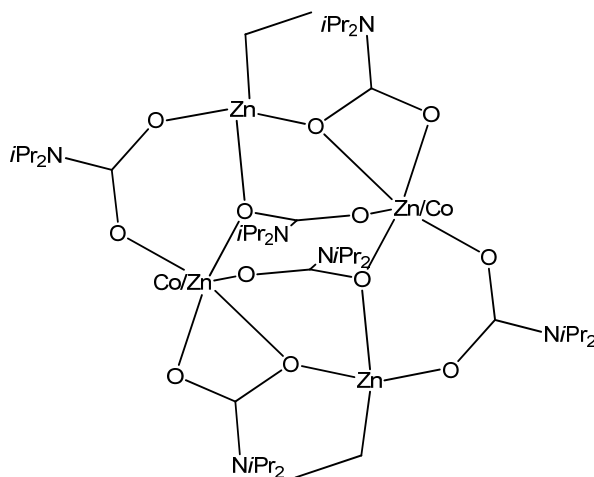
Mol. Wt. 1363.24 g/mol

Materials

[CoCl$_2$(MAP)$_2$]	0.056 g	0.162 mmol
[ZnEt(O$_2$CN(iPr)$_2$)]$_4$	0.154 g	0.162 mmol
Toluene	15 mL	

---

[a] During the refinement of the structure a disorder of the Et groups was detected. A problem which remained was the high rest electron density near the Zn atoms. The rest electron density can be explained by the presence of some molecules in which instead of Et groups Cl is connected to the zinc atom (in average every fourth Et group is replaced by Cl).

Experimental

[CoCl$_2$(MAP)$_2$] (0.056 g, 0.162 mmol) in toluene (10 mL) was added to a toluene (5 mL) solution of [ZnEt(O$_2$CN(*i*Pr)$_2$)]$_4$ (0.154 g, 0.162 mmol). The solution was stirred at 20°C for 3 h. Then the solvent was removed in vacuum. Recrystallization from toluene at -20°C affords purple-coloured crystals.

Yield

33%   0.072 g   0.053 mmol

EA (C$_{58.8}$H$_{107}$Cl$_{0.6}$Co$_{1.5}$N$_6$O$_{12}$Zn$_{2.5}$)

calcd.: C [%] 53.01, H [%] 8.16, N [%] 6.18
found: C [%] 52.47, H [%] 8.35, N [%] 6.62

IR (solid CsI):

3431 (w) $\tilde{\upsilon}$(N-H); 2970 (m), 2867 (w) $\tilde{\upsilon}$(C-H); 1560 (s), 1493 (s) $\tilde{\upsilon}$(C=O); 1356 (s), 1163 (s), 1066 (m) $\tilde{\upsilon}$(C-N) cm^{-1}

UV/VIS (c=6.3*10^{-3} mol L^{-1} in toluene)

ν = 16200 cm^{-1} (λ_{max} = 617 nm), ε = 24 dm^3 mol^{-1} cm^{-1}

ν = 16900 cm^{-1} (λ_{max} = 592 nm), ε = 24 dm^3 mol^{-1} cm^{-1}

ν = 18200 cm^{-1} (λ_{max} = 549 nm), ε = 16 dm^3 mol^{-1} cm^{-1}

AAS

Zn/Co ratio 2.5/1.5

ICP

found ICP	[g/ml]	[g]	weight % in sample	molar ratio Zn/Co
Zn	2.09*10^{-5}	5.23*10^{-4}	1.38*10^{-1}	2.45/1.55
Co	1.19*10^{-5}	2.98*10^{-4}	7.83*10^{-2}	

4.5.2 Synthesis of [Zn$_5$Co$_3$(µ$_4$-O)$_2$(O$_2$CN(*i*Pr)$_2$)$_{12}$]

C$_{92}$H$_{177}$Co$_3$N$_{12}$O$_{26}$Zn$_5$
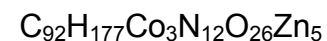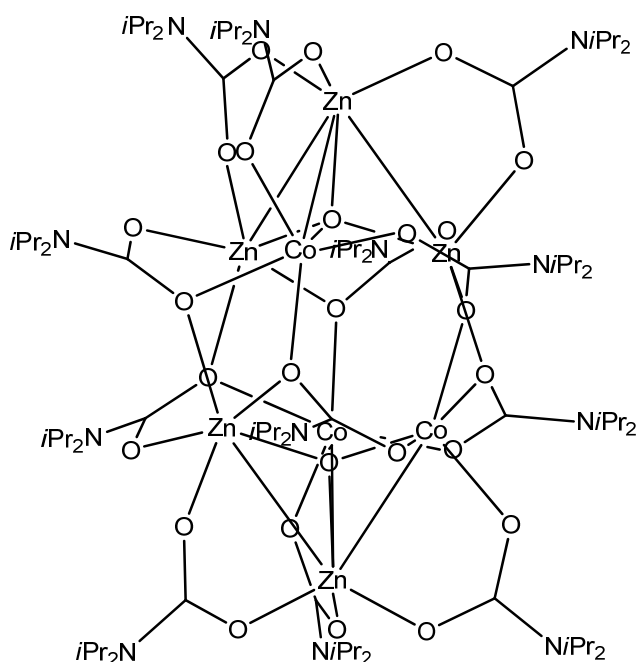
Mol. Wt. 2367.98 g/mol

Materials

[Zn$_{2.5}$Co$_{1.5}$Et$_2$(O$_2$CN(*i*Pr)$_2$)$_6$]	0.012 g
Hexane	2 mL

Experimental

From a solution of [Zn$_{2.5}$Co$_{1.5}$Et$_2$(O$_2$CN(*i*Pr)$_2$)$_6$] in hexane a new carbamate complex was crystallized, which turned out to be an octanuclear complex namely [Zn$_5$Co$_3$(µ$_4$-O)$_2$(O$_2$CN(iPr)$_2$)$_{12}$].

EA (C$_{92}$H$_{177}$Co$_3$N$_6$O$_{26}$Zn$_5$)

calcd.: C [%] 46.65, H [%] 7.56, N [%] 7.10

found: C [%] 42.44, H [%] 7.34, N [%] 6.17

IR (solid CsI):

3549 (w) $\tilde{\upsilon}$(N-H); 2963 (m), 2889 (w) $\tilde{\upsilon}$(C-H); 1566 (s), 1466 (s) $\tilde{\upsilon}$(C=O); 1358 (s), 1219 (s), 1165 (s), 1066 (s) $\tilde{\upsilon}$(C-N) cm^{-1}

UV/VIS (c=1.95*10^{-2} mol L^{-1} in toluene)

ν = 16050 cm^{-1} (λ_{max} = 623 nm), ε = 25 dm^3 mol^{-1} cm^{-1}

ν = 17010 cm^{-1} (λ_{max} = 588 nm), ε = 24 dm^3 mol^{-1} cm^{-1}

ν = 18350 cm^{-1} (λ_{max} = 545 nm), ε = 16 dm^3 mol^{-1} cm^{-1}

AAS

Zn/Co ratio 5/3

ICP

found ICP	[g/ml]	[g]	weight % in sample	molar ratio Zn/Co
Zn	1.37*10^{-5}	3.43*10^{-4}	2.28*10^{-1}	5.17/2.83
Co	6.50*10^{-6}	1.63*10^{-4}	1.08*10^{-1}	

4.5.3 Synthesis of [Zn$_{2.5}$Co$_{1.5}$(μ_4-O)(O$_2$CN(*i*Pr)$_2$)$_6$]
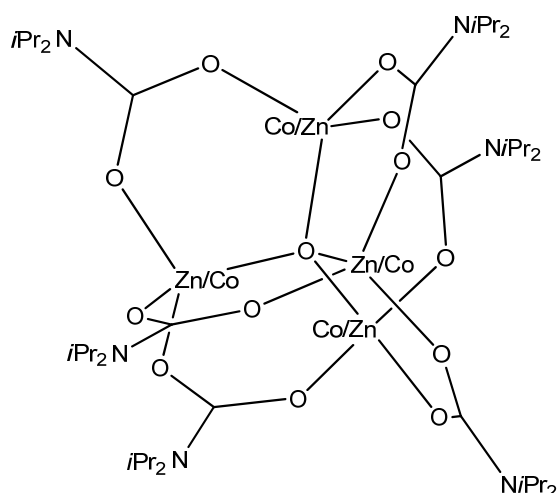
C$_{46}$H$_{90}$Co$_{1.5}$N$_8$O$_{13}$Zn$_{2.5}$

Mol. Wt. 1215.08 g/mol

Materials

[$Zn_{2.5}Co_{1.5}Et_2(O_2CN(iPr)_2)_6$]   0.011 g

Acetonitrile   2 mL

Experimental

From a solution of [$Zn_{2.5}Co_{1.5}Et_2(O_2CN(iPr)_2)_6$] in acetonitrile a new carbamate complex was crystallized, which turned out to be an tetranuclear complex namely [$Zn_{2.5}Co_{1.5}(\mu_4\text{-}O)(O_2CN(iPr)_2)_6$].

EA ($C_{42}H_{84}Co_{1.5}N_6O_{13}Zn_{2.5}*2CH_3CN$)

calcd.: C [%] 46.62, H [%] 7.56, N [%] 7.10

found: C [%] 41.09, H [%] 6.91, N [%] 6.98

IR (solid CsI):

3534 (w) $\tilde{\upsilon}$(N-H); 2955 (m), 2892 (w) $\tilde{\upsilon}$(C-H); 1573 (s), 1474 (s) $\tilde{\upsilon}$(C=O); 1345 (s), 1212 (s), 1159 (s), 1072 (m) $\tilde{\upsilon}$(C-N) cm^{-1}

UV/VIS (c=1.86*10^{-2} mol L^{-1} in toluene)

ν = 16050 cm^{-1} (λ_{max} = 623 nm), ε = 27 dm^3 mol^{-1} cm^{-1}

ν = 17000 cm^{-1} (λ_{max} = 589 nm), ε = 26 dm^3 mol^{-1} cm^{-1}

ν = 18380 cm^{-1} (λ_{max} = 544 nm), ε = 18 dm^3 mol^{-1} cm^{-1}

MS (FD+, c=1*10^{-3} mol L^{-1} in toluene)

calcd. m/z (%) = 1182.36 (100) for [$Zn_2Co_2(\mu_4\text{-}O)(O_2CN(iPr)_2)_6$]

found m/z (%) =1182.40 (100) for [$Zn_2Co_2(\mu_4\text{-}O)(O_2CN(iPr)_2)_6$]

calcd. m/z (%) = 1187.35 (100) for [$Zn_3Co(\mu_4\text{-}O)(O_2CN(iPr)_2)_6$]

found m/z (%) =1187.39 (100) for [$Zn_3Co(\mu_4\text{-}O)(O_2CN(iPr)_2)_6$]

4.5.4 Synthesis of [Zn$_{2.5}$Co$_{1.5}$Me$_2$(O$_2$CN(*i*Pr)$_2$)$_6$]

C$_{55.3}$H$_{95.6}$Cl$_{0.6}$Co$_{1.5}$N$_6$O$_{12}$Zn$_{2.5}$ [b]
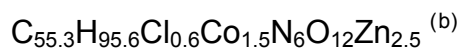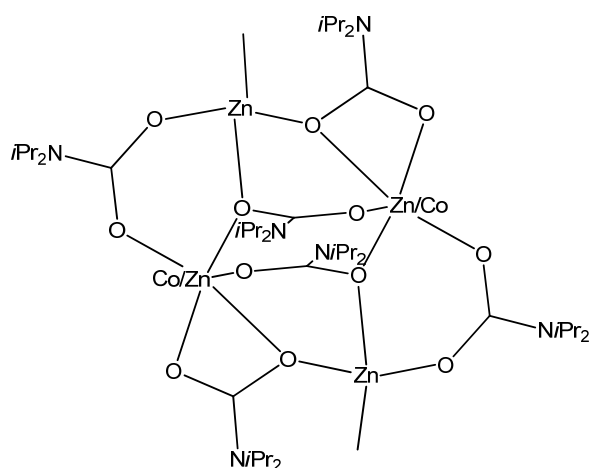
Mol. Wt. 1251.99 g/mol

Materials

[CoCl$_2$(MAP)$_2$]	0.077 g	0.222 mmol
[ZnMe(O$_2$CN(*i*Pr)$_2$)]$_4$	0.200 g	0.222 mmol
Toluene	15 mL	

Experimental

[CoCl$_2$(MAP)$_2$] (0.077 g, 0.222 mmol) in toluene (10 mL) was added to a toluene (5 mL) solution of [ZnMe(O$_2$CN(*i*Pr)$_2$)]$_4$ (0.2 g, 0.222 mmol). The reaction mixture was stirred at 20°C for 3 h. The solution was then evaporated to dryness and the solid product recrystallized from toluene at -20°C to give purple crystals.

Yield

32%	0.094 g	0.071 mmol

---

[b] A problem which remained was the high rest electron density near the Zn atoms. The rest electron density can be explained by the presence of some molecules in which instead of Me groups Cl is connected to the zinc atom (in average every fourth Me group is replaced by Cl). In addition, new problem arises due to the disorder of the solvent molecules in the crystal.

EA ($C_{55.3}H_{95.6}Cl_{0.6}Co_{1.5}N_6O_{12}Zn_{2.5}$)

calcd.: C [%] 51.82, H [%] 8.02, N [%] 6.31

found: C [%] 51.05, H [%] 7.81, N [%] 6.41

IR (solid CsI):

3427 (w) $\tilde{\upsilon}$(N-H); 2984 (m), 2874 (w) $\tilde{\upsilon}$(C-H); 1565 (s), 1498 (s) $\tilde{\upsilon}$(C=O); 1354 (s), 1153 (s), 1074 (m) $\tilde{\upsilon}$(C-N) cm^{-1}

UV/VIS (c=7.6*10^{-3} mol L^{-1} in toluene)

ν = 17000 cm^{-1} (λ_{max} = 588 nm), ε = 17 dm^3 mol^{-1} cm^{-1}

ν = 19120 cm^{-1} (λ_{max} = 523 nm), ε = 9 dm^3 mol^{-1} cm^{-1}

ν = 21050 cm^{-1} (λ_{max} = 475 nm), ε = 2 dm^3 mol^{-1} cm^{-1}

4.5.5 Synthesis of Zn/Co mixed oxide nanoparticles

Materials

$[Zn_{2.5}Co_{1.5}Et_2(O_2CN(iPr)_2)_6]$ 0.014 g   0.010 mmol

Experimental

$[Zn_{2.5}Co_{1.5}Et_2(O_2CN(iPr)_2)_6]$ (0.014 g, 0.010 mmol) were filled in a platinum crucible. The compound was heated with different heating rates (2, 5 and 10°C min^{-1}) under nitrogen atmosphere with a flow rate of 150 mL min^{-1}. The starting temperature was settled at 30°C and the end temperature was fixed at 300°C. Decomposition of the mixed Zn/Co carbamate leads to the formation of Zn/Co mixed oxide nanoparticles.

BET

BET surface: 37.2 m^2 g^{-1}

average particle size: 25±1 nm

XRD

CoO mean particle size	47.7±0.3 nm
ZnO mean particle size	7.7±0.4 nm

4.6 Synthesis of new MnCl₂ complexes with different nitrogen-bases

4.6.1 Synthesis of [Mn₂Cl₄(MAEP)₂]

$C_{16}H_{24}Cl_4Mn_2N_4$
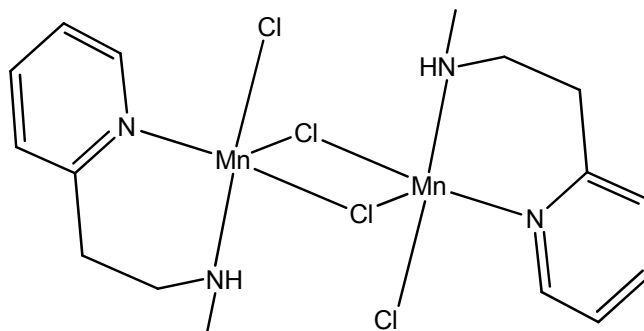
Mol. Wt. 524.07 g/mol

Materials

MnCl₂	0.22 g	1.75 mmol
MEAP	0.48 g	3.5 mmol
Methanol	20 mL	

Experimental

2-[2-(Methylamino)-ethyl]-pyridine (MAEP) (0.48 g, 3.5 mmol) in methanol (10 mL) was added to a methanol (10 mL) solution of MnCl₂ (0.22 g, 1.75 mmol). The solution was stirred at 60°C for 3 h. The reaction mixture was left over night at room temperature. The solution was separated from the precipitate and was evaporated to dryness. The solid product was recrystallized from methanol at room temperature to give colourless crystals.

Yield

61%	0.56 g	1.069 mmol

4.6.2 Synthesis of [MnCl$_2$(MAP)$_2$]

$$C_{12}H_{16}Cl_2MnN_4$$
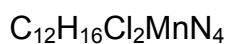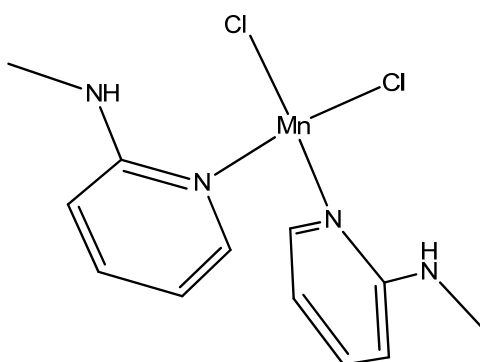
Mol. Wt. 341.01 g/mol

Materials

MnCl$_2$	0.325 g	2.58 mmol
MAP	0.558 g	5.16 mmol
Methanol	40 mL	

Experimental

2-(Methylamino)pyridine (MAP) (0.558 g, 5.16 mmol) in methanol (20 mL) was added to a methanol (20 mL) solution of MnCl$_2$ (0.325 g, 2.58 mmol). The solution was stirred at 60°C for 3 h. The reaction mixture was left over night at room temperature. The solution was evaporated to leave an oily brown compound. Every attempt to crystallize this compound failed.

4.7 Synthesis of oligonuclear mixed Zn/Mn carbamates as precursors to nanosized magnetic oxides under mild conditions

4.7.1 Synthesis of [Zn$_2$Mn$_6$(μ_4-O)$_2$(O$_2$CN(iPr)$_2$)$_{12}$]

C$_{91}$H$_{175}$Mn$_6$N$_{12}$O$_{26}$Zn$_2$
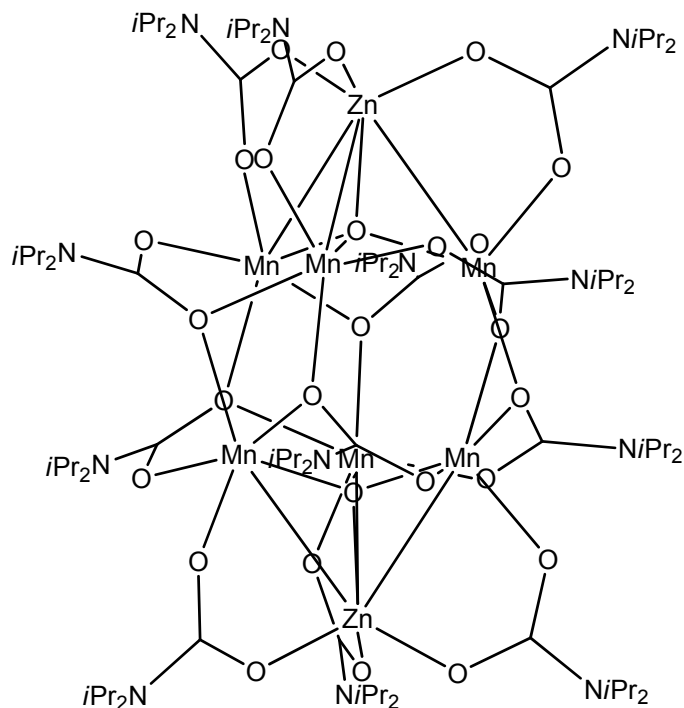
Mol. Wt. 2313.81 g/mol

Materials

MnCl$_2$ x 0.22 H$_2$O	0.255 g	1.96 mmol
MAP	0. 440 g	4.06 mmol
[ZnEt(O$_2$CN(iPr)$_2$)$_4$]	1.000 g	1.02 mmol
THF	10 mL	
Toluene	10 mL	

Experimental

2-(Methylamino)pyridine (MAP) (0.440 g, 4.06 mmol) was added to a THF (10 mL) suspension of MnCl$_2$ x 0.22 H$_2$O (0.255 g, 1.96 mmol). By the addition of the 2-(Methylamino)pyridine the white suspension of MnCl$_2$ x 0.22 H$_2$O becomes a

solution, this solution was stirred at room temperature for 1 h. Without isolating the intermediate compound to the solution was added a toluene solution (10 mL) of [ZnEt(O$_2$CN(iPr)$_2$)$_4$] (1 g, 1.02 mmol) and the solution colour changed into yellow. The solution was stirred at room temperature for 24 h, then evaporated to dryness. The solid product was recrystallized from toluene at room temperature to give colourless crystals.

Yield

28.8%   0.21 g   0.094 mmol

EA (C$_{84}$H$_{168}$Mn$_6$N$_{12}$O$_{26}$Zn$_2$*C$_7$H$_8$)

calcd.: C [%] 47.19, H [%] 7.62, N [%] 7.26

found: C [%] 47.33, H [%] 7.62, N [%] 7.46

IR (solid CsI):

3487 (w) $\tilde{\upsilon}$(N-H); 2970 (m) $\tilde{\upsilon}$(C-H); 1566 (s), 1450 (s) $\tilde{\upsilon}$(C=O); 1358 (s), 1219 (s), 1165 (s), 1065 (m) $\tilde{\upsilon}$(C-N) cm^{-1}

UV/VIS (c=3.0*10^{-3} mol L^{-1} in CHCl$_3$)

ν = 33112 cm^{-1} (λ_{max} = 301 nm), ε = 32 dm^3 mol^{-1} cm^{-1}

ν = 42016 cm^{-1} (λ_{max} = 238 nm), ε = 110 dm^3 mol^{-1} cm^{-1}

UV/VIS (c=2.6*10^{-3} mol L^{-1} in CH$_3$CN)

ν = 33112 cm^{-1} (λ_{max} = 301 nm), ε = 54 dm^3 mol^{-1} cm^{-1}

ν = 41322 cm^{-1} (λ_{max} = 242 nm), ε = 113 dm^3 mol^{-1} cm^{-1}

UV/VIS (polytetrafluoroethylene powder)

λ_{max} = 314 nm,

λ_{max} = 238 nm

MS (FD+, c=4.3*10^{-4} mol L^{-1} in toluene)

calcd. m/z (%) = 2222.70 (100)

found m/z (%) = 2222.72 (100)

4.7.2 Synthesis of [(MAP)H]⁺[(MAP)ZnCl₃]⁻

4.7.2 Synthesis of [(MAP)H]$^+$[(MAP)ZnCl$_3$]$^-$

$C_{12}H_{17}Cl_3N_4Zn$
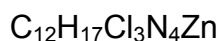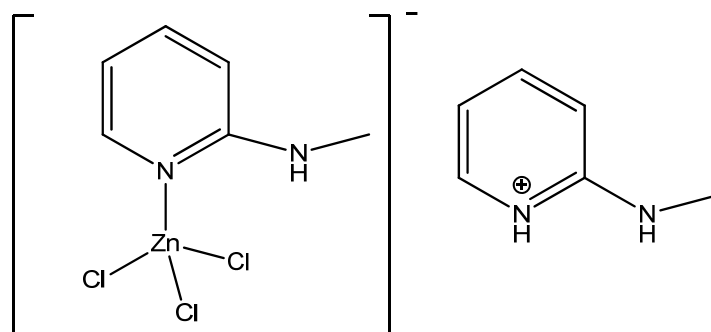
Mol. Wt. 389.02 g/mol

Materials

$MnCl_2$ x 0.22 H_2O	0.17 g	1.35 mmol
MAP	0. 29 g	2.7 mmol
$[ZnEt(O_2CN(iPr)_2)]_4$	0.64 g	0.675 mmol
H_2O	0.05 g	2.7 mmol
THF	6 mL	
Toluene	6 mL	

Experimental

2-(Methylamino)pyridine (MAP) (0.29 g, 2.7 mmol) was added to a THF (6 mL) suspension of $MnCl_2$ x 0.22 H_2O (0.17 g, 1.35 mmol). By the addition of the 2-(Methylamino)pyridine the white suspension of $MnCl_2$ becomes a solution, this solution was stirred at room temperature for 1 h. Without isolating the intermediate compound to the solution was added a toluene solution (6mL) of $[ZnEt(O_2CN(iPr)_2)]_4$ (0,64 g, 0.675 mmol) and the solution becomes yellow. The solution was stirred at room temperature for 1 h and then was added (0.05 mg, 2.7mmol) water. By the addition of water a precipitate is formed and the mixture became like a light brown suspension. The reaction mixture was further stirred at room temperature for additional 72 h and the solution colour changes to green. The green solution was separated from the precipitate and was then evaporated to dryness. The solid

product was recrystallized from toluene at room temperature to give colourless crystals.

Yield

2%	0.005 g	0.13 mmol

^{1}H NMR (200 MHz, C$_6$D$_6$):

δ = 2.55 (d, 3H, NC*H3*,), 6.00 (d, 1H, *py*), 6.39 (t, 1H, *py*), 7.13 (m, 2H, *py*), 8.38 (b, 1H, N*H*)

EA

calcd. C [%] 37.05, H [%] 4.40, N [%] 14.40

found. C [%] 39.13 H [%] 5.47., N [%] 13.75

4.7.3 Synthesis of [Zn$_2$Mn$_6$(μ_4-O)$_2$(μ_3-O)(O$_2$CN(*i*Pr)$_2$)$_{12}$]

C$_{91}$H$_{176}$Mn$_6$N$_{12}$O$_{27}$Zn$_2$
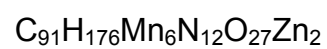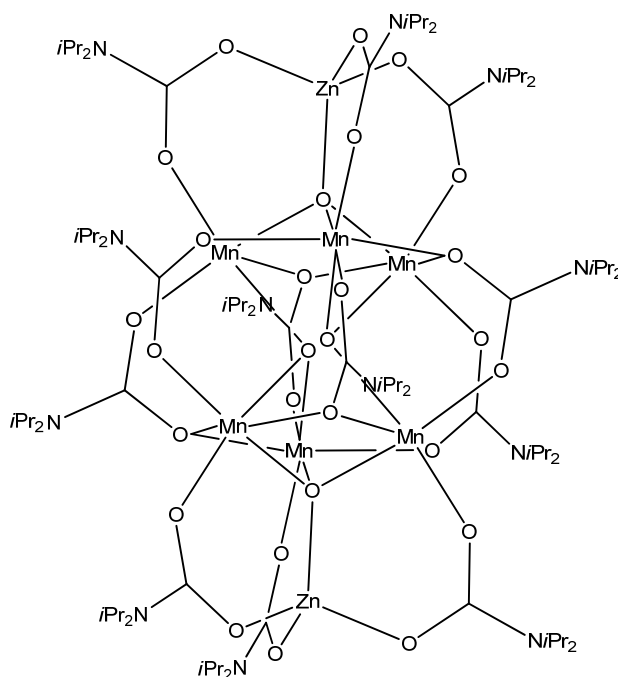
Mol. Wt. 2330.82 g/mol

Experimental

A toluene solution of $[Zn_2Mn_6(\mu_4\text{-}O)_2(O_2CN(iPr)_2)_{12}]$ (0.0231 g, 0.01 mmol) was stirred for 48 h at room temperature (allowing a few air contacts) during which time the reaction mixture changes the colour from colourless to brown. The solution was then evaporated to dryness. The solid product was recrystallized from toluene/hexane 4:1 at room temperature to give brown crystals.

Yield

97%   0.0224 g   0.0097 mmol

EA ($C_{84}H_{168}Mn_6N_{12}O_{27}Zn_2*C_7H_8$)

calcd.: C [%] 46.33, H [%] 7.61, N [%] 7.21

found: C [%] 47.07, H [%] 7.71, N [%] 7.46

IR (solid CsI):

3479 (w) $\tilde{\upsilon}$(N-H); 2970 (m) $\tilde{\upsilon}$(C-H); 1566 (s), 1466 (s) $\tilde{\upsilon}$(C=O); 1358 (s), 1211 (s), 1157 (s), 1065 (m) $\tilde{\upsilon}$(C-N) cm^{-1}

UV/VIS (c=3.0*10^{-3} mol L^{-1} in CHCl$_3$)

ν = 34013 cm^{-1} (λ_{max} = 294 nm), ε = 114 dm^3 mol^{-1} cm^{-1}

ν = 43103 cm^{-1} (λ_{max} = 232 nm), ε = 376 dm^3 mol^{-1} cm^{-1}

UV/VIS (polytetrafluoroethylene powder)

λ_{max} = 500 nm

λ_{max} = 288 nm

λ_{max} = 244 nm

MS (FD+, c=4.3*10^{-4} mol L^{-1} in toluene)

calcd. 2238.69 m/z (%) = (100)

found 2238.53 m/z (%) = (100)

4.7.3 Synthesis of Zn/Mn mixed oxide nanoparticles

Method A
Materials

$[Zn_2Mn_6(\mu_4\text{-}O)_2(O_2CN(i\text{Pr})_2)_{12}]$ 0.012 g   0.005 mmol

Experimental

$[Zn_2Mn_6(\mu_4\text{-}O)_2(O_2CN(i\text{Pr})_2)_{12}]$ (0.012 g, 0.005 mmol) were filled in a platinum crucible. The compound was heated with different heating rates (2, 5 and 10°C min^{-1}) under nitrogen atmosphere with a flow rate of 150 mL min^{-1}. The starting temperature was settled at 30°C and the end temperature was fixed at 300°C. Decomposition of the mixed Zn/Mn carbamate leads to the formation of the oxides MnO and $ZnMn_2O_4$ in a ratio 26 to 74%.

XRD

oxide phase	MnO	$ZnMn_2O_4$
composition	26%	74%

EDX

Mn:Zn ratio 3:1

TEM

mean particle size	9.0 nm
maximum particle size	23.0 nm
minimum particle size	1.9 nm
standard deviation	4.3 nm

Method B

Materials

[Zn$_2$Mn$_6$(μ_4-O)$_2$(μ_3-O)(O$_2$CN(*i*Pr)$_2$)$_{12}$]   0.019 g   0.008 mmol

Experimental

[Zn$_2$Mn$_6$(μ_4-O)$_2$(μ_3-O)(O$_2$CN(*i*Pr)$_2$)$_{12}$] (0.019 g, 0.008 mmol) were filled in a platinum crucible. The compound was heated with different heating rates (2, 5 and 10°C min^{-1}) under nitrogen atmosphere with a flow rate of 150 mL min^{-1}. The starting temperature was settled at 30°C and the end temperature was fixed at 300°C. Decomposition of the mixed Zn/Mn carbamate leads to the formation of the oxides MnO and ZnMn$_2$O$_4$ in a ratio 50 to 50%.

XRD

oxide phase	MnO	ZnMn$_2$O$_4$
composition	50%	50%

EDX

Mn:Zn ratio 3:1

TEM

mean particle size	8.4 nm
maximum particle size	18.2 nm
minimum particle size	2.5 nm
standard deviation	3.1 nm

5. Supplementary material

5.1 Crystal data and refinement details

Formula	$C_{36}H_{76}N_4O_8Zn_4$ **1**	$C_{44}H_{92}N_4O_8Zn_4$ **2**
Mr [g·mol^{-1}]	954.53	1066.70
Crystal size [mm]	0.60 x 0.50 x 0.40	0.50 x 0.25 x 0.20
Crystal system	tetragonal	triclinic
Space group	P4 (1)	*P* -1
a [Å]	13.3570(19)	12.882(3)
b [Å]	13.3570(19)	13.453(3)
c [Å]	26.598(5)	18.089(4)
α [°]	90.000(0)	83.61(3)
β [°]	90.000(0)	87.47(3)
γ [°]	90.000(0)	64.66(3)
V [Å^3]	4745.3(13)	2815.6(10)
ρ_{calc} [g·m^{-3}]	1.336	1.258
Z	4	2
F(000)	2016	1136
hkl range	-17 ≤ *h* ≤ 17	-16 ≤ *h* ≤ 16
	-12 ≤ *k* ≤ 12	-17 ≤ *k* ≤ 16
	-34 ≤ *l* ≤ 34	-23 ≤ *l* ≤ 23
θ range [°]	1.52 to 27.47	1.68 to 27.71
μ [mm^{-1}]	2.043	1.729
Reflections collected	10899	14234
Independent reflections [R_{int}]	10852 (0.0000)	9346 (0.0467)
Observed reflections [*I* > 2σ(*I*)]	8384	6314
Refined parameters / restraints	502 / 1	563 / 0
Goodness-of-fit	1.019	1.013
R_1 [*I* > 2 σ(*I*)]	0.0407	0.0471
wR2 (all data)	0.0860	0.1261
Residual electron density [e·Å^{-3}]	0.621 / -0.648	0.477 / -0.495

Formula	$C_{54}H_{108}N_6O_{13}Zn_4$ **3**	$C_{28}H_{48}N_4O_4Zn_2$ **4**
Mr [g·mol^{-1}]	2621.88	1270.88
Crystal size [mm]	0.25 x 0.25 x 0.20	0.20 x 0.20 x 0.15
Crystal system	orthorhombic	triclinic
Space group	Fdd2	P -1
a [Å]	28.663(6)	8.8950(18)
b [Å]	30.645(6)	9.0420(18)
c [Å]	15.878(3)	11.105(2)
α [°]	90.000(0)	80.75(3)
β [°]	90.000(0)	73.47(3)
γ [°]	90.000(0)	70.46(3)
V [Å^3]	13947(5)	804.8(3)
ρ_{calc} [Mg·m^{-3}]	1.249	1.311
Z	4	1
F(000)	5584	336
Range hkl (indep.set)	-36 ≤ h ≤ 36	-12 ≤ h ≤ 12
	-37 ≤ k ≤ 37	-12 ≤ k ≤ 12
	-20 ≤ l ≤ 20	-15 ≤ l ≤ 15
θ range [°]	2.48 to 27.49	3.4 to 55.4
μ [mm^{-1}]	1.415	1.526
Reflections collected	13440	5358
Independent reflections [R_{int}]	7303 (0.0464)	4193 (0.0354)
Observed reflections [$I > 2\sigma(I)$]	6518	3687
Refined parameters / restraints	396 / 10	182 / 0
Goodness-of-fit	1.035	1.042
R_1 [$I > 2\ \sigma(I)$]	0.0354	0.0428
$wR2$ (all data)	0.0882	0.1174
Residual electron density [e·Å^{-3}]	0.497 / -0.543	0.529 / -0.627

Formula	$C_{28}H_{62}N_8O_4Zn_2$ **5**	$C_{24}H_{54}N_8O_4Zn$ **6**
Mr [g·mol^{-1}]	705.64	584.12
Crystal size [mm]	0.40 x 0.40 x 0.30	0.20 x 0.14 x 0.06
Crystal system	monoclinic	monoclinic
Space group	P2 (1) / n	P2 (1) / n
a [Å]	9.2800()19	11.6812(11)
b [Å]	19.420(4)	13.6524(12)
c [Å]	10.422(2)	20.2283(18)
α [°]	90.000(0)	90.000(0)
β [°]	93.41(3)	102.741(2)
γ [°]	90.000(0)	90.000(0)
V [Å^3]	1874.9(7)	3146.5(5)
ρ_{calc} [Mg·m^{-3}]	1.250	1.233
Z	2	4
F(000)	756	1264
Range *hkl* (indep.set)	$-12 \le h \le 12$	$17 \le h \le 17$
	$-25 \le k \le 25$	$-20 \le k \le 19$
	$-13 \le l \le 13$	$-29 \le l \le 29$
θ range [°]	2.10 to 27.45	1.86 to 31.80
μ [mm^{-1}]	1.319	0.821
Reflections collected	8394	79900
Independent reflections [R_{int}]	4268 (0.0434)	10563 (0.0551)
Observed reflections [$I > 2\sigma(I)$]	3074	7822
Refined parameters / restraints	199 / 0	358 / 0
Goodness-of-fit	1.045	1.073
R_1 [$I > 2\,\sigma(I)$]	0.0488	0.0357
wR2 (all data)	0.1206	0.0981
Residual electron density [e·Å^{-3}]	0.776 / -0.443	0.744 / -0.314

Formula	$C_{29}H_{49}N_7O_2Zn$ **7**	$C_{52.60}H_{93.40}N_9O_6Zn_3$ **8**
Mr [g·mol^{-1}]	593.12	1144.07
Crystal size [mm]	0.17 x 0.16 x 0.15	0.40 x 0.20 x 0.20
Crystal system	tetragonal	monoclinic
Space group	I-4	C2 / c
a [Å]	23.861(3)	21.446(4)
b [Å]	23.861(3)	15.867(3)
c [Å]	12.0663(17)	36.361(8)
α [°]	90.000(0)	90.000(0)
β [°]	90.000(0)	94.04(3)
γ [°]	90.000(0)	90.000(0)
V [Å^3]	6870.1(16)	12342(4)
ρ_{calc} [Mg·m^{-3}]	1.147	1.231
Z	8	8
$F(000)$	2544	4880
Range hkl (indep.set)	$-28 \leq h \leq 28$	$-29 \leq h \leq 29$
	$0 \leq k \leq 28$	$-21 \leq k \leq 21$
	$0 \leq l \leq 14$	$-49 \leq l \leq 49$
θ range [°]	1.89 to 25.08	1.60 to 29.00
μ [mm^{-1}]	0.748	1.207
Reflections collected	57156	104515
Independent reflections [R_{int}]	6128 (0.1263)	16341 (0.0608)
Observed reflections [$I > 2\sigma(I)$]	4423	-
Refined parameters / restraints	366 / 0	713 / 0
Goodness-of-fit	1.082	1.049
R_1 [$I > 2\,\sigma(I)$]	0.0594	0.0461
$wR2$ (all data)	0.1123	0.1564
Residual electron density [e·Å^{-3}]	1.679 / -0.638	0.551 / -0.537

Formula	$C_{12}H_{16}Cl_2CoN_4$ **9**	$C_8H_{12}Cl_2CoN_2$ **10**
Mr [g·mol^{-1}]	346.12	266.03
Crystal size [mm]	0.60 x 0.60 x 0.55	0.35 x 0.30 x 0.30
Crystal system	monoclinic	monoclinic
Space group	P2 (1) / c	P2 (1) / c
a [Å]	12.732(3)	12.681(3)
b [Å]	7.9800(16)	6.7560(14)
c [Å]	14.617(3)	13.337(3)
α [°]	90.000(0)	90.000(0)
β [°]	96.53(3)	103.05(3)
γ [°]	90.000(0)	90.000(0)
V [Å^3]	1475.5(5)	1113.1(4)
ρ_{calc} [g·m^{-3}]	1.558	1.587
Z	4	4
F(000)	708	540
hkl range	$-17 \leq h \leq 17$	$-17 \leq h \leq 17$
	$-10 \leq k \leq 8$	$-7 \leq k \leq 9$
	$-20 \leq l \leq 20$	$-18 \leq l \leq 18$
θ range [°]	1.61 to 30.03	3.14 to 30.00
μ [mm^{-1}]	1.516	1.978
Reflections collected	24584	7248
Independent reflections [R_{int}]	4226 (0.0195)	3234 (0.0400)
Observed reflections [$I > 2\sigma(I)$]	3678	2266
Refined parameters / restraints	182 / 0	119 / 0
Goodness-of-fit	1.027	1.034
R_1 [$I > 2\,\sigma(I)$]	0.0305	0.0444
wR2 (all data)	0.0802	0.1180
Residual electron density [e·Å^{-3}]	0.526 / -0.523	0.953 / -0.741

Formula	$C_{16}H_{24}Cl_2CoN_4$ **11**	$C_{58.8}H_{107}Cl_{0.6}Co_{1.5}N_6O_{12}Zn_{2.5}$ [a] **12**
Mr [g·mol^{-1}]	402.22	1363.24
Crystal size [mm]	0.30 x 0.20 x 0.20	0.30 x 0.20 x 0.20
Crystal system	monoclinic	triclinic
Space group	P2 (1) / n	P-1
a [Å]	9.998(2)	12.191(2)
b [Å]	6.6600(13)	12.594(3)
c [Å]	13.279(3)	13.095(3)
α [°]	90.000(0)	116.34(3)
β [°]	99.22(3)	95.32(3)
γ [°]	90.000(0)	100.53(3)
V [Å^3]	872.8(3)	1736.7(9)
ρ_{calc} [g·m^{-3}]	1.531	1.303
Z	2	1
F(000)	418	724
hkl range	$-13 \leq h \leq 14$	$-15 \leq h \leq 15$
	$-9 \leq k \leq 9$	$-16 \leq k \leq 16$
	$-18 \leq l \leq 18$	$-16 \leq l \leq 16$
θ range [°]	2.38 to 30.00	1.73 to 27.43
μ [mm^{-1}]	1.293	1.285
Reflections collected	5014	14834
Independent reflections [R_{int}]	2535 (0.0291)	7894 (0.0530)
Observed reflections [$I > 2\sigma(I)$]	2072	-
Refined parameters / restraints	107 / 0	400 / 0
Goodness-of-fit	1.063	1.010
R_1 [$I > 2\,\sigma(I)$]	0.0368	0.0469
$wR2$ (all data)	0.0959	0.1080
Residual electron density [e·Å^{-3}]	1.038 / -0.614	0.778 / -0.556

[a] During the refinement of the structure a disorder of the Et groups was detected. A problem which remained was the high rest electron density near the Zn atoms. The rest electron density can be explained by the presence of some molecules in which instead of Et groups Cl is connected to the zinc atom (in average every fourth Et group is replaced by Cl).

Formula	$C_{92.20}H_{177}Co_3N_{12}O_{26}Zn_5$ **13**	$C_{46}H_{90}Co_{1.5}N_8O_{26}Zn_{2.5}$ **14**
Mr [g·mol⁻¹]	4747.80	1215.08
Crystal size [mm]	0.25 x 0.20 x 0.20	0.35 x 0.30 x 0.30
Crystal system	triclinic	monoclinic
Space group	P-1	P2 (1) / c
a [Å]	15.062(3)	14.321(3
b [Å]	15.173(3)	35.817(7)
c [Å]	15.893(3)	24.108(5)
α [°]	65.93(3)	90.00
β [°]	67.16(3)	99.44(3)
γ [°]	88.02(3)	90.00
V [Å³]	3022.9(10)	12198(4)
ρ_{calc} [g·m⁻³]	1.304	1.323
Z	1	4
F(000)	1254	5132
hkl range	-18 ≤ *h* ≤ 19	-20 ≤ *h* ≤ 20
	-19 ≤ *k* ≤ 19	-50 ≤ *k* ≤ 50
	-20 ≤ *l* ≤ 20	-33 ≤ *l* ≤ 33
θ range [°]	1.54 to 27.50	1.42 to 30.00
μ [mm⁻¹]	1.442	1.432
Reflections collected	25184	71386
Independent reflections [R_{int}]	13616 (0.0700)	35552 (0.0806)
Observed reflections [*I* > 2σ(*I*)]	8480	19442
Refined parameters / restraints	680 / 0	1322 / 0
Goodness-of-fit	1.084	1.015
R_1 [*I* > 2 σ(*I*)]	0.1072	0.0608
wR2 (all data)	0.3283	0.1604
Residual electron density [e·Å⁻³]	1.880 / -1.127	1.212 / -0.994

Formula	$C_{55.3}H_{95.6}Cl_{0.6}Co_{1.5}N_6O_{12}Zn_{2.5}$ [b] **15**	$C_{16}H_{24}Cl_4Mn_2N_4$ **17**
Mr [g·mol^{-1}]	1251.99	524.07
Crystal size [mm]	0.30 x 0.25 x 0.25	0.30 x 0.20 x 0.15
Crystal system	triclinic	monoclinic
Space group	P-1	P2 (1) / n
a [Å]	14.013(3)	10.971(2)
b [Å]	15.536(3)	14.929(3)
c [Å]	17.012(3)	12.844(3)
α [°]	76.49(3)	90.000(0)
β [°]	77.96(3)	92.39(3)
γ [°]	74.98(3)	90.000(0)
V [Å^3]	3434.6(12)	2101.8(7)
ρ_{calc} [g·m^{-3}]	1.211	1.656
Z	2	4
F(000)	1324	1064
hkl range	-18 ≤ *h* ≤ 19	-15 ≤ *h* ≤ 15
	-21 ≤ *k* ≤ 21	-21 ≤ *k* ≤ 21
	-23 ≤ *l* ≤ 23	-18 ≤ *l* ≤ 18
θ range [°]	2.27 to 29.16	2.09 to 30.03
μ [mm^{-1}]	1.296	1.718
Reflections collected	34158	11840
Independent reflections [R_{int}]	18347 (0.0226)	6131 (0.0174)
Observed reflections [*I* > 2σ(*I*)]	-	5416
Refined parameters / restraints	736 / 0	245 / 0
Goodness-of-fit	1.086	1.038
R_1 [*I* > 2 σ(*I*)]	0.0443	0.0292
wR2 (all data)	0.1365	0.724
Residual electron density [e·Å^{-3}]	2.243 / -0.493	0.677 / -0.572

[b] A problem which remained was the high rest electron density near the Zn atoms. The rest electron density can be explained by the presence of some molecules in which instead of Me groups Cl is connected to the zinc atom (in average every fourth Me group is replaced by Cl). In addition, new problem arises due to the disorder of the solvent molecules in the crystal.

Formula	C$_{91}$H$_{175}$Mn$_6$N$_{12}$O$_{26}$Zn$_2$ **19**	C$_{12}$H$_{17}$Cl$_3$N$_4$Zn **20**
Mr [g·mol^{-1}]	2313.81	389.02
Crystal size [mm]	0.22 x 0.18 x 0.16	0.20 x 0.12 x 0.12
Crystal system	orthorhombic	monoclinic
Space group	P b c n	P2 (1) / n
a [Å]	22.466(11)	7.4320(15)
b [Å]	23.113(12)	14.229(3)
c [Å]	23.385(11)	15.378(3)
α [°]	90.000(0)	90.00(0)
β [°]	90.000(0)	90.88(3)
γ [°]	90.000(0)	90.00(0)
V [Å^3]	12143(11)	1626.0(6)
ρ$_{calc}$ [g·m^{-3}]	1.266	1.589
Z	4	4
F(000)	4892	792
hkl range	0 ≤ h ≤ 31	-10 ≤ h ≤ 10
	0 ≤ k ≤ 31	-19 ≤ k ≤ 20
	0 ≤ l ≤ 32	-21 ≤ l ≤ 21
$θ$ range [°]	1.74 to 30.03	1.95 to 30.06
$μ$ [mm^{-1}]	1.057	1.998
Reflections collected	289662	8934
Independent reflections [R$_{int}$]	17779 (0.0661)	4739 (0.0417)
Observed reflections [I > 2σ(I)]	12823	3239
Refined parameters / restraints	622 / 0	195 / 0
Goodness-of-fit	1.044	1.027
R_1 [I > 2 σ(I)]	0.0516	0.0412
$wR2$ (all data)	0.1565	0.1021
Residual electron density [e·Å^{-3}]	2.303 / -0.741	0.412 / -0.774

Formula	$C_{91}H_{176}Mn_6N_{12}O_{27}Zn_2$
	21
Mr [g·mol^{-1}]	2330.82
Crystal size [mm]	0.12 x 0.12 x 0.06
Crystal system	triclinic
Space group	P-1
a [Å]	14.776(7)
b [Å]	14.852(8)
c [Å]	17.114(8)
α [°]	74.003(13)
β [°]	66.337(10)
γ [°]	60.644(8)
V [Å^3]	2984(3)
ρ_{calc} [g·m^{-3}]	1.297
Z	2
F(000)	1232
hkl range	-15 ≤ *h* ≤ 17
	-16 ≤ *k* ≤ 17
	0 ≤ *l* ≤ 20
θ range [°]	1.71 to 25.03
μ [mm^{-1}]	1.076
Reflections collected	50334
Independent reflections [R_{int}]	10543 (0.0760)
Observed reflections [$I > 2\sigma(I)$]	7029
Refined parameters / restraints	623 / 202
Goodness-of-fit	1.049
R_1 [$I > 2\,\sigma(I)$]	0.0567
wR2 (all data)	0.1480
Residual electron density [e·Å^{-3}]	0.807 / -0.697

6. Publications

1. "Synthesis and Characterisation of Some New Zinc Carbamate Complexes Formed by CO_2 Fixation and Their Use as Precursors for ZnO Particles under Mild Conditions" D. Domide, E. Kaifer, J. Mautz, O. Walter, S. Behrens, H. J. Himmel *Eur. J. Inorg. Chem.* **2008**, 3177–3185

2. "Electron density controlled carbamate ligand binding mode: towards a better understanding of metalloenzyme activity" C. Neuhäuser, D. Domide, J. Mautz, E. Kaifer, H. J. Himmel *Dalton Trans. (Communication)* **2008**, 1821-1824

3. "Synthesis of Trinuclear, Dinuclear and Mononuclear Carbamato-Zinc Complexes from Tetranuclear Precursors: A Top-Down Synthetic Approach to New Carbamates" D. Domide, C. Neuhäuser, E. Kaifer, H. Wadepohl, H. J. Himmel *Eur. J. Inorg. Chem.* **2009**, 2170–2178

4. "Synthesis of Oligonuclear Mixed Zn/Co Carbamates as Precursors to Nanosized Magnetic Oxides Under Mild Conditions" D. Domide, O. Walter, S. Behrens, E. Kaifer, H. J. Himmel unpublished results

5. "Synthesis and Reactivity of a New Oxidation-Labile Heterobimetallic Mn_6Zn_2 Carbamate Cluster and Precursor to Nanosized Magnetic Oxide Particles" D. Domide, O. Hübner, S. Behrens, O. Walter, H. Wadepohl, E. Kaifer, H. J. Himmel unpublished results

7. References

[1]   D. Walther, M. Ruben, S. Rau, *Coord. Chem. Rev.* **1999**, *182*, 67

[2]   Albert L. Lehninger, David L. Nelson, Michael M. Cox, *Lehninger Principles of Biochemistry* **2004**

[3]   E. J. Badin, M. Calvin, *J. Am. Chem. Soc.* **1950**, *72*, 5266

[4]   M. Calvin, *Chemical and Engineering News* **1953**, *31*, 1622

[5]   M. Calvin, *Science* **1962**, *135*, 879

[6]   T. C. Taylor, I. Andersson, *Nat. Struct. Biol.* **1996**, *3*, 95

[7]   P. Böger, *Naturwiss. Rundsch.* **1975**, *88*, 429

[8]   M. M. Halmann, *Chemical Fixation of Carbon Dioxide. Methods for Recycling CO₂ into Useful Products*, CRC Press, Boca Raton **1993**

[9]   D. Walther, *Coord. Chem. Revs.* **1987**, *79*, 135

[10]   P. Braunstein, D. Matt, D. Nobel, *Chem. Rev.* **1988**, *88*, 747

[11]   A. R. Cutler, P. K. Hanna, J. C. Vites, *Chem. Rev.* **1988**, *88*, 1363

[12]   P. C. Ford, A. Rokicki, *Adv. Organomet. Chem.* **1988**, *28*, 139

[13]   W. Leitner, *Coord. Chem. Rev.* **1996**, *153*, 257

[14]   D. H. Gibson, *Chem. Rev.* **1996**, *96*, 2063

[15]   E. Dinjus, R. Fornika, B. Cornils, W. A. Hermann, *Applied Homogeneous Catalysis with Organometallic Compounds*, VCH, Weinheim, **1997**, *2*, 1997

[16]   M. Aresta, E. Quaranta, I. Tommasi, *New. J. Chem.* **1994**, *18*, 133

[17]   U. Abram, D. B. Dell'Amico, F. Calderazzo, S. Kaskel, L. Labella, L. Marchetti, R. Rovai, J. Strähle, *J. Chem. Soc. Chem. Commun.* **1997**, *20*, 1941

[18]   D. Belli, D. B. Dell'Amico, F. Calderazzo, L. Labella, C. Maichle-Moessmer, J. Strähle, *J. Chem. Soc. Chem. Commun.* **1994**, *13*, 1555

[19]   A. Belforte, D. B. Dell'Amico, F. Calderazzo, U. Giurlani, L. Labella, *Gazz. Chim. Ital.* **1993**, *123*, 119

[20]   A. Bacchi, D. B. Dell'Amico, F. Calderazzo, U. Giurlani, G. Pelizzi, L. Rocchi, *Gazz. Chim. Ital.* **1992**, *122*, 429

[21]   I. Abrahams, M. A. Malik, M. Montevalli, D. O'Brien, *J. Chem. Soc. Dalton Trans.* **1995**, *6*, 1043

[22]   C. C. Chang, B. Srinivas, M. L. Wu, W. H. Chiang, M. Y. Chiang, C. S. Hsiung, *Organometallics* **1995**, *14*, 5150

[23] D. Walther, E. Dinjus, *Z. Chem.* **1981**, *21*, 415

[24] D. Walther, V. Herzog, *Z. Chem.* **1987**, *27*, 373

[25] D. Walther, *Z. Chem.* **1989**, *29*, 146

[26] S. Sakaki, K. Kitaura, K. Morokuma, *Inorg. Chem.***1982**, *21*, 760

[27] M. Rosi, A. Sgamellotti, F. Tarantelli, C. Floriani, *Inorg. Chem.* **1987**, *26*, 3805

[28] D. B. Dell'Amico, F. Calderazzo, U. Giurlani, *Chem. Commun.* **1986**,1000

[29] A. Belforte, F. Calderazzo, *J. Chem. Soc., Dalton Trans.* **1989**, 1007

[30] A. Belforte, D. B. Dell'Amico, F. Calderazzo, *Chem. Ber*. **1988**, *121*, 1891

[31] U. Giurlani, *Tesi di laurea*, Universita` di Pisa, Pisa, Italy **1986**

[32] M. T. Caudle, R. A. Nieman, V. G. Young, *Inorg. Chem.* **2001**, *40*, 1571

[33] K. C. Yang, C. C. Chang, C. S. Yeh, G. H. Lee, S. M. Peng, *Organometallics* **2001**, *20*, 126

[34] M. T. Caudle, J. B. Benedict, C. K. Mobley, N. A. Straessler, T. L. Groy, *Inorg. Chem*. **2002**, *41*, 3183

[35] D. B. Dell'Amico, F. Calderazzo, M. Dell' Innocenti, B. Güldenpfennig, S. Ianelli, G. Pelizzi, P. Robino, *Gazz. Chim. Ital.* **1993**, *123*, 283

[36] D. B. Dell'Amico, F. Calderazzo, M. Dell' Innocenti, B. Güldenpfennig, S. Ianelli, G. Pelizzi, *Gazz. Chim. Ital.* **1990**, *120*, 819

[37] G. A. Horley, M. F. Mahon, K. C. Molloy, P. W. Haycock, C. P. Myers, *Inorg. Chem.* **2002**, *41*, 5052

[38] A. Belforte, F. Calderazzo, P. F. Zanazzi, *J. Chem. Soc., Dalton Trans*. **1988**, 2921

[39] A. Belforte, *PhD Thesis*, Scuola Normale Superiore di Pisa, Pisa, Italy **1990**

[40] W. Bünder, E. Weiss, *Z. Naturforsch.* **1978**, *33b*, 1235

[41] D. B. Dell'Amico, F. Calderazzo, B. Giovannitti, G. Pelizzi, *J. Chem. Soc., Dalton Trans*. **1984**, 647

[42] S. Schenk, J. Notni, U. Köhn, K. Wermann, E. Anders, *Dalton Trans.* **2006**, 4191

[43] Y. Tang, W. S. Kassel, L. N. Zakharov, A. L. Rheingold, R. A. Kemp, *Inorg. Chem.* **2005**, *44*, 359

[44] M. B. Hursthouse, M. A. Malik, M. Motevalli, P. O'Brien, *J. Chem. Soc., Chem. Commun.* **1991**, 1690

[45]   M. A. Malik, M. Motevalli, P. O'Brien, *Inorg. Chem.* **1995**, *34*, 6223

[46]   D. B. Dell'Amico, F. Calderazzo, L. Labella, F. Marchetti, I. Mazzoncini, *Inorg. Chim. Acta* **2006**, *359*, 3371

[47]   J. Klunker, M. Biedermann, W. Schäfer, H. Hartung, *Z. anorg. allg. Chem.* **1998**, *624*, 1503

[48]   S. Inoue, M. Nakui, F. Kojima, *Chem. Lett.* **1984**, 619

[49]   C. S. McCowan, T. L. Groy, M. T. Caudle, *Inorg. Chem.* **2002**, *41*, 1120

[50]   C. S. McCowan, M. T. Caudle, *Dalton Trans.* **2005**, 238

[51]   P. F. Haywood, M. R. Hill, N. K. Roberts, D. C. Craig, J. J. Russell, R. N. Lamb, *Eur. J. Inorg. Chem.* **2008**, 2024

[52]   M. T. Caudle, C. K. Mobley, L. M. Bafaro, R. LoBrutto, G. T. Yee, T. L. Groy, *Inorg. Chem.* **2004**, *43*, 506

[53]   D. B. Dell'Amico, C. Bradicich, F. Calderazzo, A. Guarini, L. Labella, F. Marchetti, A. Tomei, *Inorg. Chem.* **2002**, *41*, 2814

[54]   A. Bacchi, D. B. Dell'Amico, F. Calderazzo, U. Giurlani, G. Pelizzi, L. Rocchi, *Gazz. Chim. Ital.* **1992**, *122*, 429

[55]   M. R. Hill, A. W. Jones, J. J. Russell, N. K. Roberts, R. N. Lamb, *J. Mater. Chem.* **2004**, *14*, 3198

[56]   M. R. Hill, J. J. Russell, R. N. Lamb, *Chem. Mater.* **2008**, *20*, 2461

[57]   M. R. Hill, P. Jensen, J. J. Russell, R. N. Lamb, *Dalton Trans.* **2008**, 2751

[58]   M. L. Kahn, A. Glaria, C. Pages, M. Monge, L. S. Macary, A. Maisonnat, B. Chaudret, *J. Mater. Chem.* **2009**, *19*, 4044

[59]   J. Lewinski, W. Marciniak, J. Lipkowski, I. Justyniak, *J. Am. Chem. Soc.* **2003**, *125*, 12698

[60]   J. Lewinski, K. Suwala, M. Kubisiak, Z. Ochal, I. Justyniak, J. Lipkowski, *Angew. Chem. Int. Ed.* **2008**, *47*, 7888

[61]   Q. Zhang, C. S. Dandeneau, X. Zhou, G. Cao, *Adv. Mater.* **2009**, *21*, 4087

[62]   K. Keis, E. Magnusson, H. Lindstrom, S. E. Lindquist, A. Hagfeldt, *Sol. Energy Mater. Sol. Cells* **2002**, *73*, 51

[63]   A. B. F. Martinson, T. W. Hamann, M. J. Pellin, J. T. Hupp, *Chem. Eur. J.* **2008**, *14*, 4458

[64]   Q. Zhang, T. P. Chou, B. Russi, S. A. Jenekhe, G. Cao, *Angew. Chem.* **2008**, *120*, 1

[65]   M. Monge, M. L. Kahn, A. Maisonnat, B. Chaudret, *Angew. Chem. Int. Ed.* **2003**, *42*, 5321

[66]   M. L. Kahn, M. Monge, V. Colliere, F. Senocq, A. Maisonnat, B. Chaudret, *Adv. Funct. Mater.* **2005**, *15*, 458

[67]   M. L. Kahn, M. Monge, E. Snoeck, A. Maisonnat, B. Chauret, *Small.* **2005**, *1*, 221

[68]   M. L. Kahn, T. Cardinal, B. Bousquet, M. Monge, V. Jubera, B. Chauret, *Chem. Phys. Chem.* **2006**, *7*, 2392

[69]   A. Orlov, A. Roy, M. Lehmann, M. Driess, S. Polarz, *J. Am. Chem. Soc.* **2007**, *129*, 371

[70]   A. Roy, S. Polarz, S. Rabe, B. Rellinghaus, H. Zahres, F. E. Kruis, M. Driess, *Chem. Eur. J.* **2004**, *10*, 1565

[71]   S. Polarz, A. Roy, M. Merz, S. Halm, D. Schröder, L. Scheider, G. Bacher, F. E. Kruis, M. Driess, *Small.* **2005**, *1*, 540

[72]   S. Polarz, F. Neues, M. Van der Berg, W. Grünert, L. Khodeir, *J. Am. Chem. Soc.* **2005**, *127*, 12028

[73]   V. Ischenko, S. Polarz, D. Grote, V. Stavarache, K. Fink, M. Driess, *Adv. Funct. Mater.* **2005**, *15*, 1945

[74]   S. Polarz, J. Strunk, V. Ischenko, M. Van der Berg, O. Hinrichsen, M. Muhler, M. Driess, *Angew. Chem.* **2006**, *118*, 3031

[75]   C. Lizandara-Pueyo, M. W. E. van den Berg, A. De Toni, T. Goes, S. Polarz, *J. Am. Chem. Soc.* **2008**, *130*, 16601

[76]   S. Polarz, A. V. Orlov, M. W. E. van den Berg, M. Driess, *Angew. Chem. Int. Ed.* **2005**, *44*, 7892

[77]   M. Van der Berg, S. Polarz, O. P. Tkachenko, K. V. Klementiev, M. Bandyopadhyay, L. Khodeir, H. Gies, M. Muhler, W. Grünert, *J. Catal.* **2006**, *241*, 446

[78]   S. Polarz, A. Roy, M. Lehmann, M. Driess, F. E. Kruis, A. Hoffmann, P. Zimmer, *Adv. Funct. Mater.* **2007**, *17*, 1385

[79]   S. Polarz, A. Orlov, F. Schüth, A. H. Lu, *Chem. Eur. J.* **2007**, *13*, 592

[80] J. H. Fendler, F. C. Meldrum, *Adv. Mater.* **1995**, *7*, 607

[81] C. N. R. Rao, G. U. Kulkarni, P. J. Thomas, P. P. Edwards, *Chem. Soc. Rev.* **2000**, *29*, 27

[82] N. Toshima, T. Yonezawa, *New J. Chem*. **1998**, *22*, 1179

[83] M. Niederberger, N. Pinna, J. Polleux, A. Antonietti, *Angew. Chem.* **2004**, *116*, 2320; *Angew. Chem. Int. Ed*. **2004**, *43*, 2270

[84] M. Jansen, *Angew. Chem.* **2002**, *114*, 3896; *Angew. Chem. Int. Ed*. **2002**, *41*, 3746

[85] N. Herron, D. L. Thorn, *Adv. Mater.* **1998**, *10*, 1173

[86] V. Ischenko, S. Polarz, D. Grote, V. Stavarache, K. Fink, M. Driess, *Adv. Funct. Mater.* **2005**, DOI: 10.1002/adfm.200500087

[87] S. L. Cumberland, K. M. Hanif, A. Javier, G. A. Khitrov, G. F. Strouse, S. M.Woessner, C. S. Yun, *Chem. Mater.* **2002**, *14*, 1576

[88] M. Niederberger, G. Garnweitner, N. Pinna, M. Antonietti, *J. Am. Chem. Soc*. **2004**, *126*, 9120

[89] S. Mathur, M. Veith, M. Haas, A. Shen, N. Lecerf, V. Huch, S. Hufner, R. Haberkorn, H. P. Beck, M. Jilavi, *J. Am. Ceram. Soc.* **2001**, *84*, 1921

[90] J. F. Eichler, O. Just, W. S. Rees, *J. Mater. Chem.* **2004**, *14*, 3139

[91] G. A. Seisenbaeva, E. V. Suslova, M. Kritikos, V. G. Kessler, L. Rapenne, M. Andrieux, F. Chassagneux, S. Parola, *J. Mater. Chem.* **2004**, *14*, 3150

[92] S. Mathur, M. Veith, R. Rapalaviciute, H. Shen, G. F. Goya, W. L. Martins, T. S. Berquo, *Chem. Mater.* **2004**, *16*, 1906

[93] J. H. Thurston, T. O. Ely, D. Trahan, K. H. Whitmire, *Chem. Mate*r. **2003**, *15*, 4407

[94] H. O. Davies, A. C. Jones, T. J. Leedham, P. O'Brien, A. J. P. White, D. J. Williams, *J. Mater. Chem*. **1998**, *8*, 2315

[95] C. L. Carnes, P. N. Kapoor, K. J. Klabunde, J. Bonevich, *Chem. Mater.* **2002**, *14*, 2922

[96] M. Veith, S. Mathur, C. Mathur, *Polyhedron* **1998**, *17*, 1005

[97] L. G. Hubert-Pfalzgraf, *Coord. Chem. Rev.* **1998**, *180*, 967

[98] L. G. Hubert-Pfalzgraf, *Inorg. Chem. Commun.* **2003**, *6*, 102

[99] H. Falk, J. Hübner, P. J. Klar, W. Heimbrodt, *Phys. Rev. B* **2003**, *68*, 165203

[100] Z. Xiao, H. Matsui, N. Hasuike, H. Harima, H. Tabata, *J. Appl. Phys.* **2008**, *103*, 043504

[101] M. Snure, D. Kumar, A. Tiwari, *JOM* **2009**, *61*, 72

[102] L. Poul, S. Ammar, N. Jouini, F. Fiévet, F. Villain, *Solid State Sc.* **2001**, *3*, 31

[103] M. A. Malik, P. O'Brien, *Polyhedron* **1997**, *16*, 3593

[104] M. Westerhausen, T. Bollwein, A. Pfitzner, T. Nilges, H. J. Deiseroth, *Inorg. Chim. Acta* **2001**, *312*, 239

[105] C. H. Park, S. B. Zhang, S. H. Wei, *Phys. Rev. B* **2002**, *66*, 73202/1

[106] H. Kunkely, A. Vogler, *J. Chem. Soc., Chem. Commun.* **1990**, 1204

[107] F. Decremps, J. Pellicer-Porres, A. M. Saitta, J. C. Chervin, A. Polian, *Phys. Rev. B* **2002**, *65*, 092101/1

[108] C. J. Pan, H. C. Hsu, H. M. Cheng, C. Y. Wu, W. F. Hsieh, *J. Solid State Chem.* **2007**, *180*, 1188

[109] J. M. Calleja, M. Cardona, *Phys. Rev. B* **1977**, *16*, 3753

[110] A. Weibel, R. Bouchet, F. Boulc'h, P. Knauth, *Chem. Mater.* **2005**, *17*, 2378

[111] L. Poul, S. Ammar, N. Jouini, F. Fiévet, F. Villain, *Solid State Sciences* **2001**, *3*, 31

[112] D. Domide, E. Kaifer, J. Mautz, O. Walter, S. Behrens, H. J. Himmel, *Eur. J. Inorg. Chem.* **2008**, 3177

[113] R. Schwesinger, *Nachr. Chem. Tech. Lab*. **1990**, *38*, 1214

[114] V. Raab, J. Kipke, R. M. Gschwind, J. Sundermeyer, *Chem. Eur. J.* **2002**, *8*, 1628

[115] U. Wild, O. Hübner, A. Maronna, M. Enders, E. Kaifer, H. Wadepohl, H. J. Himmel, *Eur. J. Inorg. Chem.* **2008**, 4440

[116] M. Reinmuth, U. Wild, E. Kaifer, M. Enders, H. Wadepohl, H. J. Himmel, *Eur. J. Inorg. Chem.* **2009**, 4795

[117] D. Domide, C. Neuhäuser, E. Kaifer, H. Wadepohl, H. J. Himmel, *Eur. J. Inorg. Chem.* **2009**, 2170

[118] C. Neuhäuser, D. Domide, J. Mautz, E. Kaifer, H. J. Himmel, *Dalton Trans.* **2008**, 1821

[119] P. M. Richards, R. K. Quinn, B. Morosin, *J. Chem. Phys.* **1973**, *59*, 4474

[120] D. B. Dell'Amico, F. Calderazzo, L. Labella, C. M. Mössmer, J. Strähle, *J. Chem. Soc., Chem. Commun.* **1994**, 1555

[121] J. I. Langford, A. J. C. Wilson, *J. Appl. Cryst.* **1978**, *11*, 102

[122] DENZO-SMN, Data processing software, Nonius **1998**; ttp://www.nonius.com.

[123] *SAINT*, Bruker AXS, **2007**

[124] G. M. Sheldrick, *TWINABS*, Bruker AXS, **2004-2008**

[125] G. M. Sheldrick, *SHELXS-97*, *Program for Crystal Structure Solution*, University of Göttingen, **1997**; http://shelx.uni-ac.gwdg.de/SHELX/index.html.

[126] G. M. Sheldrick, *SHELXL-97*, *Program for Crystal Structure Refinement*, University of Göttingen, **1997**; http://shelx.uni-ac.gwdg.de/SHELX/index.html.

[127] *International Tables for X-ray Crystallography*, Vol. 4, Kynoch Press, Birmingham, U.K., **1974**

[128] L. Zsolnai, G. Huttner, *XPMA*, University of Heidelberg, **1994**; http://www.uni-heidelberg.de/institute/fak12/AC/huttner/software/software.html.

[129] R. Soltek, *Winray 32*, University of Heidelberg, **2000**; http://www.uni-heidelberg.de/institute/fak12/AC/huttner/software/software.html.

[130] Ortep-3 for Windows: L. J. Farrugia, *J. Appl. Cryst.* **1997**, *30*, 565

[131] POVRay for Windows Version 3.6, *Vision Raytracer* **2007**.

[132] F. Decremps, J. Pellicer-Porres, A. M. Saitta, J.-C. Chervin, A. Polian, *Phys. Rev. B* **2002**, *65*, 092101/1

8. Acknowledgements

„Hiermit erkläre ich an Eides statt, dass ich die vorliegende Arbeit selbständig und ohne unerlaubte Hilfsmittel durchgeführt habe."

Heidelberg, im November 2010

Dan Domide